

The role of prohibitin-2 in podocytes –  
mitochondrial function and beyond

Inaugural-Dissertation

zur

Erlangung des Doktorgrades

der Mathematisch-Naturwissenschaftlichen Fakultät

der Universität zu Köln

vorgelegt von

Christina Ising  
aus Steinfurt

Berichterstatter: Prof. Dr. Thomas Langer  
(Gutachter)

Prof. Dr. Thomas Benzing

Tag der mündlichen Prüfung: 20. Januar 2014

## Table of contents

### Table of contents

Table of contents .....	I
List of figures .....	V
List of tables .....	VI
Abbreviations .....	VII
1 Abstract .....	1
2 Zusammenfassung .....	2
3 Introduction.....	4
3.1 Podocytes in glomerular diseases .....	4
3.2 SPFH domain-containing protein family .....	5
3.2.1 General information .....	5
3.2.2 Podocin .....	6
3.2.3 Prohibitins .....	6
3.3 Regulation of metabolism by mTOR signaling.....	8
3.3.1 The mTOR pathway .....	8
3.3.2 Role of mTOR signaling in podocytes .....	10
4 Thesis aims .....	12
5 Material and methods .....	14
5.1 Material.....	14
5.1.1 Chemicals, reagents and solutions .....	14
5.1.2 Assays/Kits .....	19
5.1.3 Buffers and solutions .....	20
5.1.4 Oligonucleotides .....	27
5.1.5 Plasmids .....	29
5.1.6 Antibodies .....	30
5.1.7 Enzymes .....	32
5.1.8 Materials .....	32
5.1.9 Equipment.....	34
5.1.10 Software .....	37
5.2 Methods.....	38
5.2.1 Working with nucleic acids .....	38
5.2.1.1 Polymerase chain reaction (PCR) .....	38
5.2.1.2 Restriction and purification of plasmids, vectors and PCR products.....	38

## Table of contents

5.2.1.3	Ligation.....	38
5.2.1.4	Recombination .....	38
5.2.1.5	RNA extraction and cDNA synthesis .....	39
5.2.1.6	TaqMan® assay .....	39
5.2.1.7	DNA sequencing .....	39
5.2.1.8	Dual-luciferase® reporter assay .....	39
5.2.2	Bacteria.....	40
5.2.2.1	Chemical transformation of E.coli.....	40
5.2.2.2	Isolation of plasmid DNA and diagnostic digest.....	40
5.2.3	Cell culture .....	40
5.2.3.1	Cells .....	40
5.2.3.2	Freezing and thawing of cells .....	40
5.2.3.3	Passaging of cells .....	41
5.2.3.4	Doxycycline-treatment of mouse podocytes .....	41
5.2.3.5	Transient expression of plasmids in 293T HEK cells.....	41
5.2.3.6	Virus production .....	41
5.2.3.7	Infection of cells with virus and selection.....	42
5.2.3.8	Immunofluorescence on cells .....	42
5.2.4	Protein biochemistry .....	42
5.2.4.1	Protein extraction .....	42
5.2.4.2	Protein measurement .....	43
5.2.4.3	Co-immunoprecipitation.....	43
5.2.4.4	SDS-polyacrylamide-gelelectrophoresis.....	44
5.2.4.5	Western Blot.....	44
5.2.4.6	Colloidal coomassie staining .....	45
5.2.5	Antibody production .....	45
5.2.5.1	Purification of recombinant protein .....	45
5.2.5.2	Immunization of mice and hybridoma generation .....	47
5.2.5.3	ELISA .....	47
5.2.6	Worm experiments.....	48
5.2.6.1	Worm strains .....	48
5.2.6.2	RNA interference.....	48
5.2.6.3	Touch assay .....	49

## Table of contents

5.2.6.4	Microinjection .....	49
5.2.6.5	Immunofluorescence on worms.....	49
5.2.7	Mouse experiments.....	50
5.2.7.1	Mouse strains and animal care.....	50
5.2.7.2	Serum analysis.....	51
5.2.7.3	Extraction of DNA from mouse tissue.....	51
5.2.7.4	Polymerase-chain reaction (PCR) for genotyping purposes.....	51
5.2.7.5	Albumin ELISA .....	52
5.2.7.6	Creatinine Assay .....	52
5.2.7.7	PAS staining.....	52
5.2.7.8	Specific immunohistochemistry .....	53
5.2.7.9	Electron microscopy and immunogold labeling .....	54
5.2.7.10	Glomeruli isolation .....	54
5.2.7.11	Tamoxifen diet .....	55
5.2.7.12	Rapamycin injection.....	55
5.2.8	Human tissue .....	55
5.2.8.1	Immunofluorescence on human tissue.....	55
5.2.9	Statistical analysis.....	56
6	Results .....	57
6.1	Loss of PHB2 leads to severe glomerular disease .....	57
6.1.1	Podocyte-specific <i>Phb2</i> -knockout mice ( <i>Phb2<sup>pk0</sup></i> ) develop albuminuria and die prematurely.....	57
6.1.2	<i>Phb2<sup>pk0</sup></i> mice develop glomerulosclerosis .....	59
6.1.3	<i>Phb2<sup>het</sup></i> mice present with changes in mitochondrial ultrastructure .....	60
6.1.4	Glomeruli of <i>Phb2<sup>pk0</sup></i> mice display no increased rate of apoptosis at day 21 .....	61
6.1.5	PHB2 is required to maintain structural integrity of podocyte foot processes .....	62
6.1.6	Inducible depletion of <i>Phb2</i> results in loss of slit diaphragm function ...	63
6.2	PHB2 as a novel slit diaphragm protein.....	65
6.2.1	PHB2 localizes to the slit diaphragm.....	65
6.2.2	PHB1 and PHB2 co-immunoprecipitate with podocin .....	67

## Table of contents

6.2.3	PHB-2 co-localizes with MEC-2 at touch receptor punctae and regulates touch sensation in <i>C. elegans</i> .....	69
6.3	PHB2 in metabolic signaling.....	72
6.3.1	Podocyte-specific knockout of the insulin receptor ( <i>Insr</i> ) and IGF-1 receptor ( <i>Igf1r</i> ) prolongs survival of <i>Phb2<sup>pko</sup></i> mice .....	72
6.3.2	Inhibition of mTOR signaling increases lifespan of <i>Phb2<sup>pko</sup></i> mice.....	74
7	Discussion .....	79
7.1	PHB2 – a slit diaphragm protein?.....	79
7.1.1	The phenotype of <i>Phb2<sup>pko</sup></i> mice is similar to slit diaphragm protein-deficient mice .....	79
7.1.2	PHB2 is necessary for the function of the slit diaphragm complex.....	81
7.1.3	<i>Phb2</i> -deficiency in podocytes affects mitochondrial and non-mitochondrial functions.....	82
7.2	PHB2 is linked to the regulation of cell metabolism .....	84
7.2.1	<i>Phb2</i> -deficiency influences metabolic signaling via the insulin and IGF-1 receptor .....	84
7.2.2	Dysregulated mTOR signaling leads to glomerular diseases.....	86
7.2.3	Hypothesis: Loss of PHB2 sensitizes the insulin receptor .....	88
8	Conclusion.....	91
9	Publications .....	93
9.1	Publications in academic journals.....	93
9.2	Publications in international academic conferences .....	93
10	References .....	94
11	Danksagung .....	111
12	Erklärung .....	112
13	Curriculum vitae .....	113

## List of figures

### List of figures

Figure 1: The three layers of the glomerular filtration barrier .....	4
Figure 2: Multimeric ring complexes of prohibitins .....	7
Figure 3: mTOR pathway.....	10
Figure 4. Podocyte-specific <i>Phb2</i> -knockout mice ( <i>Phb2<sup>pko</sup></i> ) develop albuminuria and die prematurely.....	58
Figure 5. <i>Phb2<sup>pko</sup></i> mice develop glomerulosclerosis.....	60
Figure 6. <i>Phb2<sup>het</sup></i> mice present with changes in mitochondrial ultrastructure.....	61
Figure 7. Glomeruli of <i>Phb2<sup>pko</sup></i> mice display no increased rate of apoptosis at day 21 .....	62
Figure 8. PHB2 is required to maintain structural integrity of podocyte foot processes .....	63
Figure 9. Inducible depletion of <i>Phb2</i> results in loss of slit diaphragm function .....	64
Figure 10. PHB2 localizes to the slit diaphragm .....	66
Figure 11. PHB1 and PHB2 co-immunoprecipitate with podocin.....	68
Figure 12. PHB-2 co-localizes with MEC-2 at touch receptor punctae and regulates touch sensation in <i>C. elegans</i> .....	71
Figure 13: Loss of the insulin receptor but not IGF-1 receptor prolongs lifespan of <i>Phb2<sup>pko</sup></i> mice.....	73
Figure 14: Podocyte-specific knockout of the insulin receptor ( <i>Insr</i> ) and IGF-1 receptor ( <i>Igf1r</i> ) prolongs survival of <i>Phb2<sup>pko</sup></i> mice .....	74
Figure 15. Generation and validation of an inducible <i>Phb2</i> shRNA podocyte cell line .....	76
Figure 16. Inhibition of mTOR signaling increases lifespan of <i>Phb2<sup>pko</sup></i> mice .....	78
Figure 17. Hypothesis: Loss of PHB2 sensitizes the insulin receptor .....	89
Figure 18. Why does loss of PHB2 lead to glomerular disease? .....	91

## List of tables

### List of tables

Table 1. List of chemicals, reagents and solutions .....	14
Table 2. List of assays and kits.....	19
Table 3. Composition of buffers and solutions.....	20
Table 4. List of oligonucleotides used for cloning .....	27
Table 5. List of oligonucleotides used for genotyping .....	27
Table 6. List of oligonucleotides for sequencing .....	28
Table 7. List of shRNAs .....	28
Table 8. List of TaqMan® probes .....	29
Table 9. List of plasmids .....	29
Table 10. List of primary antibodies.....	30
Table 11. List of secondary antibodies .....	31
Table 12. List of enzymes.....	32
Table 13. List of materials.....	32
Table 14. List of equipment .....	34
Table 15. List of software.....	37
Table 16. List of online software .....	37

## Abbreviations

### Abbreviations

μl	microliter
4E-BP1	eukaryotic initiation factor 4-binding protein
AMPK	AMP-activated protein kinase
APS	ammonium persulfate
b	base
BSA	bovine serum albumin
CaCl <sub>2</sub>	calcium chloride
cDNA	complementary DNA
CKD	chronic kidney disease
DAB	3,3'-diaminobenzamide
DAPI	4',6-diamidino-2-phenylindole
DEG/eNaC	degenerin/epithelial Na <sup>+</sup> channels
DNA	deoxyribonucleic acid
dNTP	deoxyribonucleotide triphosphate
DRM	detergent resistant membrane
dsRNA	double stranded RNA
DTT	dithiothreitol
EC	endothelial cell
ECL	enhanced chemoluminescence
EDTA	ethylenediaminetetraacetic acid
eIF4E	eukaryotic initiation factor 4E
ETC	electron transport chain
FBS	fetal bovine serum
fl/fl	flox/flox
FOXO1	forkhead box O1 (mammalian protein)
FP	foot process
FSGS	focal segmental glomerulosclerosis
G	standard gravity
GBM	glomerular basement membrane
GFP	green fluorescent protein
H	human
HEBS	HEPES-buffered saline solution
HEK	human embryonic kidney
het	heterozygous
His	histidine-tag
HPRT1	hypoxanthine phosphoribosyltransferase 1
HRP	horse radish peroxidase
IF	immunofluorescence
IGF-1	insulin-like growth factor 1
<i>Igf1r</i>	insulin-like growth factor 1 receptor (mammalian gene)
IgG	immunoglobulin G
IHC	immunohistochemistry
<i>Insr</i>	insulinreceptor (mammalian gene)
IP	immunoprecipitation

## Abbreviations

IPTG	isopropyl-thio- $\beta$ -d-galactoside
IRS	Insulin receptor substrate
kb	kilobase
KCl	potassium chloride
kDa	kilodalton
KO	knockout
l	liter
LB	lysogeny broth
m	mouse
MEF	mouse embryonic fibroblast
MgSO <sub>4</sub>	magnesium sulfate
ml	milliliter
mRNA	messenger RNA
mTOR	mammalian target for rapamycin (mammalian protein)
mTORC1	mammalian target for rapamycin complex 1
mTORC2	mammalian target for rapamycin complex 2
mtUPR	mitochondrial unfolded protein response
NaCl	sodium chloride
NCBI	National Center for Biotechnology Information
NDS	normal donkey serum
NEB	New England Biolabs
NGM	nematode growth medium
<i>Nphs2</i>	podocin (mammalian gene)
OPA1	optical atrophy 1
OXPPOS	oxidative phosphorylation system
PAGE	polyacrylamide gel electrophoresis
PAN	puromycin aminonucleoside
PAS	periodic acid schiff
PBS	phosphate-buffered saline
PCR	polymerase chain reaction
PFA	paraformaldehyde
PHB1	prohibitin-1 (mammalian protein)
<i>Phb1</i>	prohibitin-1 (mammalian gene)
<i>phb-1</i>	prohibitin-1 ( <i>C. elegans</i> gene)
PHB-1	prohibitin-1 ( <i>C. elegans</i> protein)
PHB2	prohibitin-2 (mammalian protein)
<i>Phb2</i>	prohibitin-2 (mammalian gene)
<i>phb-2</i>	prohibitin-2 ( <i>C. elegans</i> gene)
PHB-2	prohibitin-2 ( <i>C. elegans</i> protein)
PI3K	phosphoinositide 3-kinase
pko	podocyte-specific KO
PMSF	phenylmethylsulfonyl fluoride
pS6RP	phospho S6 ribosomal protein
PVDF	polyvinylidene difluoride
RNA	ribonucleic acid
RNAi	RNA interference

## Abbreviations

ROS	reactive oxygen species
RT	room temperature
S6RP	S6 ribosomal protein
SDS	sodium dodecyl sulfate
SE	standard error
shRNA	short hairpin RNA
SEM	standard error of the mean
SOC	super optimal broth medium
SPFH	stomatins, prohibitins, flotillins and HflK/C
TAE	tris-acetate-EDTA
TBS	tris-buffered saline
TEM	transmission electron microscope
TEMED	N,N,N',N'-tetramethylethylenediamine
T <sub>m</sub>	melting temperature
Tris	tris(hydroxymethyl)aminomethane
TRP	transient receptor potential
TSC1	tuberous sclerosis complex 1 (mammalian protein)
<i>Tsc1</i>	tuberous sclerosis complex 1 (mammalian gene)
TSC2	tuberous sclerosis complex 2 (mammalian protein)
UV	ultraviolet
V	volts
WB	Western blot
WT	wildtype

## 1 Abstract

Diseases of the kidney filtration barrier are a major cause of renal failure and cardiovascular mortality. Podocytes maintain the glomerular filtration barrier and podocyte dysfunction leads to the development of glomerulosclerosis, i.e. glomerular scarring. Mutations in the SPFH domain-containing protein podocin, which is localized to the specialized cell-cell contact of podocytes, the slit diaphragm, can cause one of the most frequent glomerulopathies, FSGS. Podocin is one of the most extensively studied proteins in podocytes but nothing is known about other SPFH domain-containing proteins in podocytes so far. Since it has been speculated that mitochondrial dysfunction may contribute to podocyte injury in glomerular diseases this thesis work investigated the podocyte-specific function of a mitochondrially localized SPFH domain-containing protein, prohibitin-2 (PHB2). PHB2 is important for maintaining normal cristae structures and proper mitochondrial function.

Podocyte-specific loss of PHB2 in mice resulted in the development of progressive albuminuria, glomerulosclerosis and endstage renal failure. Unexpectedly, immunofluorescence stainings and immunogold labeling detected PHB2 not only in mitochondria but also at the slit diaphragm. PHB2 co-precipitated with podocin, thereby suggesting an extramitochondrial role of PHB2 at the slit diaphragm. Supporting these results, the ortholog of PHB2 in *C. elegans* was also not restricted to mitochondria but associated with a mechanosensory complex containing the podocin ortholog MEC-2. Given the high similarity of the mechanosensory complex in worms and the slit diaphragm complex in mammals, functional assays of the mechanosensor were performed. Knockdown of *phb-2* as well as loss of *mec-2* in the mechanosensitive neurons resulted in impaired touch sensitivity, showing a functional impact of PHB2 on this conserved protein-lipid supercomplex.

Furthermore, it was shown before that loss of insulin signaling increases lifespan of *Phb2/phb-2*-deficient yeast and worms. Therefore, apart from the findings at the slit diaphragm, the impact of PHB2 on podocyte metabolism was investigated. *Phb2*-deficiency in podocytes led to increased activity of mTORC1. Treatment of these animals with rapamycin or additional knockout of the insulin and IGF-1 receptor prolonged survival despite progressive albuminuria. Collectively, these data indicate that loss of PHB2 at the slit diaphragm resulted in the development of albuminuria but loss of podocytes was dependent on metabolic dysregulation.

### 2 Zusammenfassung

Erkrankungen des Nierenfilters stellen eine der Hauptursachen für Nierenversagen und kardiovaskuläre Mortalität dar. Podozyten sind ein wichtiger Bestandteil der glomerulären Filtrationsbarriere und eine podozytäre Dysfunktion führt zur Proteinurie und Glomerulosklerose, d.h. glomerulären Vernarbung. Mutationen in dem SPFH-Domänen-Protein Podocin, das an den spezialisierten Zell-Zell-Kontakt von Podozyten, die Schlitzmembran, lokalisiert, führen zu einer der häufigsten Glomerulopathien, der FSGS. Podocin gehört zu den am meisten untersuchten Proteinen im Podozyten, jedoch ist über weitere SPFH-Domänen-Proteine in diesem Zelltyp bisher nichts bekannt. Da spekuliert wird, dass eine mitochondriale Dysfunktion zum Podozytenschaden in glomerulären Erkrankungen beitragen könnte, beschäftigt sich diese Doktorarbeit mit der podozyten-spezifischen Funktion eines mitochondrial-lokalisierten SPFH-Domänen-Proteins, Prohibitin-2 (PHB2). PHB2 ist unter anderem wichtig für den Aufbau und Erhalt der Cristae-Strukturen sowie normale mitochondriale Funktionen.

Der Podozyten-spezifische Verlust von PHB2 führt in Mäusen zur Entwicklung einer fortschreitenden Albuminurie, Glomerulosklerose und terminalem Nierenversagen. Dabei konnten Immunfluoreszenz- und Immunogoldfärbungen PHB2 nicht nur in Mitochondrien, sondern auch an der Schlitzmembran nachweisen. PHB2 ko-präzipitierte mit Podocin, was eine extramitochondriale Rolle von PHB2 an der Schlitzmembran nahelegt. Darüber hinaus fand sich das PHB2-Ortholog in *C. elegans* nicht nur in Mitochondrien, sondern auch im mechanosensorischen Komplex, der das Podocin-Ortholog MEC-2 enthält. In Anbetracht der hohen Vergleichbarkeit des mechanosensorischen Komplexes in Würmern und dem Schlitzmembrankomplex in Säugern wurden funktionelle Assays des Mechanosensors durchgeführt. Sowohl eine verringerte *phb-2*-Expression als auch der Verlust von *mec-2* in den mechanosensitiven Neuronen führte zu einer verringerten Berührungssensitivität. Dies deutet auf einen funktionellen Einfluss von PHB2 auf diesen konservierten Protein-Lipid-Superkomplex hin.

Ferner wurde bereits gezeigt, dass der Verlust des Insulinsignalweges die Lebensspanne von *Phb2/phb-2*-defizienten Hefen und Würmern verlängert. Deshalb wurde – unabhängig von den Erkenntnissen an der Schlitzmembran – der Einfluss von PHB2 auf den Metabolismus von Podozyten untersucht. Eine *Phb2*-Defizienz in

## Zusammenfassung

Podozyten führt zu einer erhöhten Aktivierung von mTORC1. Die Behandlung dieser Tiere mit Rapamycin sowie der zusätzliche Verlust des Insulin- und IGF-1-Rezeptors verlängerten das Überleben der Tiere trotz fortschreitender Albuminurie. Zusammengefasst bedeutet dies, dass das Fehlen von PHB2 an der Schlitzmembran zur Entstehung der Albuminurie beiträgt, während der Verlust der Podozyten vermutlich auf eine metabolische Dysregulierung in Folge einer Dysregulation des Insulin/mTOR-Signalweges zurückzuführen ist.

### 3 Introduction

#### 3.1 Podocytes in glomerular diseases

Glomerular diseases represent a major cause of chronic kidney disease (CKD) affecting more than 5% of all human beings world-wide. They share common features e.g. loss of plasma proteins into the urine (albuminuria and proteinuria) and glomerular degeneration, fibrosis and scarring (glomerulosclerosis). Both, proteinuria and chronic kidney disease are independently associated with increased risk for endstage renal failure and cardiovascular diseases [1,2].

Each human kidney contains about one million small filtering units, the glomeruli. Blood plasma has to pass the glomerular filtration barrier, which is responsible for the size- and charge-selectivity of the kidney filter and produces an almost protein-free ultrafiltrate. The glomerular filtration barrier is composed of three layers: fenestrated endothelium, glomerular basement membrane and podocytes [3,4] (**Figure 1**).

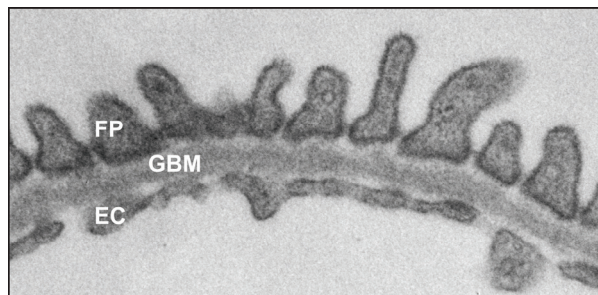


**Figure 1: The three layers of the glomerular filtration barrier**

The glomerular filtration barrier consists of three layers that are important for filtration of blood plasma: podocytes with their foot processes (FP), glomerular basement membrane (GBM) and fenestrated endothelial cells (EC).

Podocytes are the visceral epithelial cells of the kidney glomerulus. They elaborate long interdigitated foot processes that completely enwrap the glomerular capillaries in a complex network. The intercellular slit inbetween neighbouring foot processes is bridged by a continuous membrane-like cell junction, the slit diaphragm [3].

Genetic studies of the last decade showed that glomerular podocytes are essential for the function and integrity of the kidney filter and critically involved in the development of proteinuria [5,6]. Podocyte injury in renal diseases is reflected by foot process effacement, i.e. retraction of the membrane extensions, and ultimately cell

death. Since podocytes are terminally differentiated epithelial cells, podocyte loss inevitably leads to a reduced cell number which is negatively correlated with renal survival [7,8]. Not only inflammation, toxins and mechanical stress but also gene mutations can be the cause of podocyte injury [9]. Numerous studies within the last decades on hereditary glomerular diseases identified mutations in genes encoding for proteins that localize to the podocyte slit diaphragm, e.g. cytoskeleton-associated CD2AP [10,11], the immunoglobulin family member nephrin [12,13], the ion channel TRPC6 [14,15] and the SPFH domain-containing protein podocin [16–19].

### **3.2 SPFH domain-containing protein family**

#### **3.2.1 General information**

The SPFH domain-containing protein family was named after the initials of the proteins in this family: stomatins, prohibitins, flotillins and HflK/C. Initially, the SPFH domain was identified in stomatins and database searches revealed that other proteins like prohibitins contain a strikingly similar domain (also called PHB domain) [20]. The SPFH domain is not only conserved among different proteins but also across species [20–22]. Among others, erlins and podocin as well as the podocin homolog MEC-2 in *C. elegans* are prominent members of this protein family [3,23,24]. Many SPFH domain-containing proteins form homo-oligomers by interacting via the SPFH domain [25–27]. However, also hetero-oligomers exist as shown for the complexes that are made up of prohibitin-1 and prohibitin-2 [28]. Most of the SPFH domain-containing proteins have been shown to be enriched in detergent resistant membranes (DRM) [21,29–34], but so far no common function could be attributed to all members of this family. The SPFH domain is suggested to be either a protein-binding or a lipid-binding motif but no protein-binding partner was identified which is universal for all family members [21]. Since many of the SPFH domain-containing proteins are associated with DRMs - which are defined by their specific lipid composition [35] – it seems to be very probable that this domain is necessary for specific protein-lipid interactions [21]. This has already been shown for podocin/MEC-2, which bind to cholesterol in the plasma membrane [24], but still needs to be proven for other members of the SPFH domain-containing protein family.

### 3.2.2 Podocin

Podocin is an integral membrane protein encoded by *NPHS2*. It consists of one transmembrane domain and a carboxy-terminal cytoplasmic tail. The protein sequence shows strong homology to the corresponding regions of stomatin family proteins [16,36]. During glomerular development podocin is expressed in “mesonephric podocytes from the S-shaped body and, later, in the metanephric kidney, in the future podocytes at the late S-shaped body stage” [36]. In the mature kidney podocin expression is exclusively detectable in podocytes where the protein is localized at the slit diaphragm [36]. *NPHS2* mutations are involved in the development of a familial form of early-onset steroid-resistant nephrotic syndrome progressing towards focal segmental glomerulosclerosis (FSGS) as well as in sporadic cases of the disease and late-onset inherited FSGS [16,17,37–41]. *NPHS2*-knockout mice develop normally but show massive proteinuria shortly after birth due to severe podocyte foot process effacement resulting in end-stage renal failure and premature death within the first weeks of life [18].

In the nematode *C. elegans* MEC-2 - the worm homolog of podocin – is located along regular touch punctae along the six touch receptor neuron processes. Here, MEC-2 is part of a multiprotein-channel complex that is needed to convert mechanical stimuli into electrical signals [42,43]. MEC-2 regulates the function of MEC-4/MEC-10, two degenerin/epithelial Na<sup>+</sup> channels (DEG/ENaC) that transduce gentle body touch sensation [42,44,45]. In mammals, the ion channel TRPC6 - a member of the transient receptor potential (TRP) superfamily - is associated with the slit diaphragm [14,15], where it interacts with other slit diaphragm proteins [14,24]. TRP channels are mechanically gated ion channels [46] which can be regulated by podocin [24]. This renders the slit diaphragm a possible mechanosensitive structure which can more easily be studied in *C. elegans* [47].

### 3.2.3 Prohibitins

Prohibitin-1 (PHB1) and prohibitin-2 (PHB2) are two closely related proteins that reside within the inner mitochondrial membrane. Unconventional sorting sequences target both proteins to mitochondria, where they are inserted into the inner membrane by TIM23-translocase activity. Protein structure analysis revealed that they are anchored to the membrane by a hydrophobic stretch located at the amino terminal end while the large carboxy terminal end, which consists of a PHB-domain

## Introduction

and a coiled coil domain, is exposed to the intermembrane space [28,48]. PHB1 and PHB2 directly interact by forming multimeric ring complexes (**Figure 2**) and stabilize each other [28,49,50].

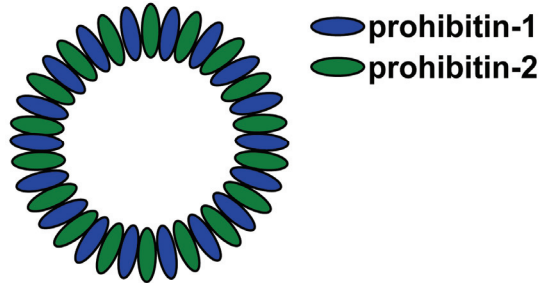


**Figure 2: Multimeric ring complexes of prohibitins**

Prohibitin-1 and prohibitin-2 are assembled in heteromeric ring structures and thereby stabilize each other. (Figure adapted from Osman et al., 2009 [51])

Prohibitins are involved in numerous functions within the cell. Not only are they needed for the maintenance of the mitochondrial membrane and cristae structure but also serve a scaffolding function during biogenesis of oxidative phosphorylation system (OXPHOS) complexes [52,53]. Moreover, prohibitins seem to be important for the regulation of apoptosis [53–56] and can reside within the nucleus where they modulate transcriptional activity [54,57–60]. Nevertheless, it is generally conceived that the majority of prohibitins is localized within the mitochondrial compartment. Prohibitins are upregulated in various types of cancers e.g. breast cancer [61] and gastric cancer [62] but seem to have protective roles in many normal tissues. For example PHBs are required to prevent ethanol-mediated damage of pancreatic  $\beta$ -cells [55,63] and can stop the progression of TGF- $\beta$ 1-induced renal tubulointerstitial lesions [64].

In 2008, Merkwirth et al. [53] showed that cellular depletion of PHB2 in mouse embryonic fibroblasts (MEFs) led to decreased levels of PHB1, markedly reduced proliferation and an increased susceptibility to apoptotic stimuli. The cells exhibited disorganized and swollen mitochondrial cristae structures. However, mitochondrial membrane potential and enzymatic activities of respiratory complexes were unaffected. An impaired processing of the dynamin-like GTPase OPA1 (optic atrophy 1) was identified as the primary cellular defect in the absence of prohibitins [53]. Correct cleavage of OPA1 into five different short and long isoforms is required

## Introduction

for mitochondrial fusion, thereby promoting cristae maintenance and remodeling [65–68].

Universal knockout of *Phb2* in a mouse model resulted in no viable offspring [53,59]. Recently, loss of regular mitochondrial cristae structures and impaired OPA1 cleavage was demonstrated in a neuronal-specific *Phb2*-knockout mouse model *in vivo* [69], thereby confirming the phenotype that was observed in isolated *Phb2*-deficient MEFs [53]. *Phb2*-deficiency in *C. elegans* led to increased fat utilization, increased mitochondrial proliferation, consequent cellular damage and an ultimately reduced lifespan. However, loss of PHB-2 increased lifespan of already long-lived insulin receptor/*daf-2*-mutant worms and partially restored the metabolic defects observed in *Phb2*-deficient worms, thereby linking prohibitins to the metabolic signaling pathways [70]. Furthermore, a recent study in prohibitin-deficient yeast cells revealed that loss of prohibitins leads to increased mitochondrial proteotoxic stress, which activates the mitochondrial untranslated protein response (mtUPR). This effect can be reversed under dietary restriction i.e. less nutrient signaling, probably via decreasing cytoplasmic mRNA translation [71]. In conclusion, experiments in yeast and worm link PHB2 to the action of insulin.

### 3.3 Regulation of metabolism by mTOR signaling

#### 3.3.1 The mTOR pathway

The nutrient-sensing Ser/Thr kinase mammalian target of rapamycin (mTOR) is one of the central regulators for metabolism in cells and organisms. mTOR can assemble with other proteins into two distinct complexes, mTORC1 and mTORC2. In the rapamycin-sensitive mTORC1 complex mTOR associates with raptor and regulates temporal aspects of cell growth whereas the rapamycin-insensitive mTORC2 complex contains rictor and controls spatial aspects of cell growth [72–76]. To exert its function mTORC1 signaling increases e.g. transcription and protein synthesis but inhibits autophagy. The mTORC2 complex mainly regulates actin organization [77].

The activity of mTOR complexes is regulated by different upstream signals that either downregulate or upregulate mTOR activity. On the one hand, stress signals like hypoxia as well as low cellular energy states downregulate mTOR signaling to arrest cell growth [78–81]. Hypoxia increases the HIF1-mediated expression of REDD,

## Introduction

which activates the tuberous sclerosis complex consisting of the heterodimer TSC1 and TSC2. TSC1-TSC2 negatively regulate mTOR activity via Rheb [82–84]. Low cellular energy leads to activation of AMP-activated protein kinase (AMPK), which activates TSC2, resulting in the inhibition of mTORC1 activity [80,85]. On the other hand, amino acids and growth factors increase mTOR signaling. So far, it is not clear how the amino acid status is communicated to the mTOR complex, but one hypothesis is that it works independent of the TSC complex by direct activation of Rheb, which in turn activates the mTOR complex. Two of the most important activators of the mTOR pathway are the growth factors insulin and insulin-like growth factor 1 (IGF-1). Each binds to its specific receptor at the plasma membrane and inhibits TSC1-TSC2 via the phosphoinositide 3-kinase (PI3K) pathway, thereby promoting activation of mTOR and cell growth [86–90] (**Figure 3**).

Two of the best understood downstream mediators of mTOR function are the ribosomal S6 kinase S6K1 and the eukaryotic initiation factor 4-binding protein 4E-BP1. mTORC1 activation leads to phosphorylation of S6K1, which then phosphorylates the 40S ribosomal protein S6, ultimately leading to translation of proteins necessary for ribosomal biogenesis [91]. Moreover, mTORC1 signaling promotes phosphorylation of 4E-BP1, leading to the release of eukaryotic initiation factor 4E (eIF4E) [91,92]. Both downstream effectors initiate protein translation and can be used as *in vitro* and *in vivo* readout for mTORC1 activity [93].

## Introduction

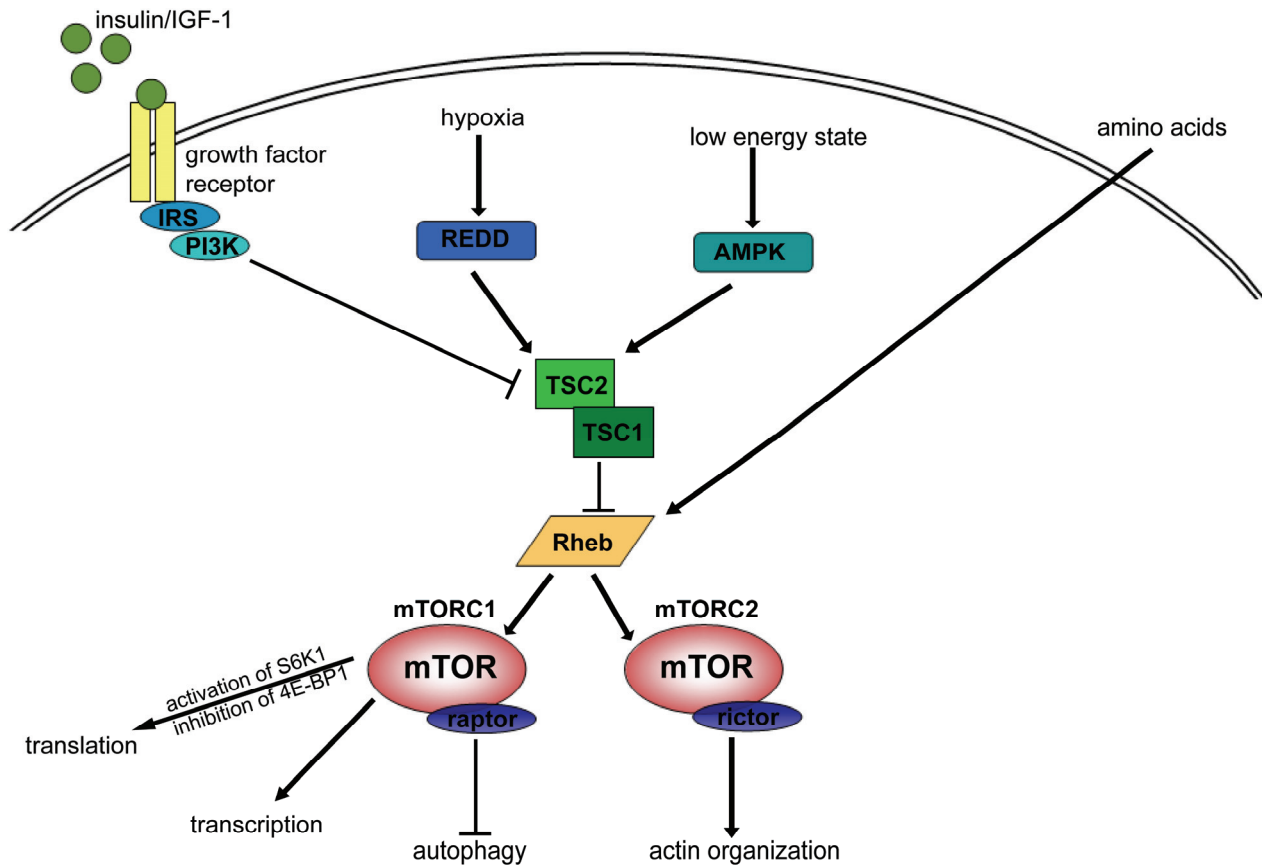


**Figure 3: mTOR pathway**

The mTOR pathway can be activated by different signals. Insulin and IGF-1 are acting via growth factor receptors and the PI3K pathway to inhibit the TSC1-TSC2 complex. Hypoxia mediates inhibition of TSC1-TSC2 via increasing expression of REDD. Low energy states are sensed by AMPK, which also acts on the TSC complex. Amino acids most likely act downstream of the TSC complex by activating Rheb. The two mTOR-complexes contain either mTOR and raptor (mTORC1) or mTOR and rictor (mTORC2). The mTORC1 complex controls temporal aspects of cell growth by regulation of e.g. translation, transcription and autophagy whereas the mTORC2 complex regulates spatial aspects of cell growth via actin organization. (Figure adapted from Wullschleger et al., 2006 [77])

### 3.3.2 Role of mTOR signaling in podocytes

Several studies revealed that patients with glomerular diseases like FSGS [94] and diabetic nephropathy [95–99] may benefit from mTORC1 inhibition by rapamycin treatment. However, rapamycin treatment also frequently leads to the development of *de novo* proteinuria, especially in transplant patients [100–102]. To further understand the role of mTOR in podocytes Gödel et al. [95] generated a podocyte-specific raptor-knockout mouse to specifically abrogate function of the mTORC1 complex. These mice developed albuminuria at the age of four weeks and later

## Introduction

displayed with glomerulosclerosis, resulting in an increased mortality rate after eight months of age. By using an inducible mouse model they also showed that mTORC1 function is not only important for the development but also for the maintenance of the glomerulus during adulthood. Ablation of mTORC2 function by podocyte-specific deletion of rictor did not lead to any overt phenotype under normal conditions, but these mice developed albuminuria when they were exposed to stress cues. However, a combination of raptor- and rictor-knockout led to a much faster progressing and more severe phenotype compared to the knockout of raptor alone [95]. In line with these findings, podocyte-specific depletion of the insulin receptor led to the development of proteinuria and first subtle changes in foot process structures at the age of five weeks. Histologically, these mice showed features of diabetic nephropathy [103]. Another study used a podocyte-specific TSC1-knockout mouse, thereby increasing mTORC1 activity. These mice developed albuminuria already at the age of two weeks and foot process effacement at four weeks of age. In addition, this phenotype was inducible in adult animals as well and the effects could be reversed by treatment with rapamycin [104]. These studies clearly demonstrate that a balance in mTORC1 activity is crucial for a healthy glomerular metabolism, but further work is needed to better understand the effects of different mTOR activity states in glomerular health and disease [105].

#### 4 Thesis aims

The SPFH domain-containing protein podocin, a component of the protein-lipid supercomplex at the slit diaphragm of podocytes, is one of the best studied proteins in podocyte biology. Mutations in *NPHS2*, the gene encoding for podocin, are causing frequent glomerulopathies in humans. So far, little is known about the role of other SPFH domain-containing proteins in podocytes. Therefore, this PhD work investigated the role of prohibitin-2, another SPFH domain-containing protein with primarily mitochondrial function, in podocytes. Furthermore, recent reports from worms and yeast suggest a link between PHB2 and insulin signaling [70,71]. Since mTOR activity downstream of insulin signaling seems to be dysregulated in glomerulosclerosis [95,104,105], the connection between PHB2 and insulin/mTOR signaling was explored further.

Therefore, the major aims for this thesis were:

1. Generation and characterization of podocyte-specific *Phb2*-knockout mice

Conditional *Phb2 flox/flox* mice were mated to podocyte-specific Cre mice (*NPHS2.cre* mice) to generate podocyte-specific *Phb2*-knockout mice (*Phb2<sup>pk0</sup>* mice). The development of glomerular disease in these mice was analyzed at day 14, 21 and 28 after birth by measuring urinary albumin-to-creatinine ratio with a combination of an ELISA and a colorimetric assay. Moreover, PAS staining, specific immunohistochemistry and electron microscopy were used to further characterize these mice.

2. Determination of the localization of PHB2 in podocytes and investigation of a possible interaction with podocin

To assess localization of PHB2 in podocytes two different techniques, immunofluorescence and immunogold labeling, were applied. To analyze a possible interaction with podocin co-immunoprecipitation experiments were performed from overexpressed and endogenous samples.

3. Analysis of a functional impact of PHB2 on the protein-lipid supercomplex

Immunofluorescence stainings were used to confirm the conserved localization of PHB-2 to the protein-lipid supercomplex in *C. elegans*. Gentle

## Thesis aims

touch assays were used to investigate a functional role of PHB-2 in touch sensation.

### 4. Analysis of an impact of the insulin and IGF-1 receptor on the development of glomerular disease in *Phb2*<sup>pk0</sup> mice

Conditional *Phb2 flox/flox* mice were mated to *Insr flox/flox* / *Igf1r flox/flox* mice and *NPHS2.cre* mice to generate *Phb2*<sup>pk0</sup>/*Insr*<sup>pk0</sup>/*Igf1r*<sup>pk0</sup> mice. Lifespan of these animals was recorded and albuminuria at different time points assessed in coomassie gels.

### 5. Determination of a role of mTOR activation in the development of glomerular disease in *Phb2*<sup>pk0</sup> mice

Kidney sections from *Phb2*<sup>pk0</sup> were stained by specific immunohistochemistry for mTORC1 activity. *Phb2*<sup>pk0</sup> mice were treated with the mTORC1 inhibitor rapamycin and albuminuria by means of a coomassie gel as well as survival was assessed.

## 5 Material and methods

### 5.1 Material

#### 5.1.1 Chemicals, reagents and solutions

**Table 1. List of chemicals, reagents and solutions**

<i>Chemicals/Reagents/Solutions</i>	<i>Product no.</i>	<i>Provider</i>
2-Mercaptoethanol	M3148	Sigma
Agarose	A9539-500G	Sigma
Ammonium persulfate (APS)	A0834	Applichem
Ammonium sulfate	3746	Carl Roth
Ampicillin Sodium Salt	K029	Carl Roth
ANTI-FLAG <sup>®</sup> M2 Affinity Gel	A2220	Sigma
Bacto <sup>™</sup> yeast extract	212750	BD Biosciences
Blasticidin S	ant-bl-1	InvivoGen
Boric acid	100165	Merck
Bovine Serum Albumin (BSA)	A7030	Sigma
Bovine Serum Albumin (BSA), 10 mg/ml	B9001	New England BioLabs
Bovine Serum Albumin (BSA), fraction V	1066	Gerbu
Bromphenol Blue	A512	Carl Roth
Cacodylic acid sodium salt trihydrate	5169	Carl Roth
Calcium chloride dihydrate	HN04	Carl Roth
Cholesterol	C8667	Sigma
Citric acid monohydrate	27490	Sigma
Collagen I, bovine	A1064401	Invitrogen
Collagenase Type 1A	C9891	Sigma
Coomassie brilliant blue G-250	161-0406	BioRad
Coumeric Acid	C9008	Sigma
D(+)-Glucose monohydrate	1040740	Merck
DAB substrate (10x)	1855920	Thermo Scientific
Deoxyribonuclease I, bovine (DNase)	D5319	Sigma

## Material and methods

<i>Chemicals/Reagents/Solutions</i>	<i>Product no.</i>	<i>Provider</i>
Deoxyribonucleotide triphosphate (dNTP)-mix	200415	Stratagene
Dimethyl sulfoxide (DMSO) Hybri-Max	D2650	Sigma
Dithiothreitol (DTT)	6908	Carl Roth
Doxycycline hyclate	A2951	Applichem
Dulbecco's Modified Eagle Medium (DMEM)	D6429	Sigma
Ethanol 96% + 1% Methyl ethyl ketone	WAL641.5000	Th.Geyer Group
Ethanol 99% + 1% Methyl ethyl ketone	A5007	Applichem
Ethanol absolut	9065	Carl Roth
Ethidiumbromide solution (1%)	2218	Carl Roth
Ethylene glycol-bis(2-aminoethylether)- <i>N,N,N',N'</i> -tetraacetic acid (EGTA)	E3889	Sigma
Ethylenediaminetetraacetic acid disodium salt dihydrate (EDTA)	E5134	Sigma
Fetal Bovine Serum (FBS)	S 0115	Biochrom AG
Formaldehyde solution 37%	2137.1011	Th.Geyer Group
Freund's adjuvant, complete	F5581	Sigma
Freund's adjuvant, incomplete	F5506	Sigma
GeneRuler 1kb DNA Ladder	SM0311	Fermentas
GeneRuler 50bp DNA Ladder	SM0373	Fermentas
Glycerol	3783	Carl Roth
Glycine	3908	Carl Roth
HAT supplement 100x	21060-017	Gibco
Heparin-Rotexmedica	3862340	Rotexmedica
HEPES Buffer 1M	H0887	Sigma
Histo-Clear	905006	Biozym
Histomount	HS-103	National Diagnostics
Hydrochlorid acid 2 N	T134	Carl Roth
Hydrogen Peroxide 30%	107209	Merck
Igepal® CA-630	I8896	Sigma
Imidazole	X998	Carl Roth

## Material and methods

<i>Chemicals/Reagents/Solutions</i>	<i>Product no.</i>	<i>Provider</i>
Incidin Plus	3011520	Ecolab
Interferon gamma, murine	1476960100	provitro
Isopropanol	5752.3	Carl Roth
Isopropyl-thio- $\beta$ -d-galactoside (IPTG)	A1800	Applichem
Kanamycin sulfate	K4000	Sigma
Ketavet® 100 mg/ml		Pfizer
LB-Agar	X965	Carl Roth
LB-Medium	X964	Carl Roth
L-Glutamine 200mM	25030-081	Gibco
Lipofectamine-2000	11668-027	Invitrogen
Loading Dye Solution (6X)	R0611	Thermo Scientific
Luminol	9253	Fluka
Lysozyme	A3711	Applichem
Magnesium chloride hexahydrate	105833	Merck
Magnesium sulfate heptahydrate	P027	Carl Roth
Mayer's hematoxylin	MHS16	Sigma
MEM non-essential amino acids (MEM NEAA) 100x	11140-050	Gibco
Methanol	4627	Carl Roth
MitoTracker® Red FM	M22425	Invitrogen
N,N,N',N'-tetramethylethylenediamine (TEMED)	2367	Carl Roth
Ni-NTA agarose	30210	Qiagen
NEBuffer 3	B7003	New England BioLabs
Ni-NTA agarose	R901-01	Qiagen
Normal Donkey Serum	017-000-121	Dianova
Opti-MEM®	31985-047	Invitrogen
Osmium tetroxide	8371	Carl Roth
PageRuler Plus Prestained Protein Ladder	26620	Fermentas
Paraformaldehyde (PFA)	P6148	Sigma

## Material and methods

<i>Chemicals/Reagents/Solutions</i>	<i>Product no.</i>	<i>Provider</i>
Passive Lysis Buffer 5x	E1941	Promega
Penicillin-Streptomycin 10,000 U/mL	15140-122	Gibco
Peptone from casein, enzymatic digest	82393	Sigma
Periodic acid 99%	3257	Carl Roth
Phenylmethylsulfonyl fluoride (PMSF)	P7626	Sigma
Phosphoric acid 85%	79617	Sigma
PIPES disodium salt	P3768	
Polyacrylamide	T802	Carl Roth
Polyethylenglykol 400	0144	Carl Roth
Ponceau S	P7170	Sigma
Potassium chloride	6781	Carl Roth
Potassium dihydrogen phosphate	P-018	Carl Roth
ProLong Gold antifade reagent with DAPI	P-36931	Invitrogen
Protein A Sepharose	10-1041	Invitrogen
Protein G Sepharose	GEHE17-0618-01	VWR
Proteinase K	82456	Sigma
Pure acetic acid 99% - 100%	7332	Carl Roth
Puromycin	ant-pr-1	InvivoGen
Qiazol	79306	Qiagen
Rapamycin	R-5000	LC Labs
RNase-free water Ultra Pure	10977-035	Invitrogen
Rompun® 2%		Bayer HealthCare
RPMI-1640 medium	31870025	Gibco
RPMI-1640 medium	R8758	Sigma
Schiff's reagent	109033	Merck
Sodim citrate dihydrate	194868	MP Biomedicals
Sodium acetate	6268	Merck
Sodium azide	S2002	Sigma
Sodium chloride	3957	Carl Roth
Sodium chloride solution 0,9%, isotonic	3563293	AlleMan Pharma

## Material and methods

<i>Chemicals/Reagents/Solutions</i>	<i>Product no.</i>	<i>Provider</i>
Sodium deoxycholate	D6750	Sigma
Sodium dodecyl sulfate (SDS) pellets	CN30	Carl Roth
Sodium fluoride	S-1504	Sigma
Sodium hydrogen carbonate	106329	Merck
Sodium hydroxide	402	J.T. Baker
Sodium hydroxide solution 2 N	T135	Carl Roth
Sodium hypochlorite solution 12%	9026	Carl Roth
Sodium orthovanadate	S6508	Sigma
Sodium pyruvate 100 mM	11360-070	Gibco
Sodium pyruvate 100 mM	S8636	Sigma
Sodium(di-) hydrogen phosphate heptahydrate	106574	Merck
Sodium(tetra-) diphosphate decahydrate	106591	Merck
Spectinomycin dihydrochloride pentahydrate	567570	Merck
Spermidine HCl	S2501	Sigma
TE buffer	60191	Invitrogen
Tetramethylbenzidine (TMB)	T2885	Sigma
Tissue-Tek® O.C.T.™ compound	4583	Sakura
Tris Hydrochlorid (HCl)	9090	Carl Roth
Triton X-100	108603	Merck
Trizma Base	T1503	Sigma
Trypsin-EDTA Solution (1x)	T3924	Sigma
Tryptone	1010817	MP Biomedicals
Tween®20	3472	Caesar&Lorentz
Tween®80	9139	Carl Roth
Uranyl acetate	19481	Ted Pella Inc.
Uranyl acetate dihydrate	73943	Sigma
Vectastain® R.T.U. Elite™ ABC reagent	PK-7100	Vector Laboratories
Zeocin	ant-zn-1	InvivoGen

## 5.1.2 Assays/Kits

Table 2. List of assays and kits

<i>Assay/Kit</i>	<i>Product no.</i>	<i>Provider</i>
Avidin/Biotin Blocking Kit	SP-2001	Vector Laboratories
BCA Protein Assay Kit	23227	Pierce/Thermo Scientific
Big Dye® Terminator v3.1 Cycle Sequencing Kit	4337455	Applied Biosystems
Creatinine (urinary) Assay Kit	500701	Cayman
DAB Substrate Kit	34002	Pierce/Thermo Scientific
Direct-zol™ RNA Mini Prep Kit	R2052	ZymoResearch
Dual-Luciferase® Assay System	E1910	Promega
Epoxy Embedding Medium Kit	45359	Sigma
GeneJet™ PCR Purification Kit	K0702	Fermentas
GeneJet™ Gel Extraction Kit	K0692	Fermentas
GeneJet™ Plasmid Miniprep Kit	K0503	Fermentas
GoTaq® Flexi DNA Polymerase	M8301	Promega
High Capacity cDNA Reverse Transcription	4368814	Applied Biosystems
KOD Hot Start DNA Polymerase Kit	71086	Merck/Novagen
Lowicryl® K4M Polar Kit	15923	Polysciences
Mouse Albumin ELISA Kit	E99-134	Bethyl Laboratories
NucleoBond® Xtra Midi Prep Kit	740410	Macherey-Nagel
REDtaq® ReadyMix™ PCR Reaction Mix	R2523	Sigma
SuperSignal West Femto Chemiluminescent Substrate	34095	Pierce/Thermo Scientific
TaqMan® Universal Master Mix II	4440040	Applied Biosystems
Venor® GeM Mycoplasma Detection Kit	11-1050	Minerva Biolabs

## Material and methods

<i>Assay/Kit</i>	<i>Product no.</i>	<i>Provider</i>
Zenon® Tricolor Rabbit IgG Labeling Kit	Z25360	Molecular Probes

### 5.1.3 Buffers and solutions

**Table 3. Composition of buffers and solutions**

<i>Buffer/Solution</i>	<i>Composition</i>
Anesthesia	6.8 ml 0.9% NaCl 1 ml 100 mg/ml Ketavet® 0.4 ml Rompun®
Antibody Buffer A	1% (w/v) BSA 0.5% (v/v) Triton X-100 0.05% (w/v) NaN <sub>3</sub> 1 mM EDTA in 1x PBS
Antibody Buffer B	0.2% (w/v) BSA in Antibody Buffer A
Base Solution	0.025 N NaOH 0.2 mM EDTA pH 12
Blocking Solution	5% (v/v) NDS 0.1% (v/v) Triton-X100 in 1x PBS
Borate Buffer (40x)	1 M boric acid 500 mM NaOH pH 9.2
Cell Culture Medium (HEK 293T)	10% (v/v) FBS in DMEM
Cell Culture Medium (Hybridoma)	10% (v/v) FBS 100 U/ml Penicillin-Streptomycin 2 mM L-Glutamin 0.5 mM Sodium pyruvate (Gibco) 1x HAT supplement

## Material and methods

<i>Buffer/Solution</i>	<i>Composition</i>
	1x MEM NEAA in RPMI-1640 (Gibco)
Cell Culture Medium (Mouse Podocytes)	10% (v/v) FBS 10 mM HEPES 1 mM Sodium pyruvate (Sigma) in RPMI-1640 (Sigma)
Cell Freezing Solution	45% (v/v) FBS 45% (v/v) DMEM or RPMI-1640 10% (v/v) DMSO
Citrate Buffer (10mM)	1.26 mM Citric acid 8.74 mM Sodium citrate pH 6
Colloidal Coomassie Stock Solution	755 mM (NH <sub>4</sub> ) <sub>2</sub> SO <sub>4</sub> 2.55% (v/v) Phosphoric acid 0.1% (w/v) Coomassie brilliant blue G-250
Colloidal Coomassie Solution	80% Colloidal Coomassie Stock Solution 20% (v/v) Methanol
Developer Solution	48 mM Sodium acetate 13.4% (v/v) H <sub>2</sub> O <sub>2</sub> 98 µg/ml TMB pH 5.2
ECL Detection Solution	100 mM Tris 1,25 mM Luminol 0,2 mM Coumaric acid 0,75% (v/v) H <sub>2</sub> O <sub>2</sub> pH 8.5
Electron Microscopy Antibody Buffer	1% BSA 0.5% Tween®20 0.1% Triton X-100

## Material and methods

<i>Buffer/Solution</i>	<i>Composition</i>
	0.1 M Tris
Electron Microscopy Fixation Buffer	4% (v/v) PFA 2% (v/v) Glutaraldehyde 0.1 M Cacodylate
Elution Buffer	20 mM Tris 150 mM NaCl 300 mM Imidazole pH 8
Fixing Solution for Worms	1% (v/v) formaldehyde in 1x MRWB
Fixing Solution for Coomassie	25% (v/v) isopropanol 10% (v/v) acetic acid
HBSS (1x)	1x HBSS solution A 1x HBSS solution B
HBSS Solution A (10x)	5.4 mM KCl 0.3 mM Na <sub>2</sub> HPO <sub>4</sub> 0.4 mM KH <sub>2</sub> PO <sub>4</sub> 4.2 mM NaHCO <sub>3</sub> 137 mM NaCl 5.6 mM D-glucose pH 7.4
HBSS Solution B (10x)	1.3 mM CaCl <sub>2</sub> 0.5 mM MgCl <sub>2</sub> 0.6 mM MgSO <sub>4</sub>
HEBS (2X)	50 mM HEPES 280 mM NaCl 10 mM KCl 1.5 mM Na <sub>2</sub> HPO <sub>4</sub> pH 7.08

## Material and methods

<i>Buffer/Solution</i>	<i>Composition</i>
His-Buffer	50 mM Tris 150 mM NaCl 20 mM Imidazole pH 7.5
IP Buffer	20 mM Tris 1% (v/v) Triton X-100 50 mM NaCl 15 mM Na <sub>4</sub> P <sub>2</sub> O <sub>7</sub> 50 mM NaF pH 7.5
Laemmli Sample Buffer (2X)	100 mM Tris 4% (w/v) SDS 20% (v/v) Glycerol Bromphenol Blue 100 mM DTT pH 6.8
Laemmli Sample Buffer (5X)	250 mM Tris 10% (w/v) SDS 50% (v/v) Glycerol Bromphenol Blue 250 mM DTT pH 6.8
Ligation Buffer (10X)	400 mM Tris 100 mM MgCl <sub>2</sub> 100 mM DTT 5 mM ATP pH 7.8
M9 Buffer	22 mM KH <sub>2</sub> PO <sub>4</sub> 42 mM Na <sub>2</sub> HPO <sub>4</sub> 85.5 mM NaCl 1 mM MgSO <sub>4</sub>

## Material and methods

<i>Buffer/Solution</i>	<i>Composition</i>
modified RIPA Buffer	50 mM Tris-HCl 1% (v/v) Igepal® CA-630 0.25% (v/v) Sodium deoxycholate 150 mM NaCl 1 mM EDTA 1 mM NaF pH 7.4
modified Ruvkun's Witches Brew (MRWB) (2x)	160 mM KCl 40 mM NaCl 20 mM EGTA 10 mM Spermidine 30 mM PIPES 50% Methanol
Nematode Growth Medium (NGM)	51 mM NaCl 59 mM Agar Peptone 1 mM CaCl <sub>2</sub> 1 mM Mg <sub>2</sub> SO <sub>4</sub> 25 mM KH <sub>2</sub> PO <sub>4</sub> 5 µg/ml Cholesterol
Neutralization Solution	40 mM Tris-HCl pH 5
Phosphate Buffered Saline (PBS)	137 mM NaCl 2.7 mM KCl 10 mM Na <sub>2</sub> HPO <sub>4</sub> 2 mM KH <sub>2</sub> PO <sub>4</sub>
PBS-Tween	0.05% (w/w) Tween®20 in 1x PBS
Proteinase K Solution	20 µg/ml Proteinase K 50 mM Tris-HCl pH 7.8

## Material and methods

<i>Buffer/Solution</i>	<i>Composition</i>
Rapamycin Solution for injection	0.3 mg/ml Rapamycin 5% Tween®80 5% PEG400 sterile filtered with 0.22 µm filter
Rapamycin Stock Solution	6 mg/ml Rapamycin in 100% Ethanol
Resolving Gel	750 mM Tris 10% (v/v) PAA 0.2% (w/v) SDS pH 8.8
Running Buffer	25 mM Tris 192 mM Glycine 0.1% (w/v) SDS
Stacking Gel	250 mM Tris 5% (v/v) PAA 0.2% (w/v) SDS pH 6.8
Staining PBS	1 mM CaCl <sub>2</sub> 0,5 mM MgCl <sub>2</sub> in 1x PBS
SOC Medium	2% (w/v) Tryptone 0.5% (w/v) Yeast Extract 8.6 mM NaCl 2.5 mM KCl 20 mM MgSO <sub>4</sub> 20 mM Glucose
TAE (1X)	40 mM Tris 20 mM Acetic Acid 1mM EDTA pH 8.5

## Material and methods

<i>Buffer/Solution</i>	<i>Composition</i>
TBS (1x)	15 mM Tris-HCl 4.5 mM Tris 150 mM NaCl pH 7.6
TBS-Tween (1x)	15 mM Tris-HCL 4.5 mM Tris 150 mM NaCl pH 7.6 0.025% (v/v) Tween20
Transfer Buffer	25 mM Tris 188 mM Glycine 0.1% (w/v) SDS
Tris-EDTA-Tween	10 mM Tris 1 mM EDTA pH 9.0 0.05% (v/v) Tween20
Tris-Triton Buffer (TTB)	100 mM Tris-HCl 1% (v/v) Triton X-100 1 mM EDTA pH 7.4
Vehicle Solution for injection	5% (v/v) Ethanol 5% (v/v) Tween®80 5% (v/v) PEG400
Wash Buffer	30 mM Tris 300 mM NaCl 0.3% (v/v) Tween20 pH 7.5
2x YTA	85 mM NaCl 16 g/l Tryptone 10 g/l Yeast extract

### 5.1.4 Oligonucleotides

**Table 4. List of oligonucleotides used for cloning**

<i>Cloning primers</i>	<i>Sequence (5' → 3')</i>
ce phb-1 fp	CAATGTTGATGGAGGTCAACG
ce phb-1 rp	GGTGACATTCTTGTCTTGGC
ce phb-2 ORF pEntry fp	GGGGACAAGTTTGTACAAAAAGCAGGCTTGGCGAAA CAAGGGCAAGAAGC
ce phb-2 ORF pEntry rp	GGGGACCACTTTGTACAAGAAAGCTGGGTAGCGTCTT TTGTTCGGTCAC
ce pmec-17 fp	GGGGACAACCTTTGTATAGAAAAGTTGATTTTCTGAAATT ACTATTA
ce pmec-17 rp	GGGGACTGCTTTTTTGTACAACTTGTCATGATCGAAT CGTCTCACAACCT
mPhb1 Mlu1 fp	GCTGCCACGCGTACCATGGCTGCCAAAGTG
mPhb1 Not1 rp	ATGCACGCGGCCGCTCACTGGGGAAGCTGG
mPhb2 Mlu1 fp	GCTGCCACGCGTACCATGGCCCAGAACTTG
mPhb2 Not1 rp	ATGCACGCGGCCGCTCATTCTTACCCTTAATG

**Table 5. List of oligonucleotides used for genotyping**

<i>Genotyping primers</i>	<i>Sequence (5' → 3')</i>
β-globin fp	TGCTCACACAGGATAGAGAGGGCAGG
β-globin rp	GGCTGTCCAAGTGATTCAGGCCATCG
Cre fp	GGACATGTTCAAGGATCGCCAGGCG
Cre rp	GCATAACCAGTGAAACAGCATTGCTG
Dicer fp	CCTGACAGTGACGGTCCAAAG
Dicer rp	CATGACTCTTCAACTCAAACCT
iCreER(T2) fp	TCAACATGCTGCACAGGAGAT
iCreER(T2) rp	ACCATAGATCAGGCCGGTGGGT
Igf1r fp	TCCCTCAGGCTTCATCCGCAA
Igf1r rp	CTTCAGCTTTGCAGGTGCACG
Insr fp	GATGTGCACCCCATGTCTG
Insr rp	CTGAATAGCTGAGACCACAG

Material and methods

<i>Genotyping primers</i>	<i>Sequence (5' → 3')</i>
Phb2 fp	ATCGTATTGGTGGCGTGCAGCA
Phb2 rp1	CGAGGTCTGGCCCGAATGTCAT
Phb2 rp2	AGGGAGGCTTGGTTTGAGGGGA

**Table 6. List of oligonucleotides for sequencing**

<i>Sequencing primers</i>	<i>Sequence (5' → 3')</i>
ce phb-2 ORF pos. 1262 fp	CATCAATTTGTTATTGTTTTG
ce phb-2 ORF pos. 169 rp	CAATTAATTTGATCGTTATAC
ce phb-2 ORF pos. 251 fp	CACTTCAGAATCCCATGGTTC
ce phb-2 ORF pos. 658 fp	GAAAATTATGGGTTATGATC
ce phb-2 ORF pos. 963 fp	GAAGAACGATCCAGGATTTTTG
emGFP fp	GGCATGGACGAGCTGTACAA
mPhb1 pos. 428 fp	GAGAGCTGGTCTCCAG
mPhb1 pos. 601 rp	CCACCACAAATCTGGC
mPhb2 pos. 416 fp	GAGGTGCTCAAGAGTG
mPhb2 pos. 548 rp	CTGTGTA CTCTCGGC
pcDNA6 fp	CGTGTACGGTGGGAGGTCTA
pcDNA6 rp	AGGAAAGGACAGTGGGAGTG
pmec-17 pos. 216 rp	TCTCTCCAACAACTTATTGT

**Table 7. List of shRNAs**

<i>shRNAs</i>	<i>Sequence (5' → 3')/Clone ID</i>
mPhb2 shRNA 1 bottom strand	CCTGAGCTAAGTCCTAAGTTCTGGTCAGTCAGTGGCC AAAACCAGAACTTGAAGGACTTAGCTC
mPhb2 shRNA 1 top strand	TGCTGAGCTAAGTCCTTCAAGTTCTGGTTTTGGCCACT GACTGACCAGAACTTAGGACTTAGCT
mPhb2 shRNA 2	CCTGTAACAATGGACCAGCACTCGTCAGTCAGTGGCC

## Material and methods

<i>shRNAs</i>	<i>Sequence (5' → 3')/Clone ID</i>
bottom strand	AAAACGAGTGCTGCCGTCCATTGTTAC
mPhb2 shRNA 2 top strand	TGCTGTAACAATGGACGGCAGCACTCGTTTTGGCCAC TGACTGACGAGTGCTGGTCCATTGTTA
scrambled shRNA bottom strand	CCTGAAATGTACTGCGTGGAGACGTCAGTCAGTGGCC AAAACGTCTCCACGCGCAGTACATTT
scrambled shRNA top strand	TGCTGAAATGTACTGCGCGTGGAGACGTTTTGGCCAC TGACTGACGTCTCCACGCGCAGTACATTT

**Table 8. List of TaqMan® probes**

<i>TaqMan® probe</i>	<i>Assay ID</i>	<i>Provider</i>
mHPRT	Mm01545399_m1	Applied Biosystems
mPhb1	Mm01627033_g1	Applied Biosystems
mPhb1	Mm00476104_m1	Applied Biosystems

### 5.1.5 Plasmids

**Table 9. List of plasmids**

<i>Plasmid</i>	<i>Provider</i>
ce mec-2 L4440	J. Ahringer lab, Cambridge, England
ce mev-1 L4440	J. Ahringer lab, Cambridge, England
ce phb-1 L4440	generated for this thesis
ce phb-2 L4440	J. Ahringer lab, Cambridge, England
ce phb-2 pEntry	generated for this thesis
ce pmec-17 pEntry	generated for this thesis
ce pmec-17-phb-2::GFP-pDest	generated for this thesis
FLAG.hNEMO pcDNA6	Nephrolab Cologne
FLAG.mPhb1 pcDNA6	generated for this thesis
FLAG.mPhb2 pcDNA6	generated for this thesis
FLAG.mPodocin pcDNA6	Nephrolab Cologne
FLAG.RuvBI1 pcDNA6	Nephrolab Cologne
L4440	A. Fire lab, Stanford, CA, USA
mPhb2 pDonr 221	generated for this thesis

## Material and methods

<i>Plasmid</i>	<i>Provider</i>
mPhb2 psiCheck Dest LR	generated for this thesis
mPhb2 shRNA1+2 pcDNA6.2	generated for this thesis
mPhb2 shRNA1+2 pLenti4/TO/V5-Dest	generated for this thesis
pLentiTTR	Invitrogen
pMD2 VSV-G	Nephrolab Cologne
pMDL g/p	Nephrolab Cologne
pRSV	Nephrolab Cologne
pΔR8.74	D. Trono lab, Lausanne, Switzerland
scrambled shRNA pcDNA6.2	Nephrolab Cologne
scrambled shRNA pLenti4/TO/V5-Dest	generated for this thesis
scrambled shRNA TRIPZ	Thermo Scientific
V5.mPhb1 pcDNA6	generated for this thesis
V5.mPhb2 pcDNA6	generated for this thesis

### 5.1.6 Antibodies

**Table 10. List of primary antibodies**

<i>Antigen (epitope)</i>	<i>Clone</i>	<i>Product no.</i>	<i>Host</i>	<i>dilution</i>	<i>Provider</i>
cleaved caspase-3	(polyclonal)	9661	rabbit	1:200 IHC	Cell Signaling
Flag (DYKDDDDK)	(polyclonal)	F7425	rabbit	1:10,000 WB	Sigma
Flag (DYKDDDDK)	M2 (monoclonal)	F3165	mouse	1 µg IP	Sigma
mec-2			rabbit	1:100 IF	M. Chalfie
PHB1 (C-terminal)	Poly6031 (polyclonal)	603101	rabbit	1:1000 WB	BioLegend
PHB1/PHB2 mixed	(monoclonal)		mouse	undiluted IF	newly generated

## Material and methods

<i>Antigen (epitope)</i>	<i>Clone</i>	<i>Product no.</i>	<i>Host</i>	<i>dilution</i>	<i>Provider</i>
PHB2/BAP37 (C-terminal)	Poly6118 (polyclonal)	611802	rabbit	1:5 Immunogold 1:1000 WB	BioLegend
podocin (amino-acid residues 367-383)	(polyclonal)	P0372	rabbit	1:100 IF	Sigma
V5 (GKPIPPELLGLDST)	(polyclonal)	AB3792	rabbit	1:2000 WB	Millipore
V5 (GKPIPPELLGLDST)	SV5-Pk1 (monoclonal)	MCA1360	mouse	1 µg IP	Serotec
WT-1 (C-terminal)	C-19 (polyclonal)	sc-192	rabbit	1:1000 IHC	St. Cruz

**Table 11. List of secondary antibodies**

Antigen (epitope)	Product no	Dilution	Provider
Cy3-AffiniPure Donkey α-Rabbit IgG (H+L)	711-165-152	1:400	Jackson ImmunoRe search
F(ab') <sub>2</sub> fragment anti-rabbit IgG (H+L)-Biotin	711-066-152	1:500	Dianova
gold-labeled goat anti-rabbit IgG	EM.GAR15	1:10	BBInternati onal
Polyclonal goat anti-mouse immunoglobulins/HRP	P0447	1:30,000	Dako
Polyclonal goat anti-rabbit immunoglobulins/HRP	P0448	1:30,000	Dako

### 5.1.7 Enzymes

**Table 12. List of enzymes**

<i>Enzyme</i>	<i>Product no.</i>	<i>Provider</i>
Gateway® BP Clonase® II Enzyme Mix	11789020	Invitrogen
Gateway® LR Clonase® II Enzyme Mix	11791100	Invitrogen
MluI	R0198	New England Biolabs
Nco	R0193	New England Biolabs
NotI	R0189	New England Biolabs
SacI	R0156	New England Biolabs
T4 DNA Ligase	EL0011	Fermentas

### 5.1.8 Materials

**Table 13. List of materials**

<i>Material</i>	<i>Product no.</i>	<i>Provider</i>
8-Lid chain, flat	65.989.002	Sarstedt
10 cm dish for Agar Plates	82.1473	Sarstedt
BD Microlance™ 3 27 G 3/4" cannula	302200	BD Medical
BD Plastipak™ syringe, 1 ml	300013	BD Medical
BD Primaria™ cell culture dish	353803	BD Biosciences
Blotting paper (Type BF4, 580 x 580)	FT-2-521-580580G	VWR
Cell culture dishes (12-well)	3513	Corning
Cell culture dishes (6-well)	3516	Corning
Cell culture dishes (10-cm)	430167	Corning
Cell culture dish (96-well F-Form)	655180	Greiner BioOne
Cell strainer, 100 µm	352360	BD Biosciences
Combs (10 well, 1 mm) for acrylamide gels	NC3010	Invitrogen
Combs (15 well, 1 mm) for acrylamide gels	NC3015	Invitrogen

## Material and methods

<i>Material</i>	<i>Product no.</i>	<i>Provider</i>
Cover glass (round 18 mm no. 1.5)	631-0153	VWR
Cover glass (square 18 mm no. 1.5)	631-0125	VWR
Cryomold® standard	4557	Sakura
Discofix®-3	4098102	Braun
Dounce glass-glass homogenizer		Wheaton
Dynabeads® MPC®-S (magnetic particle concentrator)	A13346	Invitrogen
Fast Optical 96-well plates	4346907	Applied Biosystems
Flask rectangular 25 cm <sup>2</sup>	431463	Corning
Formvar/Carbon-coated nickel grids	S162N	Plano
Gel cassette (1 mm)	NC2010	Invitrogen
Glass cuvette		WINZER Laborglastechnik
Histosette® I	M499-11	Simport
Intrafix® SafeSet	4063000	Braun
Polypropylene conical tube (15 ml)	188271	Greiner BioOne
Polypropylene conical tube (50 ml)	227261	Greiner BioOne
MicroAmp® Optical Adhesive Film	4311971	Applied Biosystem
Micro tubes (1.5 ml)	72.690.001	Sarstedt
Micro tubes (2 ml)	72.691	Sarstedt
Millipore Immobilon-P Transfer Membranes	T831.1	Carl Roth
Multiple well cluster plate, 96-well	3596	Corning
Multiply®-µStrip 0.2 ml chain	72.985.002	Sarstedt
Nunc Cryotube™	368632	Nunc
Nunc-immuno frame	460348	Nunc
Nunc-immuno module F8 maxisorb loose	469949	Nunc
Omnifix® Solo syringe, 10 ml	4617100V	Braun
PCR Soft-tubes 0.2 ml assorted colours	711088	Biozym

## Material and methods

<i>Material</i>	<i>Product no.</i>	<i>Provider</i>
PCR Soft-tubes 0.2 ml clear	710920	Biozym
PCR Soft-tubes 0.2 ml 8 Tubes/Flat Caps	710970	Biozym
Pipette tips (200 µl yellow)	70.760.002	Sarstedt
Pipette tips (1000 µl blue)	70.762	Sarstedt
Polypropylene column	34964	Qiagen
Rotilabo®-syringe filters, 0.22 µm	P666.1	Carl Roth
Rotilabo®-syringe filters, 0.45 µm	P667.1	Carl Roth
Safe Lock 1.5 ml Eppendorf tubes	211-2130	VWR
Stripettes (5 ml)	4051	Corning
Stripettes (10 ml)	4101	Corning
Stripettes (25 ml)	4251	Corning
SuperFrost®/Plus microscope slides	H867.1	Th.Geyer Group
Syringe (Plastipak™ 1 ml)	7392/2007	BD
TipOne (0.1-10 µl XL), sterile	S1110-3810-c	Starlab
TipOne (1-200 µl beveled), sterile	S1111-1816-c	Starlab
TipOne (101-1000 µl graduated), sterile	S1111-2831-c	Starlab
Venofix® Safety 21 G 3/4"	4056520-01	Braun
Weighing tray 140 x 140 mm	2159.1	Carl Roth
Weighing tray 89 x 89 mm	2150.1	Carl Roth

### 5.1.9 Equipment

**Table 14. List of equipment**

<i>Equipment</i>	<i>Model/Product no.</i>	<i>Provider</i>
Analogue tube roller	SRT6	Stuart
Autoclave	V-150	Systec
Avanti centrifuge	J-301	Beckman
AxioCam	ICc 1	Zeiss
AxioCam	MRm	Zeiss
Axiovert microscope	200M	Carl Zeiss MicroImaging

## Material and methods

<i>Equipment</i>	<i>Model/Product no.</i>	<i>Provider</i>
Centrifuge (refrigerated)	5810 R	Eppendorf
Confocal microscope LSM/Axiobserver Z1	LSM 710	Zeiss
Cryostat	CM1850 UV	Leica
Dumont #5 forceps	14098	WPI
Dumont #55 forceps	14099	WPI
Eppendorf Research® Multipipette (10-100 µl)	3122000043	Eppendorf
Fast Real-Time PCR System	7900HT	ABI
Fusion Solo chemiluminometer	60-FU-SOLO	PeqLab
Hamilton syringe (50 µl Type 705)	549-1155	VWR
HERAcell Incubator	240	Heraeus
HERAcell Incubator	150	Heraeus
High-speed centrifuge (refrigerated)	RC-5C plus	Sorvall
Horizontal electrophoresis system	1582 - 030305	Dan-Kar
Incubator (Agarose)	T 6030	Heraeus
Innova Incubator Shaker	4400	New Brunswick Scientific
Inverted microscope	CK2	Olympus
JuLi™ Smart Fluorescence Cell Imager	DBJ01B	Bulldog Bio
Laminar Flow Cabinet	HS12	Heraeus
MacsMix Tube Rotator	MX100	Miltenyi Biotech
Microcentrifuge	5424	Eppendorf
Microcentrifuge (refrigerated)	5417R	Eppendorf
Microcentrifuge (refrigerated)	5415 R	Eppendorf
Microtome	RM2235	Leica
Mithras multimode microplate reader	LB 940	Berthold Technologies
Multifuge	4KR	Heraeus
Nanodrop Spectrophotometer	1000	PeqLab
Operating Scissor	501754	WPI
Pipetboy acu	155 015	Integra Biosciences AG

## Material and methods

<i>Equipment</i>	<i>Model/Product no.</i>	<i>Provider</i>
Pipetman Pipette set (P2, P10, P100)	F167500	Gilson
Pipetman Pipette set (P20, P200, P1000)	F167300	Gilson
Power supply (for Dan-Kar system)	EPS200	Pharmacia Biotech
Powerpac 200 Power supply	1655052	Bio-Rad
Powerpac 3000 Power supply	1655057	Bio-Rad
Shaker	KS 260	IKA
Suction Pump	MD 4C	Vacuubrand
TEM CCD camera	Megaview III	Olympus
Thermal cycler (MJ mini)	PTC-1148	Bio-Rad
Thermomixer Comfort 1.5 ml Thermoblock	5360 000.011	Eppendorf
Thermomixer Comfort shaker & heating plate	5355 000.011	Eppendorf
Transmission electron microscope	EM 902	Zeiss
Transmission electron microscope	JEM 1200	JEOL
Ultra-centrifuge (Optima)	TLX-120	Beckman
Ultra-centrifuge rotor	TLA-55	Beckman
Ultracut UCT ultramicrotome	EM FCS	Leica
Ultrasound homogenisator SONOPLUS	HD2070	Bandelin
Ultrasound water bath	2200	Branson
UV Transilluminator system	MW312	Intas
Vannas Scissors	500086	WPI
Vortex Mixer	MS525-20	Heidolph (Reax)
Water bath	WNB 22	Memmert
Water bath (digital heating bath)	HBR4	IKA
Water bath (for paraffin sections)	HI1210	Leica
XCell SureLock™ Mini-Cell electrophoresis system	100601-1408	Invitrogen

### 5.1.10 Software

**Table 15. List of software**

<i>Software</i>	<i>Version</i>	<i>Provider</i>
Adobe Illustrator CS4	14.0.0	Adobe
Adobe Photoshop	11.0.0.0	Adobe
Axiovision	4.8	Carl Zeiss MicroImaging
Edit-Seq	5.06	DNASTAR
FinchTV	01.04.2000	Geospiza Inc.
Fusion-CAPT	15.16	Vilber Lourmat
Graphpad Prism 5 for Windows	5.2	GraphPad Software Inc.
ImageJ/Fiji	1.46j	Wayne Rasband
Microsoft Office Suite	2003	Microsoft
MikroWin	2000	Berthold Technologies
Nanodrop 1000	3.7	Thermo Scientific
SDS Software	2.4	Applied Biosystems
ZEN Software	2009	Zeiss

**Table 16. List of online software**

<i>Software (online)</i>	<i>Website</i>
BLOCK-iT™ RNAi Designer	<a href="http://rnaidesigner.invitrogen.com/rnaiexpress/">http://rnaidesigner.invitrogen.com/rnaiexpress/</a>
Ensembl.org	<a href="http://www.ensembl.org/">http://www.ensembl.org/</a>
NCBI Primerblast software	<a href="http://www.ncbi.nlm.nih.gov/tools/primer-blast/">http://www.ncbi.nlm.nih.gov/tools/primer-blast/</a>
NCBI Pubmed	<a href="http://www.ncbi.nlm.nih.gov/pubmed/">http://www.ncbi.nlm.nih.gov/pubmed/</a>
NEB Double Digest Finder	<a href="http://www.neb.com/nebecomm/doubledigestcalculator.asp">http://www.neb.com/nebecomm/doubledigestcalculator.asp</a>

## 5.2 Methods

### 5.2.1 Working with nucleic acids

#### 5.2.1.1 Polymerase chain reaction (PCR)

KOD Hot Start DNA Polymerase Kit was used for DNA amplification according to the manufacturer's instructions. 100 ng template was used for amplification. Annealing temperature was chosen depending on the primer pair used (Primer  $T_m$  - (5-10) °C).

#### 5.2.1.2 Restriction and purification of plasmids, vectors and PCR products

Plasmids and vectors for cloning were digested with the following protocol: 2 µg DNA, 1 µl restriction enzyme, 3 µl NEBuffer, 0,1 µg/µl BSA (depending on which enzyme was used) and filled up with H<sub>2</sub>O to 30 µl. After mixing, this solution was incubated for two hours at 37°C. Inserts were digested with the same protocol but - without considering the concentration - 15 µl of the purified PCR product (purification done with GeneJET™ Gel Extraction Kit according to manufacturer's instructions) were applied to this mixture. After digestion the samples were loaded onto an agarose-gel and separated by applying an appropriate voltage. The expected bands were excised with a scalpel under UV light and purified by employing the GeneJET™ Gel Extraction Kit according to the manufacturer's instructions.

#### 5.2.1.3 Ligation

5 µl ligation buffer, 1 µl T4-Ligase and 1 - 2 µl digested, purified vector were mixed in a tube and filled up with H<sub>2</sub>O to 42 µl. The mixture was equally split into two tubes and 4 µl likewise digested and purified PCR product was added or 4 µl H<sub>2</sub>O as control. The samples were incubated for two hours at room temperature (RT) before transformation.

#### 5.2.1.4 Recombination

For recombination 200 ng entry clone were mixed with 300 ng destination vector and filled up with TE buffer, pH 8.0, to 9 µl. The mixture was equally split into two tubes and 1 µl clonase or 1 µl H<sub>2</sub>O was added. After mixing by pipetting up and down, the reaction was incubated for one hour at 25°C. 0.5 µl Proteinase K solution was added to each sample, followed by an additional incubation for 10 minutes at 37°C to terminate the reaction.

### 5.2.1.5 RNA extraction and cDNA synthesis

Cells were harvested in 500 µl Qiazol and RNA was extracted using the Direct-zol™ RNA MiniPrep Kit according to the manufacturer's instructions. Quality of RNA was assessed by agarose gelelectrophoresis and measurement with a NanoDrop. cDNA was transcribed from 1 µg RNA with the High Capacity cDNA Reverse Transcription Kit according to the manufacturer's instructions.

### 5.2.1.6 TaqMan® assay

For TaqMan® assays, the following mix was prepared: 12.5 µl TaqMan® Universal Mastermix II + 1.25 µl TaqMan® probe + 2 µl 25 ng/µl cDNA + 8 µl H<sub>2</sub>O. Cycling conditions: 95°C for 15 sec and 60°C for 1 min for 40 cycles. Analysis of the results was done by means of SDS software.

### 5.2.1.7 DNA sequencing

300 ng DNA were mixed with 2.25 µl sequencing buffer, 0.25 µl BigDye® Terminator and 2 pmol primer. The reaction was filled up with H<sub>2</sub>O to 10 µl. DNA was denatured for 1 min at 96°C. 40 cycles with the following conditions followed: 10 s, 96°C; 5 s, 55°C; 4 min, 60°C. For the further procedure samples were given to the Cologne Center for Genomics (CCG), University of Cologne, Germany. Sequencings were analyzed by means of FinchTV.

### 5.2.1.8 Dual-luciferase® reporter assay

40.000 HEK293T cells were seeded into one well of a flat bottom 96-well plate in the evening. Next morning, cells were transfected using Lipofectamine® 2000. Therefore, mastermix 1 was prepared as follows: 80 µl Opti-MEM® was mixed with 150 ng *Phb2* psiCHECK™ Dest LR (modified from Promega's psiCHECK™-2) and 150 ng shRNA pcDNA™ 6.2-GW/emGFP-miR/eco31 (modified from Invitrogen's pcDNA™ 6.2-GW/emGFP-miR). For mastermix 2, 80 µl Opti-MEM® was mixed with 0.75 µl Lipofectamine® 2000 and incubated for five minutes. 80 µl of mastermix 1 was mixed with 80 µl mastermix 2 and incubated for 20 minutes. 50 µl of this mix was added to one well of the 96-well plate with HEK293T cells. Every transfection was done in triplicates. The Dual-luciferase® reporter assay was performed according to the manufacturer's instructions by measuring firefly luciferase activity and *Renilla* luciferase activity with a Mithras LB 940 Microplate Reader.

### 5.2.2 Bacteria

#### 5.2.2.1 Chemical transformation of E.coli

5 µl ligation product or 2 µl recombination product were mixed with 50 µl E.coli and incubated on ice for 30 minutes. After heat shock for 45 s at 42°C the bacteria were incubated on ice for additional two minutes. 350 µl SOC medium was added and the mixture placed on a 37°C-shaker for one hour (30°C for lentiviral constructs). Afterwards, 80 µl bacteria suspension was streaked out on LB plates including the respective antibiotics. The plates were dried for 15 minutes at RT and incubated overnight at 37°C (30°C for lentiviral constructs). Next day colonies were picked into LB medium including the respective antibiotics. Bacterial cultures were grown in a 37°C-shaker (30°C for lentiviral constructs) overnight.

#### 5.2.2.2 Isolation of plasmid DNA and diagnostic digest

DNA was isolated out of bacteria with GeneJet™ Plasmid Mini-Prep Kit or NucleoBond® Xtra Midi Kit according to the manufacturer's instructions. Viral DNA constructs were filtered with a 0.22 µm syringe filter after elution. 0.5 µg DNA was used for a diagnostic digestion with the appropriate enzymes.

### 5.2.3 Cell culture

#### 5.2.3.1 Cells

Conditionally immortalized mouse podocytes were generated as previously described [106,107] and cultured in RPMI-1640 media supplemented with 10% FBS, 10 mM HEPES buffer, 1 mM sodium pyruvate and 5 ng/ml Interferone gamma. Differentiation was induced by culturing the cells at 37°C for 14 days on Primaria plastic plates (BD Biosciences) in the absence of Interferone gamma. All experiments were carried out with differentiated podocytes if not stated otherwise. HEK293T (human embryonic kidney cell line 293T) were maintained in DMEM media supplemented with 10% FBS.

#### 5.2.3.2 Freezing and thawing of cells

For freezing, cells were washed with PBS once before the addition of 1 - 2 mL trypsin. After 1 - 5 minutes incubation at 37°C, medium containing 10% FBS was

## Material and methods

added to stop the trypsin reaction. Cells were pelleted with a 5 minutes centrifugation at 200 x g, resuspended in cell freezing solution and transferred to a cryo tube for slow freezing. Storage of cells was done at -80°C or - for long-term storage - in liquid nitrogen. For thawing, a cryo tube with cells was quickly thawed up and the cell suspension transferred to a dish containing the appropriate medium.

### 5.2.3.3 Passaging of cells

Cells were washed once with PBS before the addition of 1 - 2 ml trypsin. After 1 - 5 minutes incubation at 37°C, medium containing 10% FBS was added to stop the trypsin reaction. The desired amount of cell suspension was transferred to a new dish and filled up with the appropriate medium.

### 5.2.3.4 Doxycycline-treatment of mouse podocytes

Conditionally immortalized mouse podocytes expressing a Tetracycline repressor (pLenti6/TR) and a Tetracycline-inducible shRNA construct (shRNA construct in pLenti4/TO/V5-Dest) were differentiated as described under 5.2.3.1. After 10 days of differentiation, 2 µg/ml doxycycline was added to the medium and exchanged every 24 hours. Experiments were performed after 96 hours of doxycycline-treatment.

### 5.2.3.5 Transient expression of plasmids in 293T HEK cells

HEK293T cells were transfected with a standard calcium-phosphate-method. Therefore, up to 20 µg plasmid- or vector-DNA were mixed with 500 µl CaCl<sub>2</sub>. 500 µl 2x HEBS were added dropwise. The mixture was given to the cell media and after eight hours the medium was changed. Transfection efficiency (controlled by using a GFP plasmid) was controlled after 24 hours under the microscope.

### 5.2.3.6 Virus production

For pLenti6/TR or pLenti4/TO/V5-Dest virus production a mix of three helper plasmids was prepared as follows: 2.5 µg pRSV, 3.5 µg pMD2 VSV-G, 6.5 µg pMDL g/p. 50 µl CaCl<sub>2</sub> and 10 µg pLenti6/TR or pLenti4/TO/V5-Dest were mixed. After addition of 450 µl CaCl<sub>2</sub> 500 µl 2x HEBS were added dropwise. The mixture was given to the cell media of a 10 cm HEK293T dish. The reaction was stopped after eight hours by exchanging the medium. Virus production lasted 72 hours. Then media were centrifuged for five minutes at 200 x g and the

## Material and methods

supernatant was filtered through a 0.45 µm syringe filter. The virus supernatant was stored at 4°C until it was used for infection of cells.

### 5.2.3.7 Infection of cells with virus and selection

Mouse podocytes on one 10 cm cell dish were incubated with 5 ml medium, 5 ml virus supernatant and 1x Polybrene. The medium was changed after 48 hours and infection efficiency was controlled under the microscope. Cells were treated for selection with the appropriate antibiotics until all cells on a non-infected control dish were dead.

### 5.2.3.8 Immunofluorescence on cells

For immunofluorescence staining of mouse podocytes, the cells were seeded on coverslips and differentiated at 37°C for 14 days. The cells were fixed in 4% paraformaldehyde for 15 minutes, washed three times with staining PBS before incubation in blocking solution and subsequently incubated with primary antibody overnight at 4°C in a humid chamber. After extensive washing with staining PBS an appropriate fluorophore-labeled secondary antibody was applied for one hour at RT in the dark. After three additional washing steps mounting was done in Prolong Gold antifade with DAPI. Images were acquired with an Axiovert 200 M microscope/EC Plan-Neofluar ×63/1.30 water immersion objective. Images were further processed using ImageJ/Fiji software version 1.46 and Adobe Photoshop CS4 version 11.0.0.0.

## 5.2.4 Protein biochemistry

### 5.2.4.1 Protein extraction

HEK293T cells were detached from a 10 cm dish with PBS and centrifuged for 5 minutes at 200 x g. The cell pellet was resuspended in 1 ml modified RIPA buffer including 44 µg/µl PMSF and 2 mM sodium orthovanadate as protease/phosphatase inhibitors. Mouse podocytes were scraped directly into 100 µl IP buffer including 44 µg/µl PMSF and 2 mM Na<sub>3</sub>VO<sub>4</sub> as protease/phosphatase inhibitors. The cell suspension was placed on ice for 15 minutes and vortexed every 3 - 5 minutes. A centrifugation at 4°C and 15.000 g for 15 minutes followed. The supernatant was transferred to a new vial and stored at -20°C.

## Material and methods

### 5.2.4.2 Protein measurement

To determine protein concentration the Pierce™ BCA protein assay kit was used. 5 µl of each sample or BSA standard (BSA standard prepared according to manufacturer's instructions) were pipetted into one well of a flat-bottom 96-well plate. A mastermix of 150 µl BCA reagent A and 3 µl BCA reagent B was prepared and 150 µl of this mastermix was added to each well of the flat-bottom 96-well plate containing either sample or BSA standard. The 96-well was incubated for 15 minutes at 37°C prior to measuring the absorption at 560 nm using a Mithras LB 940 Microplate Reader. Every sample or BSA standard was measured in duplicates.

### 5.2.4.3 Co-immunoprecipitation

HEK293T cells were transiently transfected using the calcium phosphate-method described under 5.2.3.5. One day after transfection cells were harvested in 10 ml 1x PBS and transferred to a 15 ml conical tube. Cells were pelleted by centrifugation at 200 x g for 1 minute at 4°C. The supernatant was discarded and the cell pellet resuspended in 1 ml modified RIPA buffer. The cell suspension was transferred to a new 1.5 ml vial and incubated on ice for 15 minutes prior to centrifugation at 20,000 x g for 15 min at 4°C. 24 µl of the supernatant was preserved, mixed with 6 µl 5× Laemmli, cooked for five minutes at 95°C and stored at -20°C for subsequent western blot analysis (i.e. lysate). The remaining supernatant was transferred to a new 1.5 ml vial and incubated with either 30 µl anti-FLAG(M2) antibody covalently coupled to agarose beads or with 1 µg of V5 antibody and 30 µl protein-G-sepharose beads, each for one hour at 4°C on an overhead shaker. After three washing steps (centrifugation at 1,000 x g for 1 minute at 4°C) with modified RIPA buffer, 30 µl of 2x Laemmli was applied to the samples before incubation of the samples for 5 minutes at 95°C. Samples were stored at -20°C.

For endogenous co-immunoprecipitation, glomeruli were isolated as described under 5.2.7.10. Isolated glomeruli were homogenized in 2 ml modified RIPA buffer with 20 strokes in a dounce glass-glass homogenizer before sonication on ice (1.5 min, 0.5 sec pulses). The suspension was transferred to a 2 ml tube and incubated on ice for 15 minutes prior to centrifugation at 20,000 x g for 15 min at 4°C. 24 µl of the supernatant was preserved, mixed with 6 µl 5× Laemmli, cooked for five minutes at 95°C and stored at -20°C for subsequent western blot analysis (i.e. lysate). The remaining supernatant was split into two tubes and incubated with either 1 µg

## Material and methods

podocin antibody (Sigma, host species: rabbit) and 30  $\mu$ l of protein-A-sepharose beads or with 1  $\mu$ g of Flag antibody (Sigma, host species: rabbit) and 30  $\mu$ l of protein-A-sepharose beads. After three washing steps (centrifugation at 1,000 x *g* for 1 minute at 4°C) with modified RIPA buffer, 30  $\mu$ l of 2x Laemmli was applied to the samples before incubation of the samples for 5 minutes at 95°C. Samples were stored at -20°C.

### 5.2.4.4 SDS-polyacrylamide-gel electrophoresis

Each gel cassette was prepared by mixing 6 ml of resolving buffer with 0.15% TEMED and 0.1% APS and adding a top layer of isopropanol. After hardening, isopropanol was removed and 1.7 ml stacking buffer mixed with 0.15% TEMED and 0.1% APS was filled in. A 10-well or 15-well comb was inserted and the stacking gel was allowed to solidify. Gels were assembled into the XCell SureLock™ Mini-Cell electrophoresis system as per manufacturer's instructions and the chamber was filled with running buffer so that the interior space between the gels was completely full and the exterior part was filled to a depth of 2 cm. Samples were loaded using a 50  $\mu$ l Hamilton syringe which was cleaned four times with running buffer between each sample. 3  $\mu$ l of Page-ruler Plus protein ladder were loaded on one well. Samples were diluted with Laemmli buffer to a final concentration of 1x Laemmli and boiled for five minutes at 95°C before they were loaded onto the SDS-polyacrylamide-gel. Electrophoresis was done using a Powerpac 3000 with 70 V for 30 minutes, followed by 1 hour 45 minutes at 25 mA per gel.

### 5.2.4.5 Western Blot

For Western Blot analysis the semi-dry method was used. Therefore, two squares of blotting paper as well as the polyacrylamide-gel were placed in transfer buffer. A Millipore Immobilon-P polyvinylidene difluoride (PVDF) membrane was soaked in methanol for one minute and then placed in transfer buffer as well. The blot was arranged as follows: one square of blotting paper, membrane, polyacrylamide-gel, one square of blotting paper. The protein transfer was achieved with a constant current of 12 V for 50 - 70 minutes. After transfer, the membrane was stained with Ponceau S to control for efficiency of the transfer. The membrane was incubated in 5% BSA for one hour at RT, washed three times for five minutes with wash buffer followed by an overnight incubation with the primary antibody diluted in wash buffer

## Material and methods

(antibody dilutions see section 5.1.6). On the next day the membrane was washed three times for five minutes with wash buffer and incubated for 30 minutes with the appropriate HRP-coupled secondary antibody diluted in wash buffer. Additional three washing steps followed before either ECL detection solution or SuperSignal West Femto Chemiluminescent Substrate was applied to the membrane. Images were taken with FUSION-Solo™.

### 5.2.4.6 Colloidal coomassie staining

To test for albuminuria, 1 µl of urine was mixed with 4 µl of distilled water and 5 µl 2x Laemmli. The mixture was incubated for five minutes at 95°C before separation on a SDS-polyacrylamid-gel (see section 5.2.4.4). The gel was incubated in 30 ml fixing solution for 30 minutes at RT on a shaker. Staining was done by applying 50 ml colloidal coomassie staining solution and incubation on a shaker at RT overnight. The gel was destained with distilled water before taking an image with a GS-800™ calibrated densitometer.

## 5.2.5 Antibody production

Antibody production was done in collaboration with Bernhard Schermer, Nephrolab Cologne, Germany.

### 5.2.5.1 Purification of recombinant protein

1 µl mPHB1 or mPHB2 pET30b Z Be (modified from Novagen's pET30b(+)) was transformed into 10 µl chemo-competent BL21 bacteria as described under 5.2.2.1. 100 µl of transformed bacteria were streaked out on an agar plate containing 20 µg/ml kanamycin. Colonies were grown overnight at 37°C. Single colonies were picked into 3 ml 2x YTA containing 20 µg/ml kanamycin and incubated on a shaker at 37°C for five hours. Two 1.5 ml tubes were filled with 1 ml bacteria culture each and IPTG was added to a final concentration of 1 mM into one of the two tubes. With a needle holes were poked into the lid of the tubes before shaking them for two hours at 37°C. Bacteria were pelleted by centrifugation at 16.000 x g for one minute at RT. Supernatant was discarded, the pellet resuspended in 100 µl 2x Laemmli and incubated for five minutes at 95°C. After separation of the samples in a SDS-polyacrylamide-gel (see section 5.2.4.4) the gel was stained with colloidal coomassie

## Material and methods

(see section 5.2.4.6) to identify well inducible clones. The remaining 1 ml bacteria culture of a well inducible clone was added to 100 ml 2x YTA containing 20 µg/ml kanamycin and incubated overnight on a shaker at 37°C. 80 ml of this overnight culture were added to 1 l 2x YTA containing 20 µg/ml kanamycin and incubated on a shaker at 37°C until OD600 = 0.6 - 0.8 was obtained. IPTG was added in a final concentration of 1 mM and the culture incubated on a shaker at 30°C for additional five hours. Bacteria were pelleted with a centrifugation at 4000 x *g* for 15 minutes at 4°C. Supernatant was discarded, the pellet resuspended in 35 ml His-buffer and transferred to a 15 ml conical tube. 1 µg/ml DNase and 200 µg/ml Lysozyme were added and the mixture was incubated on ice for 15 minutes. 1 mM PMSF was added and the bacteria lysed by sonication (7 x 10% cycles for 30 seconds with 70% power; repeated 15 times). Lysis efficiency was checked by transferring 1 ml of lysate to a new 1.5 ml tube and centrifugation at 20,000 x *g* for 10 minutes at 4°C. If the supernatant was yellow and cloudy the protocol was followed further, if it was white and clear another two repeats of sonication were applied and lysis efficiency was checked again. If lysis efficiency was ok, 1 ml of the supernatant (now called "crude lysate") was transferred to a new 1.5 ml tube and 30 µl Ni-NTA agarose was added. After incubation on an overhead shaker for 30 minutes at RT, the agarose was pelleted by centrifugation at 2,000 x *g* for two minutes at 4°C. The supernatant was transferred to a new 1.5 ml tube (= "flow-through") while the agarose was washed three times with His-buffer. 2x Laemmli was added to crude lysate, flow-through and pelleted Ni-NTA agarose in an appropriate amount to generate 1x Laemmli solutions. After incubation at 95°C for five minutes all samples and three different BSA standards (1 µg, 5 µg, 10 µg) were separated on a SDS-polyacrylamide-gel (see section 5.2.4.4) and stained with colloidal coomassie (see section 5.2.4.6). This gel was used to estimate the amount of protein in 1 ml of crude lysate. In parallel, the rest of the lysed bacteria were pelleted by centrifugation at 50,000 x *g* for 45 minutes at 4°C. The supernatant (= "crude lysate") was filtered through a 0.45 µm filter into a new 50 ml conical tube. Depending on the previous estimation of protein concentration, 1 ml Ni-NTA agarose was added for each 10 mg protein in the crude lysate. This mixture was incubated on an overhead shaker overnight at 4°C. The next morning, a polypropylene column was moistened with 10 ml His-buffer. The mixture of crude lysate and Ni-NTA

## Material and methods

agarose was applied to this column and the column washed with 50 ml His-buffer. Elution of His-tagged proteins from the Ni-NTA agarose was done by adding 100  $\mu$ l elution buffer and collecting the eluate in a new 1.5 ml tube. The elution step was done five times with fresh elution buffer. To estimate protein concentration 5  $\mu$ l of each eluate fraction was mixed with 5  $\mu$ l 2x Laemmli, incubated for five minutes at 95°C and separated together with three BSA standards (1  $\mu$ g, 5  $\mu$ g, 10  $\mu$ g) on a SDS-polyacrylamide-gel (see section 5.2.4.4). The gel was stained with colloidal coomassie (see section 5.2.4.6).

### 5.2.5.2 Immunization of mice and hybridoma generation

80  $\mu$ g of His-tagged PHB1 or His-tagged PHB2 were mixed with either 200  $\mu$ l complete Freund's adjuvant or 200  $\mu$ l incomplete Freund's adjuvant and 400  $\mu$ l sterile water. The mixture was incubated in an ultrasound bath for three minutes and then vortexed for 20 minutes before uptake in a 1 ml syringe. A Balb/c mouse was i.m. injected every second day (four times in total) with 100  $\mu$ l of this mixture containing either His-tagged PHB1 or His-tagged PHB2 (first injection with complete Freund's adjuvant, next three injections with incomplete Freund's adjuvant). Fusion with myeloma cells resulted in the generation of more than 40 prohibitin-1- and prohibitin-2-specific hybridoma cell lines producing monoclonal antibodies that were subcloned.

### 5.2.5.3 ELISA

Positive clones were identified by ELISA. Briefly, 200 ng His-tagged prohibitin-1, prohibitin-2 or a control protein were coupled to the wells of a Nunc immunosorb 8-strip by incubation overnight at 4°C. After three washing steps with PBS-Tween the strips were blocked with 1% BSA in 1x PBS for one hour at RT. Three washing steps with PBS-Tween followed. 100  $\mu$ l hybridoma supernatant was applied to the strips and incubated for one hour at RT. After three washing steps with PBS-Tween, the strips were incubated with a HRP-conjugated mouse antibody (dilution: 1:5000 in 1x PBS) for one hour at RT in the dark. Three washing steps with PBS-Tween followed. 100  $\mu$ l developer solution was applied to the strips and incubated for 15 minutes at RT in the dark (blue color). The reaction was terminated by adding 50  $\mu$ l 2 N hydrochloric acid (yellow color). Absorption at 450 nm was measured with a Mithras LB 940 Microplate Reader.

### 5.2.6 Worm experiments

All worm experiments were done in collaboration with Sibylle Brinkkötter and Puneet Bharill, Nephrolab Cologne, Germany.

#### 5.2.6.1 Worm strains

TU3568 [*sid-1(pk3321) him-5(e1490) V; lin-15B(n744) X; uls71 [pCFJ90(myo-2p::mCherry) + mec-18p::sid-1]*] were used, a kind gift of Prof. Martin Chalfie, Columbia University, New York [108]. Due to an integrated array containing *mec-18p::sid-1* in a *sid-1* mutant background it provides efficient RNA interference only in touch receptor neurons. For microinjection of the *mec-17p::phb-2::gfp* transgene WTN2 animals were used [109]. All strains were cultured at 20°C.

#### 5.2.6.2 RNA interference

RNA interference (RNAi) was performed by feeding as it is described previously [110,111] using the RNAi sensitized background of TU3568 worms. RNAi clones corresponding to the target genes *phb-1*, *phb-2*, *mec-2* and *mev-1* were used for knockdown experiments. Empty RNAi vector L4440 was used as control RNAi, *mec-2* as positive control and *mev-1*, encoding another mitochondrial protein as control for unspecific RNAi effects based on an impairment of the mitochondrial respiratory chain. All clones except *phb-1* were picked from an RNAi feeding library constructed by J. Ahringer's laboratory at the The Wellcome CRC Institute, University of Cambridge, Cambridge, England [111]. To generate a *phb-1* RNAi clone, a 0.8-kb fragment was PCR amplified using N2 genomic DNA as template and the primer pair *phb-1* fp and rp as published previously [112]. A 0.656-kb *NcoI/SacI* fragment was cloned into the likewise digested L4440 vector. The construct was electroporated into HT115 bacteria. Bacteria containing the different knockdown plasmids were seeded onto nematode growth medium - isopropyl-thio-β-d-galactoside (NGM-IPTG) plates. Plates were kept 16 hours at RT for generation of dsRNA.

Worm eggs were harvested by bleaching gravid adult animals in 0.5 N NaOH and 2 - 4% NaOCl. The eggs were washed in M9 buffer, placed on the seeded plates and grown at 20°C. Young adult hermaphrodites were tested for touch sensation as described under 5.2.6.3.

### 5.2.6.3 Touch assay

Animals were tested for response to gentle touch as described previously [113]. Briefly, each animal was touched 10 times by a thin hair at the anterior part of the body. Stopping or backward movements were scored and shown as touch response out of ten touches. The data was generated in three independent experiments using  $\geq 15$  worms each time for each data point. Statistical evaluation was done as described under 5.2.7.11.

### 5.2.6.4 Microinjection

For germline injection, the *phb-2::gfp* plasmid was prepared via multisite gateway cloning. Briefly, the promoter of *mec-17* (*mec-17p*) was cloned from a *C. elegans* library and recombined into pDONR P4-P1R according to the manufacturer's protocol. *phb-2* was cloned without stop codon from the same library and recombined into pDONR 221 according to the manufacturer's protocol. Both, *mec-17p* and *phb-2* were recombined from the pEntr plasmids into pDest MB14 to generate a plasmid expressing PHB-2::GFP under control of the *mec-17* promoter.

Lines containing extrachromosomal arrays were generated by injecting the *phb-2::gfp* plasmid at a concentration of 50 ng/ul mixed with *pmyo-2::mCherry* as a co-injection marker at the concentration of 5 ng/ul into WTN2. Single positive transgenic F1 worms were moved onto NGM plates and allowed to proliferate to form different lines.

Microinjection was performed in the lab of A. Antebi, MPI for Biology of Ageing, Cologne, Germany.

### 5.2.6.5 Immunofluorescence on worms

Antibody stainings on *mec-17p::phb-2::gfp* transgenic worms were performed using a modified Finney-Ruvkun protocol [114,115]. 1.25 ml fixing solution was added to a tube with worms and kept on dry ice for 2 - 3 hours. The worms were thawed again on ice, centrifuged at 400 x g for two minutes and the supernatant was discarded. The worms were washed with Tris-Triton-Buffer (TTB) once. After resuspension in 1%  $\beta$ -mercaptoethanol/TTB the worms were incubated at 37°C for two hours, centrifuged at 400 x g for two minutes and the supernatant was discarded. Worms were first resuspended in 1x borate buffer, the buffer was discarded and replaced by 10 mM DTT in 1x borate buffer. After gentle shaking for 15 minutes the buffer was

## Material and methods

discarded and the worms washed with 1x borate buffer once. Worms were shaken for 15 minutes in 0.3% H<sub>2</sub>O<sub>2</sub>/1x borate buffer and washed again with 1x borate buffer. Next, the worms were incubated in antibody buffer B for 15 minutes. The specimen finally was incubated with a rabbit antibody detecting the N-terminus of MEC-2 (kind gift of Prof. Martin Chalfie; dilution 1:200 in antibody buffer A) for two hours at RT. Several washing steps with antibody buffer B were followed by incubation with a Cy3-labeled secondary antibody diluted in antibody buffer A for two hours at RT (for dilution see section 5.1.6). After extensive washing with antibody buffer B the worms were mounted on slides with ProLong Gold antifade reagent with DAPI. Images were captured with an LSM 710/Axiobserver Z1 confocal microscope x40/1.1 water immersion objective operated by ZEN 2009 software. Images were further processed using ImageJ/Fiji software version 1.46 and Adobe Photoshop CS4 version 11.0.0.0.

### 5.2.7 Mouse experiments

#### 5.2.7.1 Mouse strains and animal care

Mice in which exons 3 and 4 of the *Phb2* gene are flanked by two loxP sequences [53] were mated to either NPHS2.Cre mice [116] or Tamoxifen-inducible podocin-iCreER(T2) [117] to generate podocyte-specific *Phb2* knockout mice *Phb2 flox/flox*;NPHS2.Cre (*Phb2<sup>pkO</sup>*) or tamoxifen-inducible podocyte-specific *Phb2* knockout mice *Phb2 flox/flox*;podocin-iCreER(T2) (podocin-iCreER(T2) *Phb2<sup>pkO</sup>*). The animals were backcrossed onto the C57/Bl6 background for at least 10 generations. Mice from both genders carrying the conventional NPHS2.cre transgene were included while only male mice of the *Phb2 flox/flox*;podocin-iCre(ER(T2)) were used. Mice were housed according to the standardized specific pathogen-free conditions in the University of Cologne animal facility. The Animal Care Committee of the University of Cologne reviewed and approved the experimental protocol. The mice were sacrificed once they lost 15 - 20% of their maximal body weight following federal animal care regulations. Renal tissue was embedded in OCT compound and frozen at -80°C or fixed in 4% neutral buffered formalin for 24 hours before paraffin-embedding.

## Material and methods

### 5.2.7.2 Serum analysis

Blood samples were collected in the fifth week of life with a 1 ml syringe and a 27 G cannula (both washed with heparin) from anesthetized mice. Blood samples were centrifuged at 3000 x g for 10 minutes at 4°C, supernatant (= serum) transferred to a new tube and given to the Institute for Clinical Chemistry of the University Hospital of Cologne, Germany, for quantification of serum urea and creatinine.

### 5.2.7.3 Extraction of DNA from mouse tissue

To obtain DNA from mouse tissue (ear tag or tail cut) for genotyping purposes, the tissue was mixed with 100 µl base solution. After incubation for 30 minutes at 95°C, 100 µl neutralization solution was added and the mixture stored at 4°C.

### 5.2.7.4 Polymerase-chain reaction (PCR) for genotyping purposes

For genotyping-PCRs Promega's GoTaq® Flexi DNA Polymerase was used according to the manufacturer's instructions. For sequences of primers see section 5.1.4, Table 5. For *Phb2* genotyping PCR the following mix was prepared: 5.5 µl H<sub>2</sub>O + 12.5 µl 1x RedTaq Mix + 1 µl 10 µM *Phb2* fp + 0.5 µl 10 µM *Phb2* rp1 + 0.5 µl 10 µM *Phb2* rp2 + 5 µl template. Cycling conditions for *Phb2* genotyping PCR: 1.) 2 minutes at 95°C; 2.) 30 sec at 95°C; 3.) 30 sec at 62°C; 4.) 45 sec at 72°C; 5.) repeat step 2.) - 4.) 39 times; 6.) 1 min 30 sec at 72°C. Size of expected fragments: wildtype = 378 bp, floxed allele = 506 bp.

For *Insr* genotyping PCR the following mix was prepared: 13.6 µl H<sub>2</sub>O + 5 µl 5x Green Flexi buffer + 1.5 µl 25 mM MgCl<sub>2</sub> + 0.2 µl 10 mM dNTPs + 1 µl 10 µM *Insr* fp + 1 µl 10 µM *Insr* rp + 0.2 µl 5 U/µl GoTaq® + 2.5 µl template. Cycling conditions for *Insr* genotyping PCR: 1.) 2 minutes at 95°C; 2.) 30 sec at 95°C; 3.) 45 sec at 58°C; 4.) 45 sec at 72°C; 5.) repeat step 2.) - 4.) 29 times; 6.) 1 min 30 sec at 72°C. Size of expected fragments: wildtype = 200 bp, floxed allele = 250 bp.

For *Igf1r* genotyping PCR the following mix was prepared: 13.6 µl H<sub>2</sub>O + 5 µl 5x Green Flexi buffer + 1.5 µl 25 mM MgCl<sub>2</sub> + 0.2 µl 10 mM dNTPs + 1 µl 10 µM *Igf1r* fp + 1 µl 10 µM *Igf1r* rp + 0.2 µl 5 U/µl GoTaq® + 2.5 µl template. Cycling conditions for *Igf1r* genotyping PCR: 1.) 2 minutes at 95°C; 2.) 30 sec at 95°C; 3.) 30 sec at 54°C; 4.) 40 sec at 72°C; 5.) repeat step 2.) - 4.) 24 times;

## Material and methods

6.) 1 min 30 sec at 72°C. Size of expected fragments: wildtype = 300 bp, floxed allele = 350 bp.

For *Podocin-Cre* genotyping PCR the following mix was prepared: 10.6 µl H<sub>2</sub>O + 5 µl 5x Green Flexi buffer + 1.5 µl 25 mM MgCl<sub>2</sub> + 0.2 µl 10 mM dNTPs + 1.25 µl 10 µM β-globin fp + 1.25 µl 10 µM β-globin rp + 1.25 µl 10 µM Cre fp + 1.25 µl 10 µM Cre rp + 0.2 µl 5 U/µl GoTaq<sup>®</sup> + 2.5 µl template. Cycling conditions for *Podocin:Cre* genotyping PCR: 1.) 2 minutes at 95°C; 2.) 45 sec at 95°C; 3.) 60 sec at 59°C; 4.) 45 sec at 72°C; 5.) repeat step 2.) - 4.) 29 times; 6.) 1 min 30 sec at 72°C. Size of expected fragments: internal control (β-globin band) = 494 bp, *Cre* allele = 269 bp.

For *Podocin-iCreER(T2)* genotyping PCR the following mix was prepared: 11.6 µl H<sub>2</sub>O + 5 µl 5x Green Flexi buffer + 1.5 µl 25 mM MgCl<sub>2</sub> + 0.2 µl 10 mM dNTPs + 1 µl 10 µM Dicer fp + 1 µl 10 µM Dicer rp + 1 µl 10 µM iCreER(T2) fp + 1 µl 10 µM iCreER(T2) rp + 0.2 µl 5 U/µl GoTaq<sup>®</sup> + 2.5 µl template. Cycling conditions for *Podocin-iCreER(T2)* genotyping PCR: 1.) 2 minutes at 95°C; 2.) 45 sec at 95°C; 3.) 30 sec at 57°C; 4.) 45 sec at 72°C; 5.) repeat step 2.) - 4.) 34 times; 6.) 1 min 30 sec at 72°C. Size of expected fragments: internal control (β-globin band) = 351 bp, *iCreER(T2)* allele = 500 bp.

### 5.2.7.5 Albumin ELISA

Albumin concentration in mouse urine was measured by using a mouse albumin ELISA kit according to the manufacturer's instructions.

### 5.2.7.6 Creatinine Assay

Creatinine concentration in mouse urine was measured by using a creatinine (urinary) assay kit according to the manufacturer's instructions.

### 5.2.7.7 PAS staining

Paraffin sections were deparaffinized in Histo-Clear (Xylene-like) and rehydrated in graded ethanol. After five minutes incubation in distilled water the sections were incubated in 0.9% periodic acid for 10 minutes. After washing for one minute in distilled water the sections were incubated for 10 minutes in Schiff's reagent. An additional washing step for two minutes in tap water followed before the sections were incubated in Mayer's hematoxylin solution for 10 minutes. After eight minutes in

tap water the sections were dehydrated in graded ethanol and Histo-Clear. Mounting was done with Histomount.

### 5.2.7.8 Specific immunohistochemistry

Indirect immunoperoxidase staining was performed on formalin-fixed tissue. 4  $\mu$ m thin tissue sections were deparaffinized in Histo-Clear and rehydrated in graded ethanol. Endogenous peroxidase activity was blocked with 3% hydrogen peroxidase in methanol for 15 minutes. After five minutes incubation in tap water the sections were either treated with Proteinase K solution 15 minutes (for podocin-immunohistochemistry (IHC)), cooked for 10 minutes in 10 mM citrate buffer, pH 6 (for cleaved caspase-3- IHC) or cooked for 10 minutes in Tris-EDTA-Tween (for phosphorylated S6 ribosomal protein- and WT-1-IHC) followed by three washing steps for three minutes in TBS. Blocking was done for 20 minutes in 1% BSA in TBS followed by three washing steps for three minutes in TBS. Solution A was applied for 15 minutes and then the sections were incubated with solution B for 15 minutes. After three washing steps for three minutes in TBS the sections were incubated overnight at 4°C with primary antibody diluted in TBS (for dilutions see section 5.1.6). The sections were washed repeatedly in TBS before incubation for one hour at RT with biotinylated mouse anti-rabbit secondary antibody diluted in 1% BSA in TBS. The ABC kit was used according to the manufacturer's instructions for signal amplification and 3,3'-diaminobenzamidine (DAB) was used as a chromogen. Sections were counterstained with hematoxylin for 10 seconds and washed for three minutes under running tap water. After dehydration in graded ethanol and Histo-Clear the sections were covered with Histomount. In the procedure of specific immunohistochemistry for phosphorylated S6 ribosomal protein washing was always done with TBS-Tween and blocking with 1% BSA in TBS was skipped.

Images were acquired with an Axiovert 200 M microscope/EC Plan-Neofluar x40/1.3 oil immersion or x63/1.20 water immersion objective equipped with a charge-coupled-device camera. Images were further processed using ImageJ/Fiji software version 1.46j.

Specific immunohistochemistry for cleaved caspase-3 was done in collaboration with Andreas Linkermann, Christian-Albrechts University, Kiel, Germany.

### 5.2.7.9 Electron microscopy and immunogold labeling

Mice were perfused with electron microscopy fixation buffer and the kidneys post-fixed in the same buffer for two weeks at 4°C. Sample osmication with 1% osmium tetroxid in 0.1 M cacodylate and dehydration in a graduated ethanol series as well as infiltration and flat embedding using the epoxy embedding medium kit was done according to the manufacturer's instructions. Thin (30 nm) cross sections were taken on an Ultracut UCT ultramicrotome. The sections were stained with 1.5% aqueous uranyl acetate and examined with a Zeiss EM 902 electron microscope. For immunogold labeling, fixed samples of mouse or human kidneys were embedded in acrylic Lowicryl® K4M resin according to the manufacturer's instructions and polymerized in gelatin capsules at -35°C under UV light for 24 hours followed by incubation at RT under UV light for 48 hours. Ultrathin sections (80 nm) were collected on Carbon coated nickel grids and quenched in 1% BSA/0.1 M Tris for 10 minutes. For mouse sections the antibody was diluted 1:5 in EM antibody buffer, for human sections 1:10 in electron microscopy antibody buffer. Sections were incubated with the antibody dilution for two hours at RT, washed three times for five minutes in 0.1 M Tris before incubation with 15 nm of gold-labeled goat anti-rabbit IgG (diluted 1:10 in electron microscopy antibody buffer) for one hour at RT. The sections were washed once in 0.1 M Tris and thrice in ddH<sub>2</sub>O. After staining with 2% aqueous uranyl acetate for 14 minutes and Reynold's lead citrate for 10 minutes the sections were examined with a JEOL JEM 1200 transmission electron microscope. Images were further processed with Adobe Photoshop CS4 version 11.0.0.0.

Electron microscopy was done in collaboration with Prof. Bloch, German Sport University Cologne, Germany. Immunogold labeling was done in collaboration with Prof. Kerjaschki, Medical University of Vienna, Austria.

### 5.2.7.10 Glomeruli isolation

For glomeruli isolation, the mouse was sacrificed and both kidneys together with the aorta were taken out and placed in a 10 cm dish with 1x HBSS. The aorta was cut open from the dorsal side to get access to the renal arteries. 100 µl tosylactivated Dynabeads M-450 were mixed with 10 ml 1x HBSS and 1 ml of this mixture was injected into each kidney with a 1 ml syringe and 27 G cannula via the renal artery. Kidneys were decapsulated and transferred to a 2 cm dish. They were cut into pieces

## Material and methods

with a scalpel and digested with 2 ml of 1 mg/ml Collagenase in 1x HBSS for 20 minutes on a shaker at 37°C. At first, this mixture was actively pressed through a 100 µm cell strainer into a 50 ml conical tube and the cell strainer was washed with 10 ml 1x HBSS. Then the solution was passively filtered through a new 100 µm cell strainer into a fresh 50 ml conical tube and the cell strainer was again washed with 10 ml 1x HBSS. After centrifugation at 300 x g for five minutes at 4°C the supernatant was discarded and the pellet resuspended in 2 ml 1x HBSS. The glomeruli were isolated by consecutive washing steps with a magnetic bead separator. Purity and quality of glomeruli was checked under the microscope.

### 5.2.7.11 Tamoxifen diet

Eight weeks old animals were exposed to a tamoxifen-enriched diet (400mg/kg, Harlan Laboratories) *ad libitum* for six weeks. Based on a daily intake of 5 g of food per mouse, this corresponded to an oral dose of 2 mg/d tamoxifen per mouse. To exclude any potential side effects in females only male mice were used.

### 5.2.7.12 Rapamycin injection

For rapamycin injections the protocol published by Zeng et al.[118] was used with some modifications. Animals received daily i.p. injections of either rapamycin solution or vehicle solution starting two weeks after birth until they were sacrificed because of weight loss or sickness. *Phb2<sup>pk0</sup>* were injected with either 3 µg rapamycin solution per g body weight (i.e. 10 µl 0.3 mg/ml rapamycin solution per g body weight) or the same amount of vehicle solution (i.e. 10 µl vehicle solution per g body weight). *Phb2<sup>fl/fl</sup>* mice received 3 µg rapamycin solution per g body weight (i.e. 10 µl 0.3 mg/ml rapamycin solution per g body weight). The rapamycin solution was always freshly prepared directly before injection from the rapamycin stock solution, which was stored at -20°C.

## 5.2.8 Human tissue

### 5.2.8.1 Immunofluorescence on human tissue

Human tissue samples were obtained from tumor nephrectomy samples after obtaining written consent as approved by the local ethic committee. The tissue was fixed in 4% paraformaldehyde for 15 minutes, washed three times with staining PBS

## Material and methods

before incubation in blocking solution and subsequently incubated with primary antibody overnight at 4°C in a humid chamber. After extensive washing with staining PBS an appropriate fluorophore-labeled secondary antibody was applied for one hour at RT in the dark. In the meantime, 1 µg podocin-antibody was labeled with the Zenon<sup>®</sup> Tricolor rabbit IgG labeling kit according to the manufacturer's instructions. After three additional washing steps, the tissue was incubated with the Zenon-labeled podocin antibody for 60 minutes in the dark. Three additional washing steps and a post-fixation with 4% paraformaldehyde for 15 minutes followed. After three more washing steps, mounting was done in Prolong Gold antifade with DAPI. Images were acquired with an LSM 710/Axiobserver Z1 confocal microscope x40/1.1 water immersion objective operated by ZEN 2009 software. Images were further processed using ImageJ/Fiji software version 1.46 and Adobe Photoshop CS4 version 11.0.0.0.

### **5.2.9 Statistical analysis**

All results are expressed as means ± SEM. Statistical significance was evaluated using GraphPad Prism version 4.00c for Macintosh and OASIS (Online Application for the Survival Analysis of Lifespan Assays) [119]. Unpaired Student's t-test was applied in most experiments except for survival analysis experiments where a Log Rank test [120] was performed. A *P*-value <0.05 was considered significant.

## 6 Results

### 6.1 Loss of PHB2 leads to severe glomerular disease

#### 6.1.1 Podocyte-specific *Phb2*-knockout mice (*Phb2*<sup>pk0</sup>) develop albuminuria and die prematurely

To generate a mouse line for investigation of the function of PHB2 in podocytes conditional *Phb2 flox/flox* mice [53] were mated to podocyte-specific Cre mice (*NPHS2.cre* mice) [116]. The murine *Phb2* gene is located on chromosome 6 and is composed of nine exons. In the *Phb2 flox/flox* mouse loxP sites are inserted upstream of exon 3 and downstream of exon 4 of the *Phb2* gene. Expression of a Cre-recombinase leads to deletion of the loxP-flanked exons and causes a frameshift mutation resulting in a stop of translation at amino acid 73. The truncated PHB2 protein product is inactive [53].

All mice were born following Mendelian rules (**Figure 4A**) and no overt differences became evident at birth. Interestingly, podocyte-specific *Phb2*-deficient mice (*Phb2*<sup>pk0</sup>) did not survive longer than 31 - 37 days while all Cre-negative mice (*Phb2*<sup>fl/fl</sup>) developed normally and did not show any signs of glomerular disease (**Figure 4B**). Analysis of the urinary albumin-to-creatinine ratio, which was used to determine the amount of albuminuria, revealed progressive albuminuria in *Phb2*<sup>pk0</sup> mice but not *Phb2*<sup>fl/fl</sup> mice over time. 14 days after birth albuminuria was detectable in neither *Phb2*<sup>pk0</sup> mice nor control mice whereas after 21 days *Phb2*<sup>pk0</sup> mice showed already pronounced albuminuria. At day 28 a maximum albumin-to-creatinine ratio of 430 mg/mg was reached in *Phb2*<sup>pk0</sup> mice (**Figure 4C**). In line with this finding, *Phb2*<sup>pk0</sup> mice gained less weight compared to control mice already evident at day 22 resulting in a wasting syndrome after day 29 (**Figure 4D**). Serum creatinine and serum urea levels were measured to assess renal function. Serum creatinine (**Figure 4E**) as well as serum urea levels (**Figure 4F**) were significantly increased in *Phb2*<sup>pk0</sup> mice but not control mice in their fifth week of life. This is further supporting the observation that podocyte-specific loss of PHB2 results in podocyte dysfunction, renal failure and eventually causes premature death.

## Results

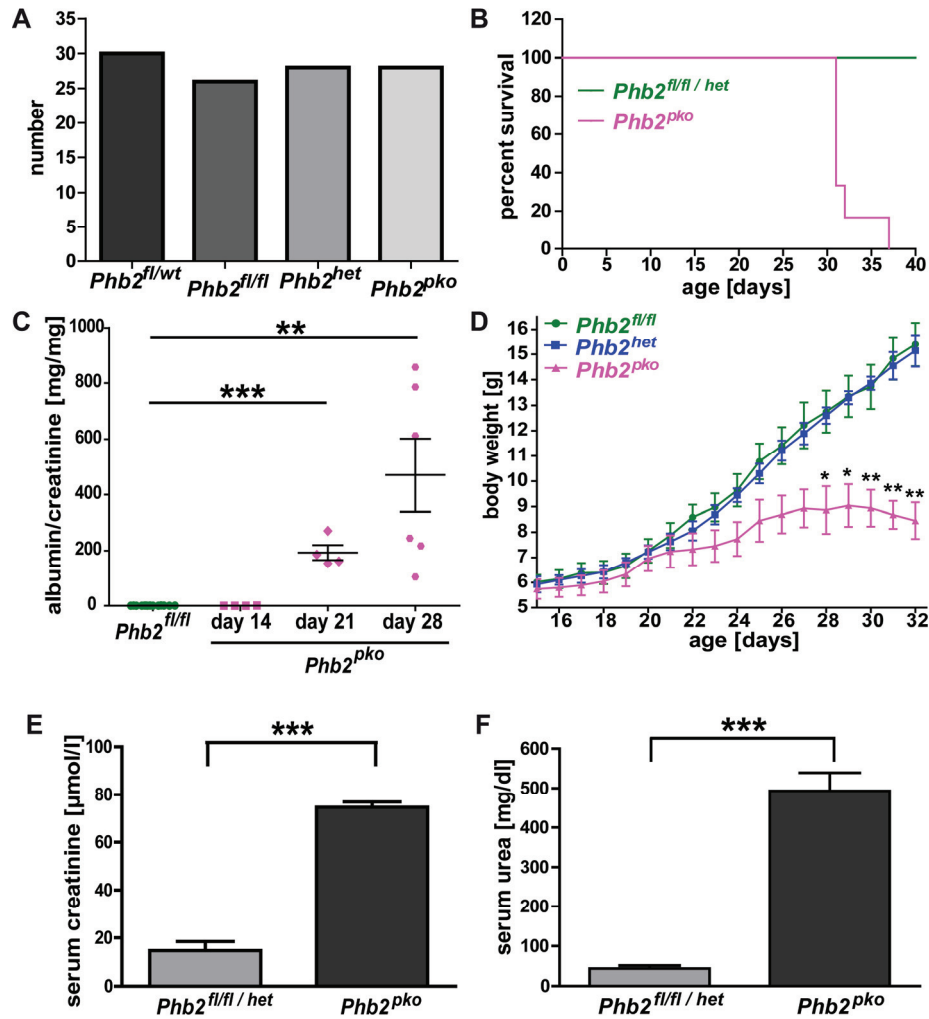


**Figure 4. Podocyte-specific *Phb2*-knockout mice (*Phb2*<sup>pko</sup>) develop albuminuria and die prematurely**

(A) *Phb2* flox/flox;*NPHS2.cre* mice are born following Mendelian rules (*Phb2*<sup>fl/wt</sup>, *Phb2* flox/wt;*NPHS2.cre* wt/wt; *Phb2*<sup>fl/fl</sup>, *Phb2* flox/flox;*NPHS2.cre* wt/wt; *Phb2*<sup>het</sup>, *Phb2* flox/wt;*NPHS2.cre* tg/wt; *Phb2*<sup>pko</sup>, *Phb2* flox/flox;*NPHS2.cre* tg/wt). (B) Kaplan-Meier survival curve showed decreased survival of *Phb2*<sup>pko</sup> mice compared to control mice (n = 5 for *Phb2*<sup>fl/fl</sup>/*het*, n = 6 for *Phb2*<sup>pko</sup>) (C) Measurement of urinary albumin-to-creatinine ratio revealed progressive albuminuria in *Phb2*<sup>pko</sup> mice (albumin-to-creatinine ratio day 14: *Phb2*<sup>fl/fl</sup> 0.09 ± 0.03 mg/mg, n = 4, vs. *Phb2*<sup>pko</sup> 0.37 ± 0.21 mg/mg, n = 4; P > 0.05; albumin-to-creatinine ratio day 21: *Phb2*<sup>fl/fl</sup> 0.65 ± 0.16 mg/mg, n = 4, vs. *Phb2*<sup>pko</sup> 193.10 ± 26.81 mg/mg, n = 4; \*\*\*P < 0.001; albumin-to-creatinine ratio day 28: *Phb2*<sup>fl/fl</sup> 0.57 ± 0.07 mg/mg, n = 4, vs. *Phb2*<sup>pko</sup> 470.40 ± 131.30 mg/mg, n = 4; \*\*P < 0.01). (D) Analysis of body weight from postnatal day 14 until day 32 (*Phb2*<sup>fl/fl</sup> or *Phb2*<sup>het</sup> vs. *Phb2*<sup>pko</sup> at days 28/29, \*P < 0.05 and at days 30-32 with \*\*P < 0.01, n = 3 for *Phb2*<sup>fl/fl</sup> and n = 4 for *Phb2*<sup>het</sup> and *Phb2*<sup>pko</sup>). (E) Measurement of serum creatinine levels of mice in their fifth week of life showed increased serum creatinine in *Phb2*<sup>pko</sup> mice (*Phb2*<sup>fl/fl</sup>/*het* 14.74 ± 3.75 μmol/l vs. *Phb2*<sup>pko</sup> 74.73 ± 2.20 μmol/l, n = 3 for both groups; \*\*\*P < 0.001). (F) Measurement of serum urea levels of mice in their fifth week of life showed higher serum urea levels in *Phb2*<sup>pko</sup> mice than control mice (*Phb2*<sup>fl/fl</sup>/*het* 44.00 ± 7.02 mg/dl vs. *Phb2*<sup>pko</sup> 493.70 ± 45.34 mg/dl, n = 3 for both groups; \*\*\*P < 0.001).

## Results

### 6.1.2 *Phb2*<sup>pk0</sup> mice develop glomerulosclerosis

To gain a better insight into the development of glomerular disease in *Phb2*<sup>pk0</sup> mice the animals were analyzed at different time points. Glomerulogenesis in mice is completed 14 days after birth. Therefore, the phenotypic analysis of *Phb2*<sup>pk0</sup> mice was started at this time point and ended with 28 days after birth, which is close to the death of the animals.

To assess glomerular morphology PAS staining of kidney sections from *Phb2*<sup>pk0</sup> mice at day 14, 21 and 28 were analyzed. Despite albuminuria being present already at day 21 no changes in glomerular morphology became evident before day 28. Here, the mice presented with tubular protein casts as well as glomerular scarring i.e. glomerulosclerosis (**Figure 5A**). Podocin was used as a marker for the integrity of the slit diaphragm. Podocin stainings revealed a regular garland-like pattern of podocin at day 14 in *Phb2*<sup>pk0</sup> mice. One week later, at day 21, podocin stainings appeared weaker and more granular indicative of an injured slit diaphragm. 28 days after birth podocin expression was nearly completely lost (**Figure 5B**). Electron micrographs revealed already at day 14 first subtle changes in foot process organization. In some areas foot process structures were completely normal while other areas showed beginning broadening of the processes. This became even more evident at day 21 when the regular foot process structure is lost nearly everywhere within a glomerulus and adjacent processes flattened. At day 28 *Phb2*<sup>pk0</sup> mice completely lost the glomerular structure (**Figure 5C**). Since PHB2 is known as a mitochondrial protein and previous reports already showed defects in mitochondrial morphology upon loss of PHB2 [53,69] the cristae structure of podocytic mitochondria in *Phb2*<sup>pk0</sup> mice was analyzed in electron micrographs. 14 days after birth no changes in mitochondrial morphology were seen. However, at day 21 the lamellar cristae structure of mitochondria in *Phb2*<sup>pk0</sup> mice was lost and the podocytes contained swollen mitochondria with disorganized cristae structures (**Figure 5D**). Because of the severe phenotype and complete loss of the glomerular structure an analysis of mitochondrial morphology in 28 days old *Phb2*<sup>pk0</sup> mice was not possible.

Taken together, *Phb2*<sup>pk0</sup> mice did not only show defects in mitochondrial morphology but also lost foot process organization and developed glomerulosclerosis.

## Results

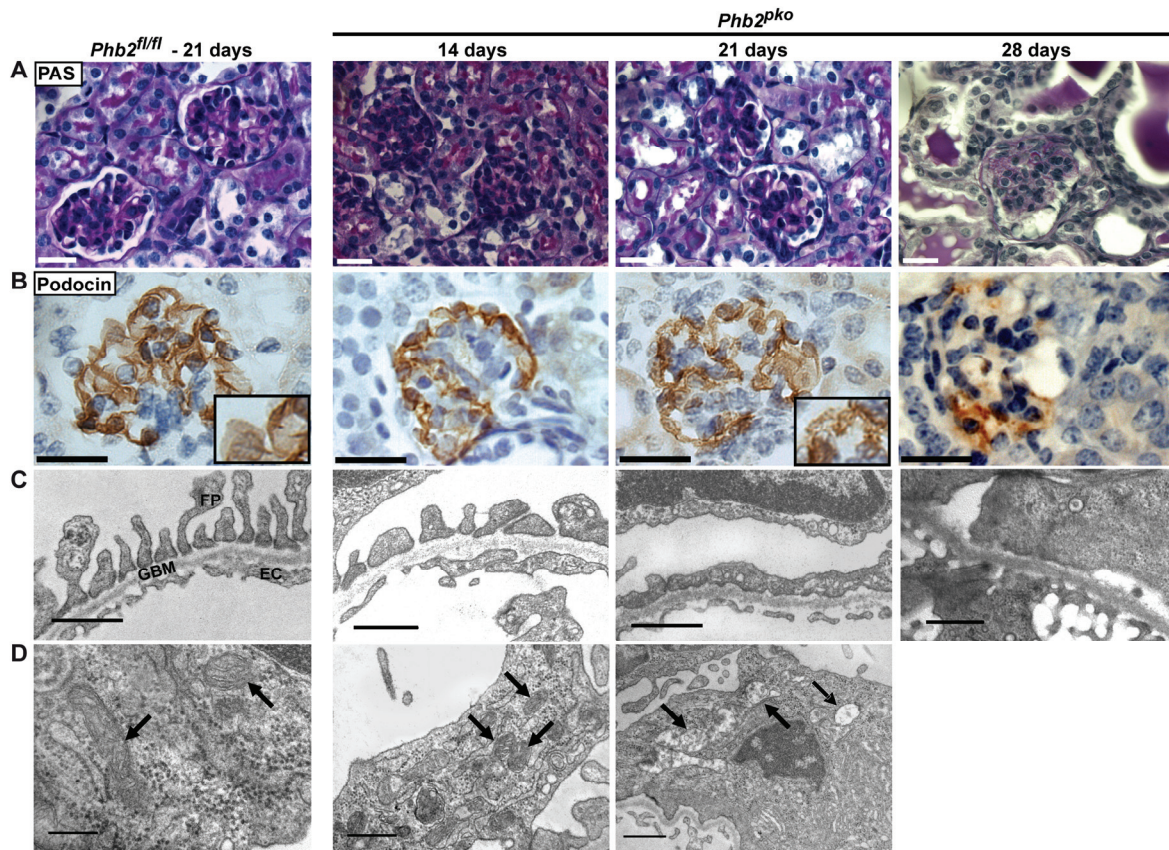


**Figure 5. *Phb2<sup>pk0</sup>* mice develop glomerulosclerosis**

Genotypes and time points as indicated in the figure. (A) PAS staining of kidney sections revealed protein casts in the tubular system and glomerulosclerosis at day 28 in *Phb2<sup>pk0</sup>* mice (scale bar 20  $\mu$ m). (B) Immunohistochemistry for podocin on kidney sections showed reduction of podocin expression over time in *Phb2<sup>pk0</sup>* mice (scale bar 20  $\mu$ m). (C) Analysis of podocyte foot processes in electron micrographs revealed progressive foot process effacement in *Phb2<sup>pk0</sup>* mice (scale bar 0.7  $\mu$ m). (D) Analysis of mitochondrial morphology in electron micrographs showed swollen and disorganized mitochondria in 21 days old but not 14 days old *Phb2<sup>pk0</sup>* mice (arrows; scale bar 0.3  $\mu$ m). FP, podocyte foot processes; GBM, glomerular basement membrane; EC, endothelial cells.

### 6.1.3 *Phb2<sup>het</sup>* mice present with changes in mitochondrial ultrastructure

To further understand the defect in *Phb2<sup>pk0</sup>* mice an electron micrograph analysis of *Phb2<sup>het</sup>* mice was performed. These mice do not show any loss of body weight or albuminuria but electron micrographs of 21 days old *Phb2<sup>het</sup>* mice revealed partially disorganized mitochondrial cristae structures, whereas foot process organization was normal (**Figure 6A+B**).

Thus, changes in mitochondrial ultrastructure do not necessarily lead to glomerular disease.

## Results

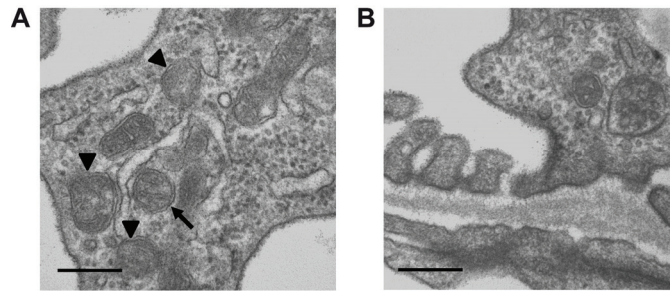


**Figure 6. *Phb2het* mice present with changes in mitochondrial ultrastructure**

(A) Electron micrograph analysis of mitochondrial cristae structures of *Phb2<sup>het</sup>* mice at day 21 revealed partially disorganized mitochondrial cristae structures (arrow = normal mitochondrial structure; arrowheads = defective mitochondrial structure; scale bar 1  $\mu$ m). (B) Electron micrograph analysis of foot process organization of *Phb2<sup>het</sup>* mice at day 21 showed no overt changes in foot process organization (scale bar 1  $\mu$ m).

### **6.1.4 Glomeruli of *Phb2<sup>pk0</sup>* mice display no increased rate of apoptosis at day 21**

Previous reports showed that loss of prohibitin-2 might render cells more susceptible to apoptosis [53,69,121,122]. Loss of the terminally differentiated podocyte cannot be compensated and seems to cause the development of albuminuria and glomerulosclerosis in other models of glomerular diseases [123–126].

To investigate if loss of podocytes causes the severe phenotype in this mouse model, kidney sections of the albuminuric *Phb2<sup>pk0</sup>* mice at day 21 and non-albuminuric control mice of the same age were stained for cleaved caspase-3, a marker for apoptotic cell death. However, no increased cleavage of caspase-3 was detected in podocytes of *Phb2<sup>pk0</sup>* mice (**Figure 7A**). Since podocyte loss does not necessarily depend on apoptosis but could also be attributed to other types of cell death the total number of podocytes per glomerulus was assessed. Therefore, kidney sections of three animals per genotype were stained for the podocyte marker protein WT-1. Podocytes from 40 glomeruli of each kidney section were counted. Interestingly, no change in podocyte cell number was detected at day 21 in *Phb2<sup>pk0</sup>* mice compared to *Phb2<sup>fl/fl</sup>* mice (**Figure 7B+C**).

Therefore, podocyte loss did not account for the development of albuminuria in *Phb2<sup>pk0</sup>* mice.

## Results

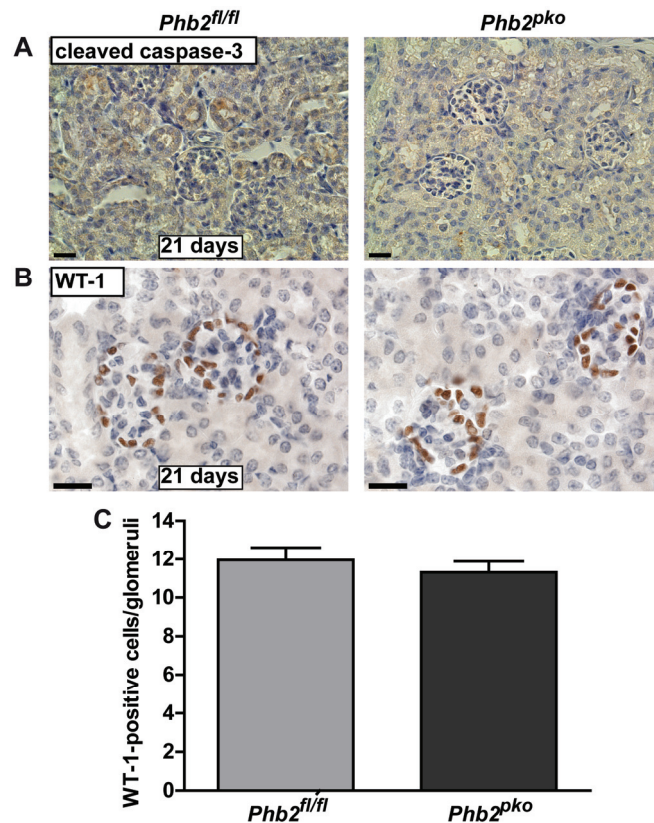


**Figure 7. Glomeruli of *Phb2<sup>pko</sup>* mice display no increased rate of apoptosis at day 21**

(A) Immunohistochemistry for cleaved caspase-3 on kidney sections of *Phb2<sup>pko</sup>* and *Phb2<sup>fl/fl</sup>* mice revealed no cleaved caspase-3-positive cells in the glomeruli of both genotypes (scale bar 20  $\mu$ m). (B) Immunohistochemistry for the podocyte marker WT-1 on kidney sections of *Phb2<sup>pko</sup>* and *Phb2<sup>fl/fl</sup>* mice (scale bar 20  $\mu$ m). (C) Quantification of WT-1-positive cells per glomerulus showed no difference in *Phb2<sup>pko</sup>* mice compared to *Phb2<sup>fl/fl</sup>* mice (*Phb2<sup>fl/fl</sup>* 11.96  $\pm$  0.65 WT-1-positive cells/glomerulus vs. *Phb2<sup>pko</sup>* 11.32  $\pm$  0.57 WT-1-positive cells/glomerulus; n = 3 for both groups, 40 glomeruli per animal counted, P > 0.05).

### 6.1.5 PHB2 is required to maintain structural integrity of podocyte foot processes

In the past decades, several studies on proteins of the slit diaphragm complex showed that an intact slit diaphragm structure is essential for a healthy glomerulus and normal albumin filtration [13,16,18,19,127]. Therefore, the structure of the slit diaphragm was analyzed in *Phb2<sup>pko</sup>* mice more closely by means of electron microscopy.

In 14 days old *Phb2<sup>pko</sup>* mice no overt changes in slit diaphragm appearance were detected (**Figure 8A**). However, at day 21 *Phb2<sup>pko</sup>* mice developed foot process effacement and loss of slit diaphragm structures became evident (**Figure 8B**).

## Results

Thus, although slit diaphragm structures between neighboring podocytes were initially formed *Phb2<sup>pk0</sup>* mice failed to maintain them over time.

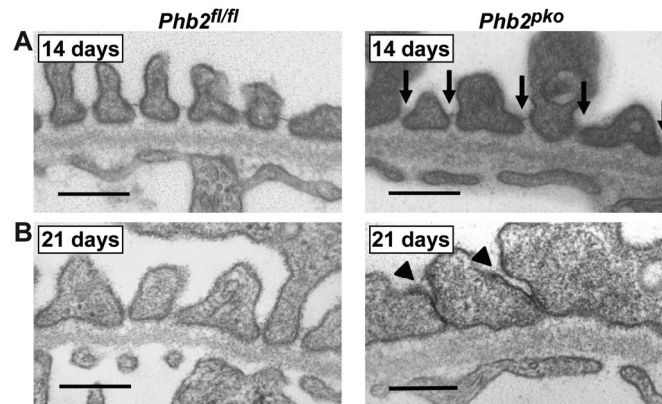


**Figure 8. PHB2 is required to maintain structural integrity of podocyte foot processes**

(A) Electron micrographs revealed no overt changes in slit diaphragm appearance in 14 days old *Phb2<sup>pk0</sup>* mice (arrows point to slit diaphragm structures in *Phb2<sup>pk0</sup>* mice; scale bar 0.3  $\mu$ m). (B) Electron micrographs demonstrated foot process effacement and loss of slit diaphragm structures in 21 days old *Phb2<sup>pk0</sup>* mice (arrow heads, scale bar 0.3  $\mu$ m).

### 6.1.6 Inducible depletion of *Phb2* results in loss of slit diaphragm function

First differences in foot process organization were already seen 14 days after birth. To exclude a developmental phenotype in *Phb2<sup>pk0</sup>* mice a second mouse model was used. Mating of tamoxifen-inducible improved Cre mice under the control of the *NPHS2* promoter (podocin-iCreER(T2)) [117] to conditional *Phb2 flox/flox* mice [53] resulted in podocin-iCreER(T2) *Phb2<sup>pk0</sup>* animals (tPod-*Phb2<sup>pk0</sup>*) and podocin-iCreER(T2) *Phb2<sup>het</sup>* animals (tPod-*Phb2<sup>het</sup>*). These mice were fed with a tamoxifen-enriched diet starting at the age of eight weeks for six weeks in total to induce Cre expression in adult animals. Only male mice were used for this study to exclude potential side-effects of tamoxifen in female mice.

PAS-staining at 2.5 weeks after end of tamoxifen treatment revealed glomerulosclerosis and tubular protein casts in tPod-*Phb2<sup>pk0</sup>* but not tPod-*Phb2<sup>het</sup>* mice (**Figure 9A**). Furthermore, at this time point podocin expression was highly reduced in these animals (**Figure 9B**). Analysis of urinary samples of tPod-*Phb2<sup>pk0</sup>* mice in a coomassie gel detected albuminuria already in the last week of tamoxifen feeding (**Figure 9C**). However, the time of onset of albuminuria and time of death

## Results

varied in between two weeks in all mice that were analyzed, probably due to different amounts of intake of the tamoxifen-enriched diet.

Taken together, the phenotype of the *Phb2*<sup>pk0</sup> mice was not developmental and could be reproduced in adult animals.

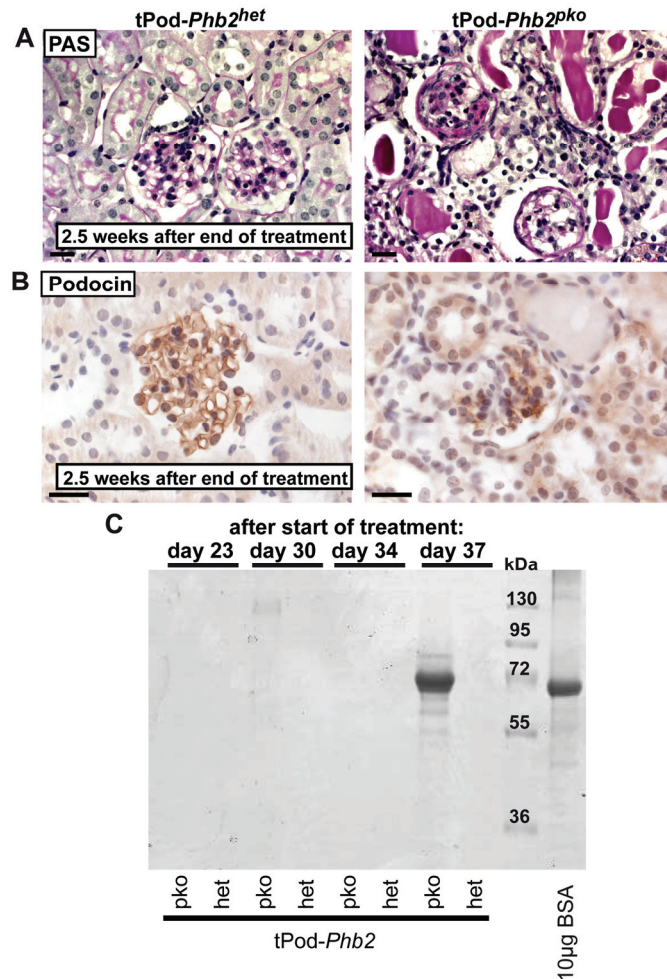


**Figure 9. Inducible depletion of *Phb2* results in loss of slit diaphragm function**

(A) PAS staining revealed glomerulosclerosis in *tPod-Phb2*<sup>pk0</sup> but not *tPod-Phb2*<sup>het</sup> mice 2.5 weeks after the end of tamoxifen treatment (scale bar 20 µm). (B) Immunohistochemistry for podocin on kidney sections of *tPod-Phb2*<sup>pk0</sup> and control mice showed loss of podocin expression 2.5 weeks after the end of tamoxifen treatment (scale bar 20 µm). (C) Coomassie stain of urinary samples detected albuminuria in *tPod-Phb2*<sup>pk0</sup> but not control mice at day 37 of tamoxifen treatment.

### 6.2 PHB2 as a novel slit diaphragm protein

#### 6.2.1 PHB2 localizes to the slit diaphragm

As loss of PHB2 not only resulted in premature death after 4-5 weeks but also led to massive albuminuria already evident three weeks after birth we tested the hypothesis that PHB2 exerts extramitochondrial functions in podocytes. To this end we assessed the localization of PHB2. Therefore, a new antibody was generated because the commercially available antibodies directed against PHB1 and PHB2 gave no reproducible results on tissue sections. Human kidney sections were stained with this self-generated antibody detecting both, PHB1 and PHB2. Co-staining for podocin showed a partial co-localization of PHB1/2 and podocin at the slit diaphragm (**Figure 10A**). The PHB1/2 antibody was validated using a co-staining with MitoTracker on immortalized podocytes (**Figure 10B**) and an ELISA (**Figure 10C**). To further prove the localization of PHB2 to the slit diaphragm immunogold labelings were performed. Immunogold labeling of a commercially available PHB2 antibody showed a clear signal in podocytes close to the slit diaphragm (**Figure 10D**) and – used as a proof of principle control – in mitochondria (**Figure 10E**). In addition, immunogold labeling with a PHB1 antibody was performed but did not give any specific signals in mitochondria or other parts of the cell.

Thus, PHB2 localized not only to mitochondria but also to the slit diaphragm of podocytes.

## Results

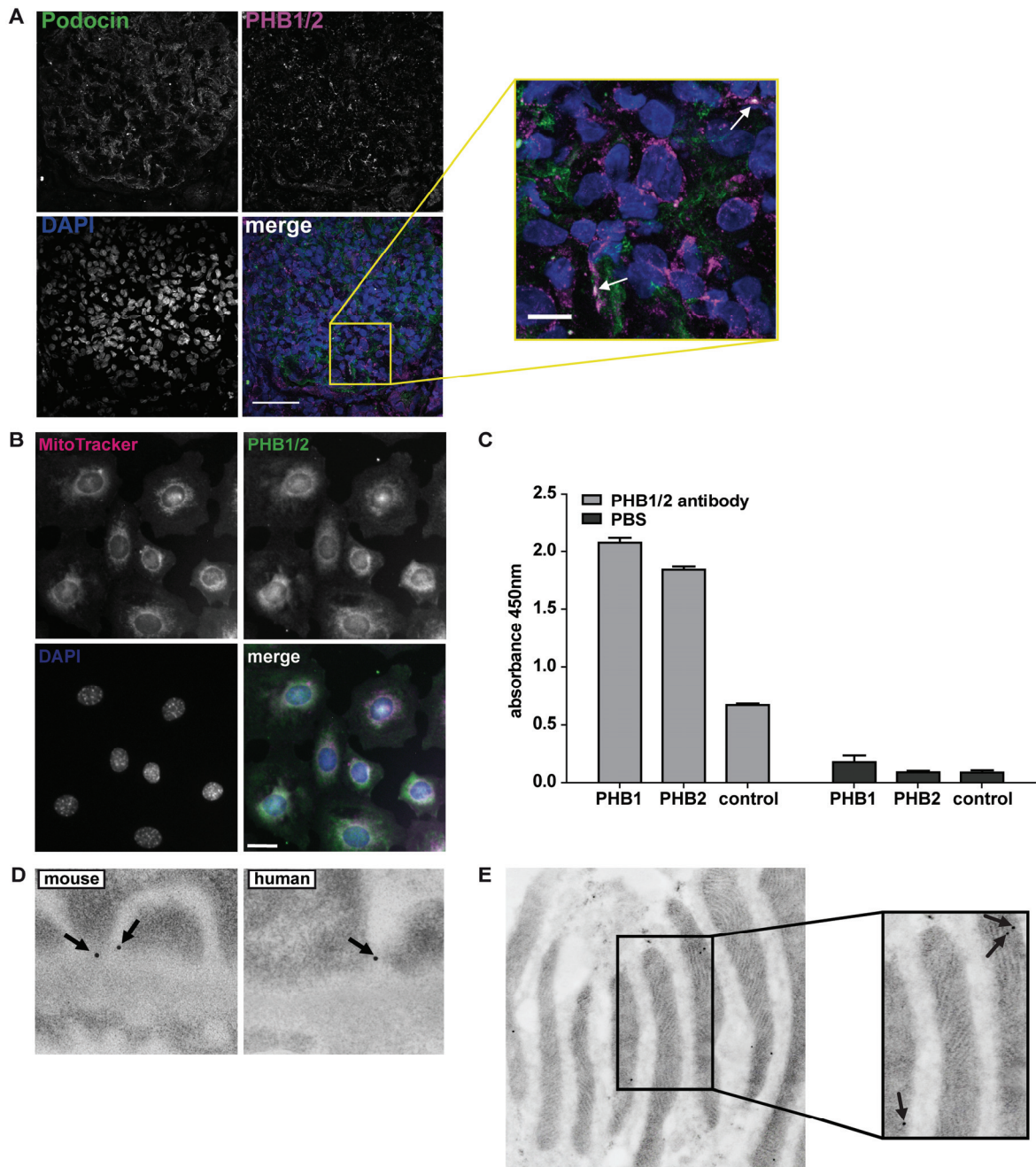


**Figure 10. PHB2 localizes to the slit diaphragm**

(A) Immunofluorescence stainings of podocin and PHB1/2 on human kidney sections showed partial co-localization (arrows show the overlap; scale bar 50  $\mu\text{m}$  in overview, 10  $\mu\text{m}$  in magnification). (B) ELISA for PHB1, PHB2 and a control protein measured in triplicates. (C) Co-staining of MitoTracker and PHB1/2 on mouse podocytes (scale bar 20  $\mu\text{m}$ ). (D) Immunogold labeling of PHB2 in mouse and human kidney sections detected PHB2 at the slit diaphragm (arrows). (E) Immunogold labeling of PHB2 revealed signals in mitochondria (arrow).

### 6.2.2 PHB1 and PHB2 co-immunoprecipitate with podocin

Previous work already showed that podocin is an important player at the slit diaphragm [33,36]. Since both, podocin and PHB2, localized to the slit diaphragm we next tested the hypothesis that both proteins co-immunoprecipitate. To test this, co-precipitation experiments after overexpression in HEK293T cells were performed. For these experiments, the known interaction of PHB1 and PHB2 served as a positive control. PHB2 co-immunoprecipitated with podocin and vice versa (**Figure 11A+B**). In addition, the interaction of PHB1 and podocin was tested and co-immunoprecipitation showed a co-immunoprecipitation of PHB1 with podocin and vice versa (**Figure 11C+D**). Both proteins did not co-immunoprecipitate with a control protein. To further substantiate this finding co-immunoprecipitations were performed with endogenous proteins. To this end, glomeruli from wildtype mice were isolated and proteins extracted before the respective antibodies were added. Here, PHB2 co-immunoprecipitated with podocin as well (**Figure 11E**). Due to technical reasons no conclusive result for the co-precipitation of PHB1 with podocin from glomerular lysates can be shown.

Taken together, PHB2 not only localized to the slit diaphragm but also co-immunoprecipitated with podocin in overexpression and glomerular lysates. Co-immunoprecipitation of PHB1 with podocin could only be shown in overexpression experiments.

## Results

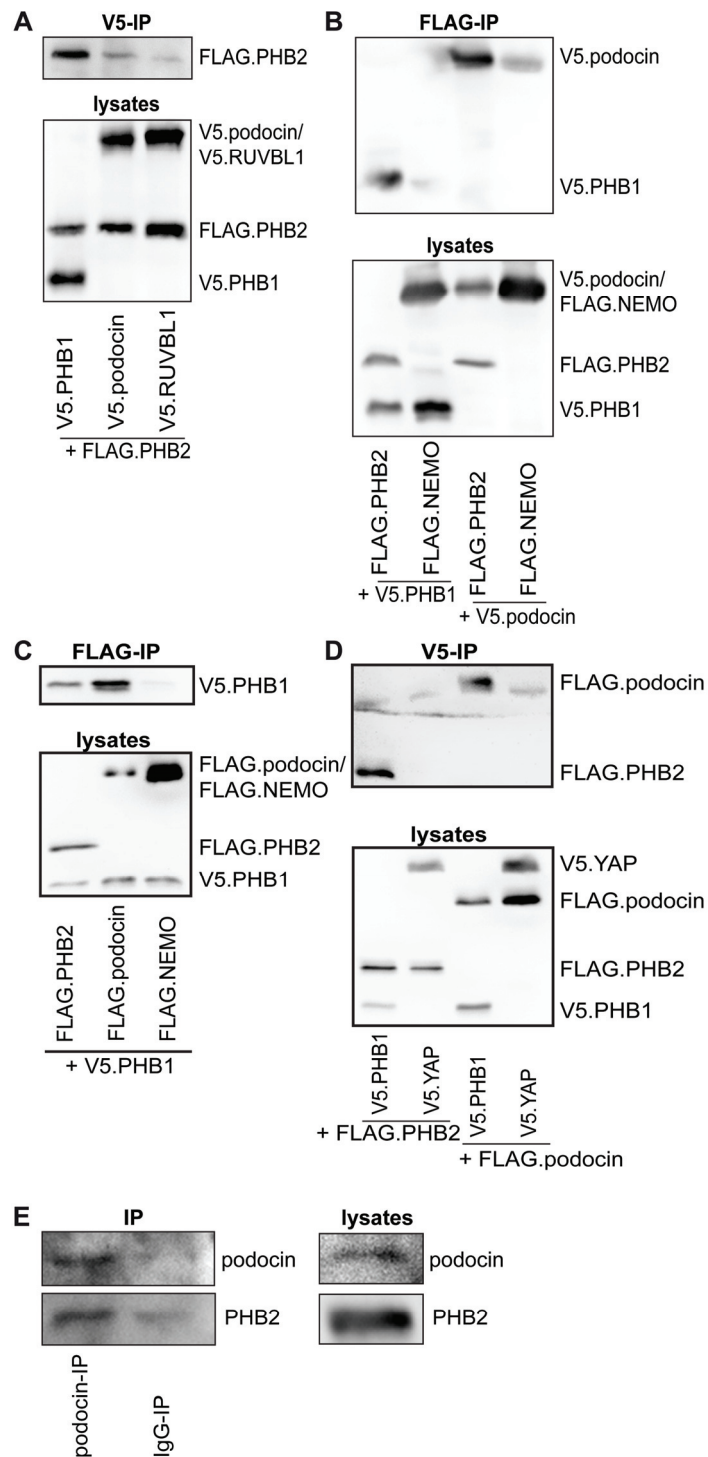


**Figure 11. PHB1 and PHB2 co-immunoprecipitate with podocin**

(A) HEK293T cells were transiently transfected as stated. Immunoprecipitation was performed using a V5 antibody and showed co-precipitation of PHB2 with podocin but not the control protein. (B) HEK293T cells were transiently transfected with the indicated constructs. Immunoprecipitation was performed using a FLAG antibody and showed co-precipitation of podocin with PHB2 but not the control protein. (C) HEK293T cells were transiently transfected with the constructs as stated. Immunoprecipitation was performed using a FLAG antibody and showed co-precipitation of PHB1 with podocin but not the control protein. (D) HEK293T cells

## Results

were transiently transfected with the indicated constructs. Immunoprecipitation was performed using a V5 antibody and showed co-precipitation of podocin with PHB1 but not the control protein. (E) Co-immunoprecipitation of podocin and PHB2 from isolated mouse glomeruli revealed co-precipitation of PHB2 with podocin endogenously.

### **6.2.3 PHB-2 co-localizes with MEC-2 at touch receptor punctae and regulates touch sensation in *C. elegans***

Localization of PHB2 to the slit diaphragm and its interaction with podocin point to an additional, extramitochondrial role of PHB2 in podocytes. This could of course also imply a functional relevance of PHB2 at the slit diaphragm complex. However, in mammals, no assays are currently available to test the functionality of the slit diaphragm experimentally. To circumvent this problem the nematode *C. elegans* can be utilized [24]. In *C. elegans*, six touch receptor neurons are necessary for conducting gentle body touch [113,128]. In these touch receptor neurons MEC-2 - the *C. elegans* homolog of podocin - is part of the multiprotein-channel complex that is localized in regular punctae along touch receptor neuron processes [42,43].

A new transgenic worm strain was generated that expressed PHB-2::GFP under control of the *mec-17* promoter, which is exclusively active in the six-touch receptor neurons [129]. In this transgenic strain PHB-2 was found around the cell body of the neurons most likely reflecting the mitochondrial localization of the protein. Additionally, staining of these worms for MEC-2 revealed a partial co-localization of PHB-2 and MEC-2 along the touch punctae (**Figure 12A**), thereby confirming the results on localization of PHB2 from section 6.2.1.

The mechanosensory machinery in *C. elegans* and the complex organization of the slit diaphragm in mammals show a high similarity [24,130]. In *C. elegans* the multiprotein-channel complex is needed to convert mechanical forces into electrical signals, thus representing a physiological response to study by performing gentle touch assays. To achieve optimal knockdown of genes in neurons of *C. elegans* a neuronal-specific RNAi strain [*sid-1(pk3321) him-5(e1490) V; lin 15B(n744) X; uls71 [pCFJ90(myo-2p::mCherry) + mec-18p::sid-1]*] can be used. By using this strain, the cell metabolism in any other cell of the body is not affected. As a whole body knockout of *phb-2* leads to infertility and shortened lifespan [70] the restriction of the knockdown to the neurons was important to exclude an influence of metabolic

## Results

changes in other cells on gentle body touch. Feeding of the neuronal-specific RNAi strain with bacteria carrying a *mec-2*-RNAi plasmid impaired touch sensitivity as reported previously [113]. Loss of either *phb-1* or *phb-2* significantly decreased touch sensitivity but to a lesser extent compared to *mec-2* deficiency. To exclude a potential effect of defects of the respiratory chain on touch sensitivity the worms were also fed with *mev-1* RNAi. *Mev-1* encodes for the succinate dehydrogenase cytochrome b, i.e. the respiratory chain complex II and its knockdown causes disruption of mitochondrial respiration [131]. However, loss of *mev-1* resulted only in a slight decrease in touch sensitivity while the difference between *mev-1*-deficient and *phb-1*- or *phb-2*-deficient worms was still highly significant (**Figure 12B**).

In summary, PHB-2 co-localized with MEC-2 at touch receptor punctae in *C. elegans*. Both, PHB-1 and PHB-2 were needed to conduct touch sensation, which was most likely independent of respiratory chain activity.

## Results

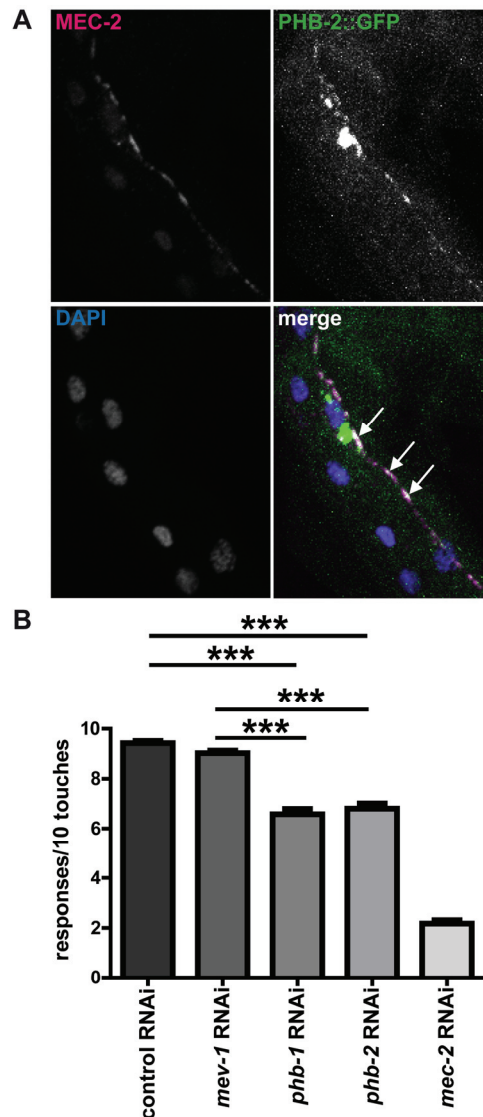


**Figure 12. PHB-2 co-localizes with MEC-2 at touch receptor punctae and regulates touch sensation in *C. elegans***

(A) Immunofluorescence stainings of MEC-2 on PHB-2::GFP expressing worms showed co-localization of PHB-2 and MEC-2 in touch punctae (arrows point at co-localization in a touch receptor neuron). (B) Touch sensitivity was reduced upon loss of either *mec-2*, *phb-1* or *phb-2* but not *mev-1*. (control RNAi  $9.42 \pm 0.09$  responses/10 touches, *mev-1* RNAi  $9.02 \pm 0.10$  responses/10 touches, *phb-1* RNAi  $6.58 \pm 0.21$  responses/10 touches, *phb-2* RNAi  $6.80 \pm 0.21$  responses/10 touches, *mec-2* RNAi  $3.38 \pm 0.22$  responses/10 touches;  $n = 50$  for all groups;  $***P < 0.001$  for control RNAi vs. *phb-1* RNAi, control RNAi vs. *phb-2* RNAi, *mev-1* RNAi vs. *phb-1* RNAi and *mev-1* RNAi vs. *phb-2* RNAi).

### 6.3 PHB2 in metabolic signaling

#### 6.3.1 Podocyte-specific knockout of the insulin receptor (*Insr*) and IGF-1 receptor (*Igf1r*) prolongs survival of *Phb2*<sup>pk0</sup> mice

In worms and yeast the deleterious effects of a *phb-2/Phb2*-deficiency could be reversed by either loss of the insulin receptor homolog *daf-2* or dietary restriction [70,71]. However, nothing is known about the impact of PHB2 on insulin signaling and the mTOR pathway in mammalian cells.

To investigate if *Phb2*<sup>pk0</sup> mice benefit from loss of insulin signaling and show reduced albuminuria and/or prolonged survival two new mouse models were generated. First, *Phb2 flox/flox* mice were mated to *Igf1r flox/flox* or *Insr flox/flox* mice. Second, these mice were mated to podocyte-specific Cre mice (*NPHS2.cre* mice) [116] to obtain mice with a podocyte-specific deficiency of either *Phb2* and *Igf1r* (*Phb2*<sup>pk0</sup>/*Igf1r*<sup>pk0</sup> mice) or *Phb2* and *Insr* (*Phb2*<sup>pk0</sup>/*Insr*<sup>pk0</sup> mice).

Survival analysis revealed that an additional *Igf1r*-deficiency did not influence the survival rate of *Phb2*<sup>pk0</sup> mice (**Figure 13A+C**). In contrast, *Phb2*<sup>pk0</sup>/*Insr*<sup>pk0</sup> as well as *Phb2*<sup>pk0</sup>/*Insr*<sup>het</sup> mice outlived *Phb2*<sup>pk0</sup> mice by 6 days in average (**Figure 13B+C**). The survival benefit reached statistically significant levels for *Phb2*<sup>pk0</sup>/*Insr*<sup>pk0</sup> mice (**Figure 13C**) and all mice developed progressive albuminuria, short-lived *Phb2*<sup>pk0</sup>/*Igf1r*<sup>pk0</sup> as well as longer-lived *Phb2*<sup>pk0</sup>/*Insr*<sup>pk0</sup> mice (**Figure 13D**).

## Results

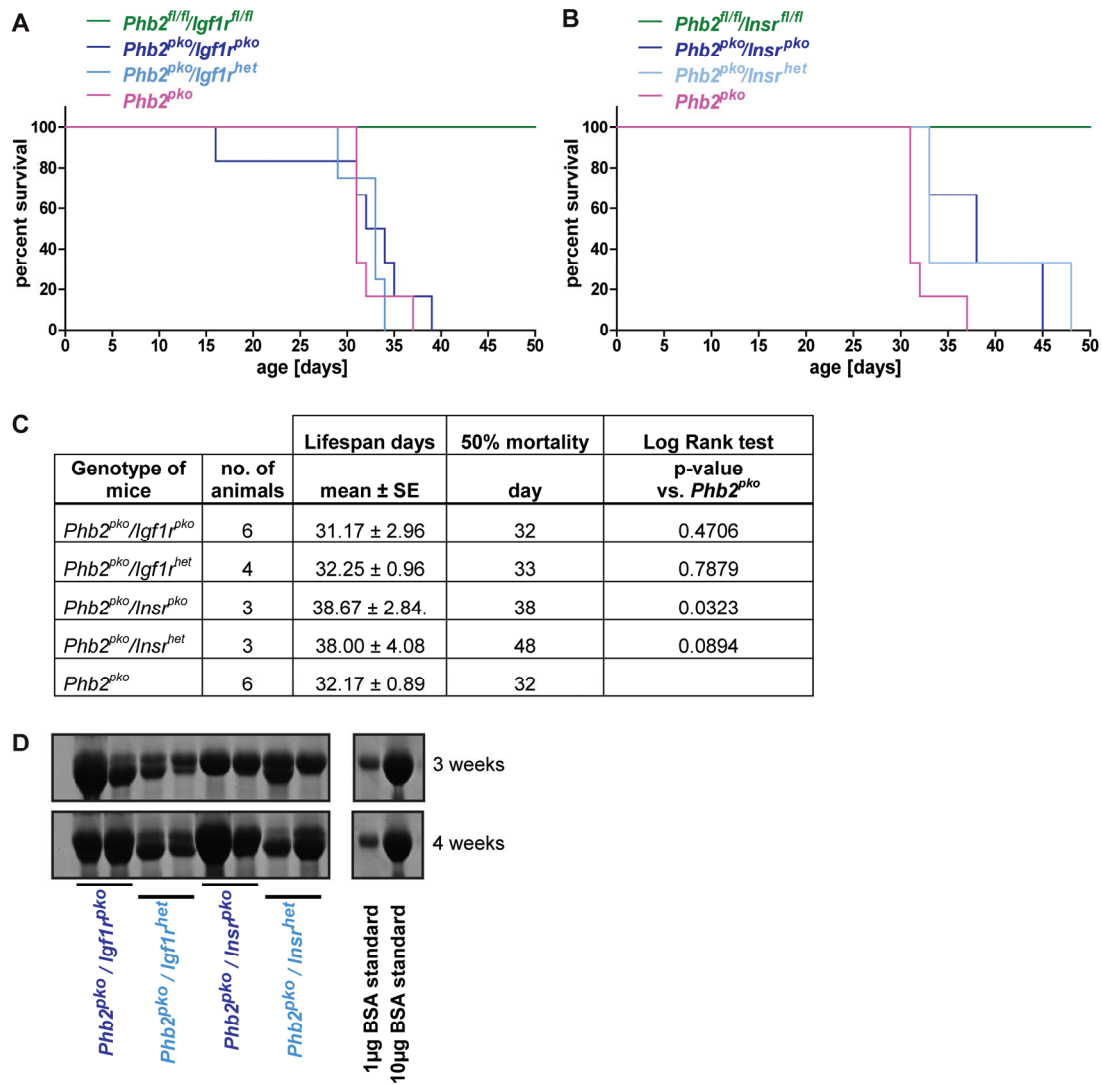


**Figure 13: Loss of the insulin receptor but not IGF-1 receptor prolongs lifespan of  $Phb2^{pko}$  mice**

(A) Kaplan-Meier survival curve revealed that the survival time of  $Phb2^{pko}$  mice is not changed by an additional  $Igf1r$ -deficiency (n = 6 for  $Phb2^{pko}/Igf1r^{pko}$ , n = 4 for  $Phb2^{pko}/Igf1r^{het}$ , n = 6 for  $Phb2^{pko}$ ). (B) Kaplan-Meier survival curve showed that an additional knockout of the insulin receptor ( $Insr$ ) prolonged lifespan of  $Phb2^{pko}$  mice (n = 3 for  $Phb2^{pko}/Insr^{pko}$ , n = 3 for  $Phb2^{pko}/Insr^{het}$ , n = 6 for  $Phb2^{pko}$ ). (C) Statistical analysis comparing all genotypes with  $Phb2^{pko}$  mice. (D) Representative coomassie stain of urinary samples revealed albuminuria in podocyte-specific double knockout-mice irrespective of their genotype.

Since the insulin receptor may compensate for the IGF-1 receptor and vice versa [132] a podocyte-specific triple knockout mouse line of  $Phb2$ ,  $Insr$  and  $Igf1r$  was generated ( $Phb2^{pko}/Insr^{pko}/Igf1r^{pko}$ ).

Analysis of survival rates showed that  $Phb2^{pko}/Insr^{pko}/Igf1r^{pko}$ ,  $Phb2^{pko}/Insr^{het}/Igf1r^{pko}$  and  $Phb2^{pko}/Insr^{pko}/Igf1r^{het}$  mice lived longer than  $Phb2^{pko}$  mice (**Figure 14A**) but this

## Results

increased survival was only statistically significant for  $Phb2^{pko}/Insr^{pko}/Igf1r^{pko}$  and  $Phb2^{pko}/Insr^{pko}/Igf1r^{het}$  mice (Figure 14B). In accordance to the results in  $Phb2^{pko}/Igf1r^{pko}$  and  $Phb2^{pko}/Insr^{pko}$  mice all analyzed genotypes of the triple knockout mice presented with massive albuminuria and there were no differences observed between the different genotypes (Figure 14C).

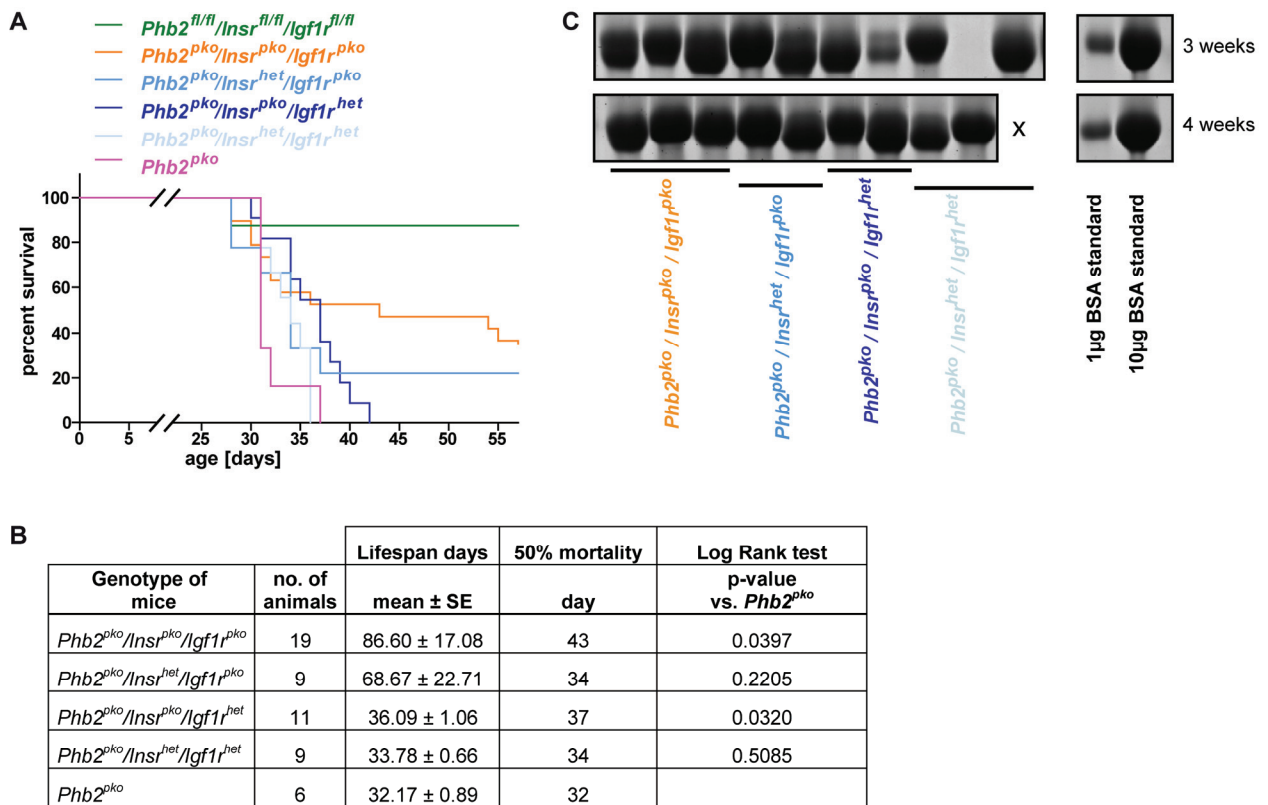


**Figure 14: Podocyte-specific knockout of the insulin receptor (*Insr*) and IGF-1 receptor (*Igf1r*) prolongs survival of  $Phb2^{pko}$  mice**

(A) Kaplan-Meier survival curve revealed prolonged survival of  $Phb2^{pko}/Insr^{pko}/Igf1r^{pko}$ ,  $Phb2^{pko}/Insr^{het}/Igf1r^{pko}$  and  $Phb2^{pko}/Insr^{pko}/Igf1r^{het}$  mice (n = 19 for  $Phb2^{pko}/Insr^{pko}/Igf1r^{pko}$ , n = 9 for  $Phb2^{pko}/Insr^{het}/Igf1r^{pko}$ , n = 11 for  $Phb2^{pko}/Insr^{pko}/Igf1r^{het}$ , n = 9 for  $Phb2^{pko}/Insr^{het}/Igf1r^{het}$ , n = 6 for  $Phb2^{pko}$ ). (B) Statistical analysis comparing all genotypes with  $Phb2^{pko}$  mice. (C) Representative coomassie stain of urinary samples showed albuminuria in all analyzed mice irrespective of their genotype (x = no urine analyzed because mouse was dead by that time).

### 6.3.2 Inhibition of mTOR signaling increases lifespan of $Phb2^{pko}$ mice

To study the role of PHB2 in metabolic signaling of podocytes in more detail a new *Phb2*-knockdown podocyte cell culture model was established. In 2008, Merkwirth et

## Results

al. showed that *Phb2*-deficiency leads to a reduced proliferation rate of the affected cells [53]. Therefore, the use of a doxycycline-inducible knockdown cell culture model was necessary. To generate an inducible *Phb2* knockdown in mouse podocytes, short hairpin RNAs (shRNAs) directed against the murine *Phb2* mRNA were designed, cloned and tested for knockdown-efficiency with a dual-luciferase assay in *mPhb2*-transfected HEK 293T cells. The combination of shRNA1 and shRNA4 gave the best knockdown result as calculated by the renilla/firefly ratios and was used for further studies (**Figure 15A**). The selected shRNAs were transferred into a doxycycline-inducible lentiviral vector (pLenti4-TO, Invitrogen) and thermo-sensitive immortalized mouse podocytes [107] were stably transduced with this vector (cell line named *mPhb2* shRNA). To control for off-target effects another cell line was generated which inducibly expressed a scrambled shRNA. The *Phb2* knockdown was confirmed by using a TaqMan® assay with probes specific for *Phb1* and *Phb2*, showing a decrease in mRNA expression of *Phb2* but not *Phb1* (**Figure 15B**). Western Blot analysis of these cells revealed significantly reduced protein levels of PHB1 and PHB2 (**Figure 15C**). This is in accordance with previous results showing that PHB1 and PHB2 interdepend and each protein needs the other for its stability [50,53,112]. In addition, the cells presented with a disrupted mitochondrial network as visualized by immunofluorescence staining for the mitochondrial marker protein Tom20 that resides within the outer mitochondrial membrane (**Figure 15D+E**).

## Results

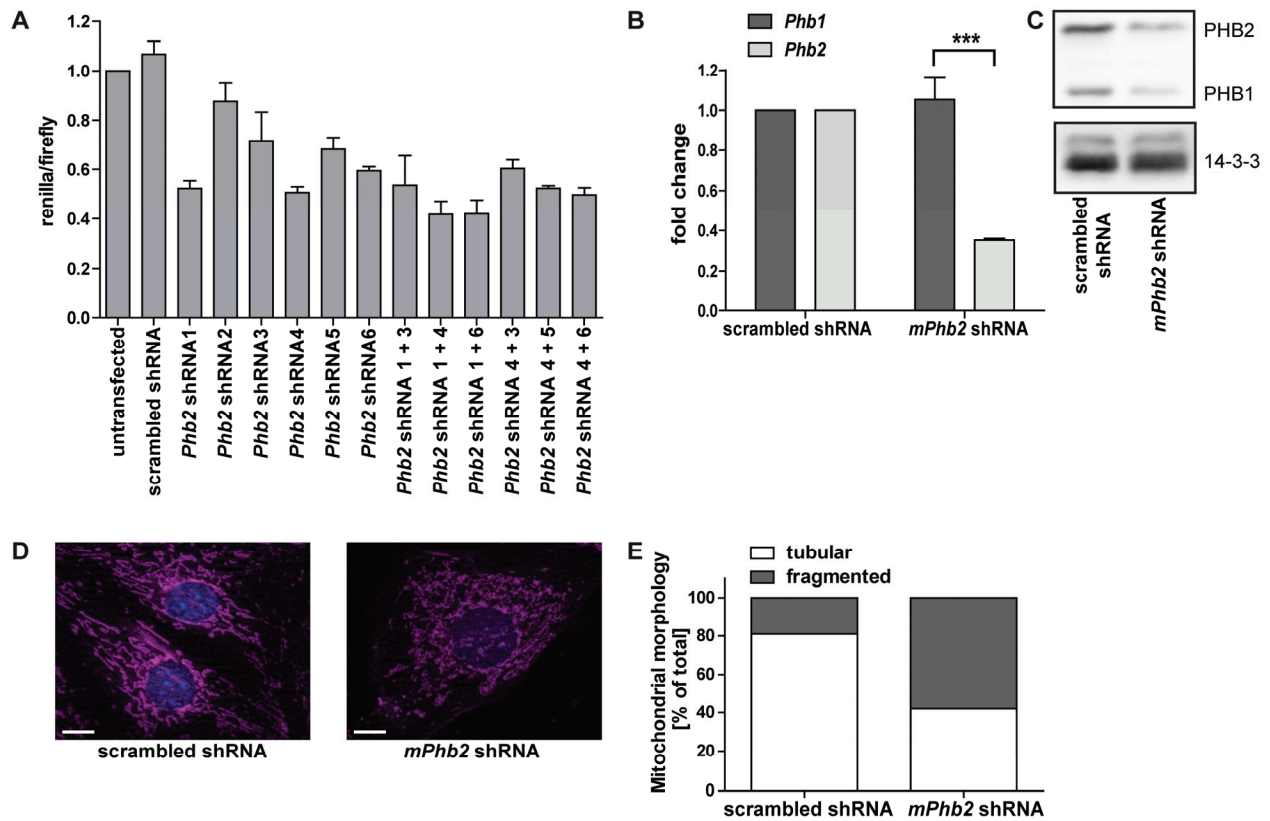


**Figure 15. Generation and validation of an inducible *Phb2* shRNA podocyte cell line**

(A) Knockdown efficiency of different shRNAs targeting murine *Phb2* mRNA was assessed by dual-luciferase assay in 293T cells (n = 3; bars represent means ± SEM). (B) *mPhb2* shRNA podocytes contained less *Phb2* mRNA than control (scrambled shRNA) podocytes as assessed in a TaqMan® assay (n = 3, bars represent mean ± SEM, \*\*\*P < 0.001). (C) Western Blot analysis revealed decreased protein levels of PHB1 and PHB2 in *mPhb2* shRNA podocytes. Staining for 14-3-3 was used as a loading control. (D) *mPhb2* shRNA podocytes presented with a disrupted mitochondrial network as seen by immunofluorescence staining with a Tom20 antibody (scale bar 10 μm). (E) Quantification of tubular and fragmented mitochondrial morphology revealed more fragmented mitochondria in *mPhb2* shRNA podocytes (n = 100 cells for *mPhb2* shRNA, n = 108 cells for scrambled shRNA).

Western Blot analysis of these *Phb2*-deficient mouse podocytes revealed an overactive signaling via the mTOR pathway as seen by increased phosphorylation of the downstream effector S6 ribosomal protein (**Figure 16A+B**). This could be blocked by treating the cells with the mTORC1-specific inhibitor rapamycin (**Figure 16A**). To show the importance of PHB2 for this signaling pathway not only in cell culture, but also in tissue, kidney sections of *Phb2<sup>pk0</sup>* and *Phb2<sup>fl/fl</sup>* mice were stained for phosphorylated S6 ribosomal protein in immunohistochemistry. Interestingly,

## Results

*Phb2<sup>pk0</sup>* but not control mice showed increased activation of S6 ribosomal protein within glomeruli (**Figure 16C**).

To investigate if the increased mTOR activity plays a role in the development of glomerular disease in *Phb2<sup>pk0</sup>* mice the mice were treated with the mTORC1-specific inhibitor rapamycin starting at the age of two weeks. At this age glomerulogenesis was completed and *Phb2<sup>pk0</sup>* mice did not present with albuminuria yet as described in section 6.1.2. Rapamycin treatment had no effect on control *Phb2<sup>fl/fl</sup>* mice. In contrast, treatment of *Phb2<sup>pk0</sup>* mice with rapamycin prolonged the mean lifespan by 10 days compared to vehicle-treated *Phb2<sup>pk0</sup>* mice (**Figure 16D+E**). Analysis of urinary samples in coomassie gels showed massive albuminuria in both, vehicle-treated and rapamycin-treated *Phb2<sup>pk0</sup>* mice (**Figure 16F**).

Thus, loss of PHB2 influenced signaling of the mTOR pathway, but treatment with rapamycin could prolong lifespan of short-lived *Phb2<sup>pk0</sup>* mice despite progressive albuminuria.

## Results

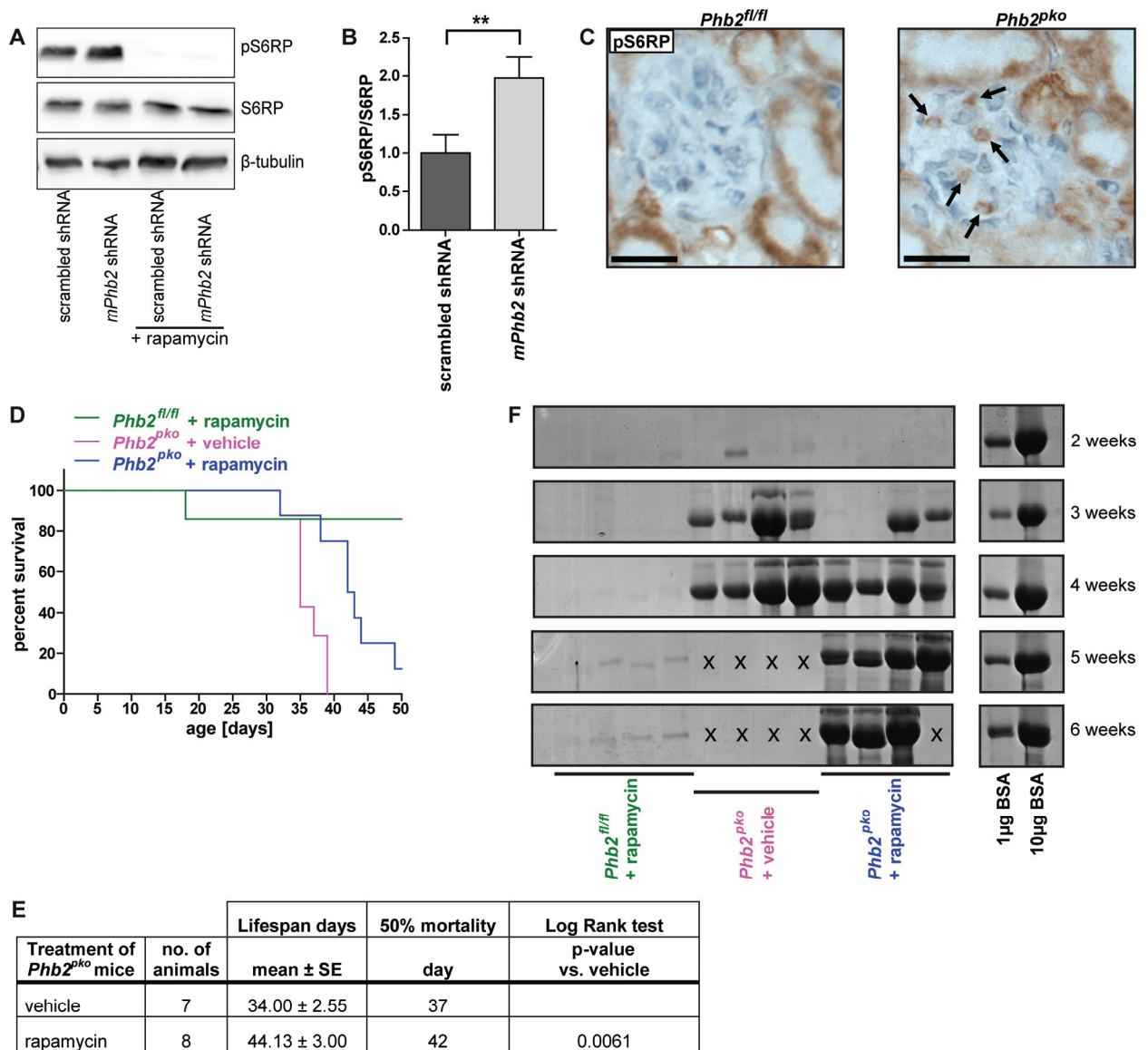


**Figure 16. Inhibition of mTOR signaling increases lifespan of *Phb2<sup>pko</sup>* mice**

(A) *Phb2*-deficient mouse podocytes showed higher levels of phosphorylated S6 ribosomal protein than control podocytes, which could be blocked by treatment with 10 ng/ml rapamycin (pS6RP = phosphorylated S6 ribosomal protein, S6RP = S6 ribosomal protein). (B) *mPhb2* shRNA podocytes had a higher ratio of pS6RP/S6RP than control (scrambled shRNA) podocytes as assessed by densitometric quantification ( $n = 5$ , bars represent mean  $\pm$  SEM,  $**P < 0.01$ ) (C) Immunohistochemistry for phosphorylated S6 ribosomal protein (pS6RP) on kidney sections revealed increased levels of pS6RP in glomeruli of *Phb2<sup>pko</sup>* compared to *Phb2<sup>fl/fl</sup>* mice (arrows point to cells showing a signal for pS6RP; scale bar 20  $\mu$ m). (D) Kaplan-Meier survival curve revealed that treatment of *Phb2<sup>pko</sup>* mice with rapamycin prolonged survival for several days compared to vehicle-treated *Phb2<sup>pko</sup>* mice ( $n = 7$  for *Phb2<sup>fl/fl</sup>* + rapamycin,  $n = 7$  for *Phb2<sup>pko</sup>* + vehicle,  $n = 8$  for *Phb2<sup>pko</sup>* + rapamycin). (E) Statistical analysis comparing rapamycin-treated *Phb2<sup>pko</sup>* mice with vehicle-treated *Phb2<sup>pko</sup>* mice. (F) Representative coomassie stain of urinary samples showed development of albuminuria in vehicle- as well as rapamycin-treated *Phb2<sup>pko</sup>* mice (x = no urine analysed because mouse was dead by that time).

## 7 Discussion

### 7.1 PHB2 – a slit diaphragm protein?

#### 7.1.1 The phenotype of *Phb2*<sup>pk0</sup> mice is similar to slit diaphragm protein-deficient mice

More than 5% of all human beings worldwide suffer from chronic kidney diseases (CKD) with great impact on quality of life and rising socio-economical burdens on our societies. Glomerular disorders, with diabetic nephropathy being the leading cause, account for the majority of cases of CKD. In the past several years, accumulating evidence suggested that glomerular podocytes are crucial for the function of the kidney filter and critically involved in the development of proteinuria [5,6]. Mutations in several genes encoding for proteins of the slit diaphragm are a major cause for the development of focal segmental glomerulosclerosis (FSGS). One of the most studied proteins at the slit diaphragm is podocin, a member of the SPFH domain protein family. Mutations in podocin cause childhood onset of proteinuria and steroid-resistant forms of focal segmental glomerulosclerosis (FSGS) [16,17,37–41]. So far, nothing is known about the function of other SPFH domain-containing proteins in podocytes, which could also be important for the development of proteinuria and glomerular disease.

PHB2 - another member of the SPFH domain-containing protein family - is known as an integral mitochondrial membrane protein. In addition to its functions in mitochondrial biogenesis and maintenance of mitochondrial DNA PHB2 seems to be involved in lots of other cellular processes like cellular signaling and apoptosis [54,133,134].

To study the function of PHB2 in podocyte biology a podocyte-specific *Phb2*-knockout mouse (*Phb2*<sup>pk0</sup>) was generated. The mice were born viable in the expected Mendelian frequency. Starting at about three weeks of age the animals showed growth retardation as compared to their littermate controls. *Phb2*<sup>pk0</sup> animals died at the age of 31 to 37 days. To obtain a better insight in podocyte biology the glomerular phenotype at different time points was analyzed. 14 days after birth, when glomerular development is completed, light microscopy of renal sections did not reveal any injury. Glomerular function as examined by urine albumin/creatinine ratios was normal. EM analysis revealed normal mitochondrial architecture. One week later

## Discussion

podocin expression was reduced and changed to a more granular pattern, indicating a change in slit diaphragm organization. In accordance to this, EM analysis of *Phb2<sup>bko</sup>* mice demonstrated highly effaced foot processes, loss of slit diaphragm structures and the animals developed albuminuria. Mitochondria structure was disorganized and with multiple swollen cristae structures. At four weeks of age, PAS staining revealed severe glomerulosclerosis and high levels of serum urea and serum creatinine revealed the progression of the disease to renal failure, leading to premature death. Podocin expression was markedly reduced and foot processes were completely effaced, which was also reflected in high, nephrotic-range levels of albuminuria. In summary, podocytes of *Phb2<sup>bko</sup>* mice showed not only disorganized mitochondrial cristae structures but also defects in foot process organization and slit diaphragm maintenance.

Interestingly, apart from loss of proper mitochondrial ultrastructures, these findings resemble the phenotype of mice lacking important components at the slit diaphragm. For example, CD2AP is part of the podocyte slit diaphragm complex and interacts with the slit diaphragm protein nephrin [135]. CD2AP-knockout mice exhibit growth retardation starting three weeks after birth and die three to four weeks later. The animals develop proteinuria at day 14 and present with glomerulosclerosis at about four weeks of age [10]. Nephrin- or podocin-knockout mice show massive foot process effacement and rapidly develop proteinuria as well. While nephrin-knockout mice die within one day after birth, podocin-knockout animals survive some days or even weeks [18,136]. To explain the differences in the onset of proteinuria and time of death between nephrin-, podocin- and CD2AP-knockout mice it was speculated that other proteins might compensate for the function of podocin and CD2AP. This could explain the slower time course of the disease in these animals compared to nephrin-knockout mice [136]. A second explanation would be the variance in genetic backgrounds, which has been shown to influence the severity of glomerular diseases [18,137].

However, the highly comparable phenotype of *Phb2<sup>bko</sup>* mice and other slit diaphragm protein-knockout mice is not the only argument for a slit diaphragm-related phenotype of *Phb2<sup>bko</sup>* animals: despite first signs of structural changes at the slit diaphragm at day 14 mitochondria of *Phb2<sup>bko</sup>* mice were unaffected and 21 days old *Phb2<sup>het</sup>* mice did not show an overt glomerular phenotype albeit disturbed

## Discussion

mitochondrial ultrastructure. Taken together, these findings point to an extramitochondrial function of PHB2 as an important factor for the maintenance of the kidney filtration barrier.

### **7.1.2 PHB2 is necessary for the function of the slit diaphragm complex**

Podocin and prohibitins are required for proper structural organization of their immediate surrounding at the slit diaphragm or mitochondria, respectively. Together with the initial findings in the *Phb2*<sup>pk0</sup> mice this raised the hypothesis that PHB2 may not only localize to mitochondria but also to the slit diaphragm and interact with podocin to further stabilize the protein-lipid supercomplex at the slit diaphragm.

Therefore, localization of PHB2 in podocytes was assessed. PHB2 was found - in addition to its known mitochondrial localization - close to the slit diaphragm in immunogold labelings as well as immunofluorescence stainings. Overexpression as well as endogenous experiments revealed co-immunoprecipitation of PHB2 with the slit diaphragm protein podocin. With regard to previous reports showing PHB2 interacting and being stable only in a complex with PHB1 it is very likely that PHB1 may also localize to the slit diaphragm. Overexpression experiments suggest a co-immunoprecipitation of podocin and PHB1. However, due to technical limitations, co-immunoprecipitation studies for PHB1 using glomerular lysates as well as immunogold labelings remained inconclusive.

The localization of PHB2 to the slit diaphragm protein-lipid supercomplex was further confirmed in *C. elegans*. Here, the PHB2 homolog (PHB-2) co-localized with the podocin homolog MEC-2 in mechanosensitive complexes along touch receptor punctae of the neurons. As a transgenic strain was utilized in which expression of the transgene was under the control of the *mec-17* promoter mislocalization due to overexpression as compared to the endogenous *phb-2* promoter and/or due to the GFP-tag cannot be excluded. However, a similar approach has been used previously to analyze localization of prohibitins in worms [70]. To assess the functionality of the complex a neuronal-specific RNAi strain was fed with either *phb-1* or *phb-2* RNAi and gentle touch assays were performed. Interestingly, *phb-1*- and *phb-2*-deficient worms showed a reduced response to gentle touches as compared to the control RNAi fed worms, suggesting a functional impact of PHB1 and PHB2 on the complex. Loss of *mev-1*, a component of the mitochondrial electron transport chain complex II, showed

## Discussion

only mild effects on mechanosensation. This indicates that the effect of *phb-1*- and *phb-2*-deficiency on the function of the multiprotein-channel complex does not depend on an overall reduction of respiratory chain activity and thereby altered cell behavior.

Although no conclusive results could be shown for the localization of PHB1 to the slit diaphragm three arguments suggest that probably both, PHB1 and PHB2, act together at the slit diaphragm: first, previous work published from different groups showed that PHB1 and PHB2 exist in multimeric ring structures and stabilize each other [28,49,50]; second, PHB1 was shown to co-precipitate with podocin in overexpression; finally, *phb-1*-deficiency led to the same decrease in touch sensitivity as *phb-2*-deficiency.

A possible mode of action of PHB2 and probably PHB1 on the functionality of the protein-lipid supercomplex could be a stabilizing effect. Thereby, loss of PHB2 could lead to increased stretch-evoked activation of the ion-channel protein transient receptor potential cation channel 6 (TRPC6) - a component of slit diaphragm supercomplex [14,15] - as suggested for podocin deficiencies as well [24,138].

The finding that PHB2 localizes to the slit diaphragm protein-lipid supercomplex is further emphasized by results from other groups, showing that prohibitins can be detected in detergent-resistant lipid rafts [30,122,139] as shown for podocin as well [140]. These specialized membrane compartments are absent in mitochondria [139], further supporting a function of prohibitins in slit diaphragm protein-lipid supercomplexes at the plasma membrane. The identification of PHB2 as a second SPFH domain-containing protein at the slit diaphragm changes the current view of our understanding of a podocin-multimeric-complex, which may also be comprised of several SPFH domain-containing proteins.

### **7.1.3 *Phb2*-deficiency in podocytes affects mitochondrial and non-mitochondrial functions**

Several lines of evidence point into the direction of not only a mitochondrial but also an extramitochondrial phenotype of *Phb2*<sup>pk0</sup> mice. As discussed in section 7.1.1 *Phb2*<sup>pk0</sup> mice rapidly developed a severe phenotype which resembled that of other slit diaphragm protein-deficient mice. Furthermore, PHB2 localized not only to

## Discussion

mitochondria, but also to the slit diaphragm complex in mammals as well as to the highly similar multiprotein-channel complex in *C. elegans* (see section 7.1.2).

Previous reports showed that *Phb2*-deficient cells are more susceptible to intrinsic apoptotic stimuli *in vitro* and *in vivo* [53,69,121,122]. A possible mechanism for the increased levels of proteinuria could be that podocytes of *Phb2<sup>pko</sup>* mice show either increased levels of mitochondria-induced apoptosis and/or detachment from the underlying GBM, consequently leading to cell loss. Interestingly, no increased caspase-3 cleavage was detected in three weeks old *Phb2<sup>pko</sup>* animals despite high albuminuric levels arguing against apoptosis as the primary mechanisms for podocyte damage at this time point. However, podocyte detachment from the GBM can also occur in the absence of apoptosis [141]. To investigate this, the overall podocyte cell number was assessed by counting WT-1-positive cells in paraffin sections, but no changes were detected in *Phb2<sup>pko</sup>* compared to *Phb2<sup>fl/fl</sup>* mice. Therefore, there is no evidence for the hypothesis that either increased apoptosis or early podocyte detachment account for the loss of podocyte function and initial development of albuminuria in *Phb2<sup>pko</sup>* mice.

However, *Phb2*-deficient podocytes clearly show a mitochondria-related phenotype in addition as seen by the detection of disorganized and swollen mitochondria cristae structures within the cells of *Phb2<sup>pko</sup>* mice. Since the respiratory chain is localized within the cristae structures and has been shown to rely on prohibitins it can be speculated that the morphological changes could decrease respiratory chain activity and increase levels of reactive oxygen species (ROS). This would modulate cell metabolism by oxidation of e.g. proteins, lipids and DNA and also influence cell viability. Interestingly, various studies on this topic revealed opposing results. On the one hand, loss of prohibitins has been shown to increase ROS production by inhibition of the respiratory chain in e.g. human endothelial cells *in vitro* [142] and human epithelial colorectal adenocarcinoma cells *in vitro* [143] as well as 3T3-L1 mouse embryonic fibroblast *in vitro* [144]. On the other hand, no or only a late impact on respiratory chain activity was seen in studies on prohibitin-deficient mouse epidermal progenitor/stem cells *in vivo* [121], mouse embryonic fibroblasts *in vitro* [53] and mouse neurons in the forebrain *in vivo* [69]. Possible reasons for these contrary results could either be cell type-specific differences in the impact of

prohibitin depletion on respiratory chain activity and consequently ROS production or variable experimental settings.

Mitochondrial dynamics are essential for a cell and mutations in genes that are important for fusion and fission events can lead to neurodegeneration [145–147]. The dynamic nature of the mitochondrial network is needed as a quality control and to mitigate the effect of damaged mitochondria. On the one hand, fusion allows redistribution of damaged content between intact and dysfunctional mitochondria, thereby maintaining the integrity of the whole network. On the other hand, fission ensures the effective elimination of damaged mitochondria by mitophagy, thus protecting the cell from mitochondria-induced apoptosis [148]. OPA1 is the central regulator of fusion at the inner mitochondrial membrane [149,150] and enhanced processing of OPA1 to shorter isoforms induces mitochondrial fragmentation [65]. Loss of PHB2 leads to unbalanced cleavage of OPA1 and subsequently fusion defects as seen by disorganized and swollen mitochondrial cristae structures [53]. Several studies have reported morphological changes of mitochondria with disturbed cristae structures in podocytes of a FSGS mouse and rat model [151,152] as well as FSGS patients [153–155]. But whether the disruption of the mitochondrial network plays a role in the development of glomerulosclerosis or if it is a secondary effect of podocyte damage still remains to be elucidated.

## **7.2 PHB2 is linked to the regulation of cell metabolism**

### **7.2.1 *Phb2*-deficiency influences metabolic signaling via the insulin and IGF-1 receptor**

Previous work from Artal-Sanz et al. [70] and Schleit et al. [71] suggests a role of PHB2 in cell metabolism via insulin/mTOR signaling. In worms, loss of PHB2 decreased survival, but increased lifespan of already long-lived *daf-2* mutant worms [70]. In yeast, *Phb2*-deficiency activated the mitochondrial untranslated protein response (mtUPR), which is associated with reduced lifespan. This effect could be inhibited by dietary restriction, thereby reducing the mtUPR [71]. Taken together, these findings raised the hypothesis of a potential link of PHB2 and insulin/mTORC1 signaling in mammalian organ systems. In contrast to nematodes, the insulin receptor

## Discussion

and the IGF-1 receptor mediate the action of growth factors on cell metabolism in mammals. Both have been shown to be expressed in podocytes [156–159].

To investigate if the deleterious effect of the podocyte-specific *Phb2*-deficiency is dependent on signaling via the insulin receptor and/or the IGF-1 receptor pathway, podocyte-specific double knockout mice were generated that either lacked PHB2 and the insulin receptor (*Phb2<sup>pko</sup>/Insr<sup>pko</sup>* mice) or PHB2 and the IGF-1 receptor (*Phb2<sup>pko</sup>/Igf1r<sup>pko</sup>* mice). Assessing survival of these animals revealed a beneficial effect on lifespan in *Phb2<sup>pko</sup>/Insr<sup>pko</sup>* but not *Phb2<sup>pko</sup>/Igf1r<sup>pko</sup>* mice compared to *Phb2<sup>pko</sup>* mice. All mice rapidly developed massive albuminuria and no differences were observed between the different genotypes. These results indicate that although filtering properties are impaired in *Phb2<sup>pko</sup>/Insr<sup>pko</sup>* the damage of podocytes which probably leads to renal failure in the end is delayed compared to *Phb2<sup>pko</sup>* mice.

Insulin and IGF-1 cannot only bind and activate their specific receptor, but insulin can also bind to the IGF-1 receptor and IGF-1 to the insulin receptor with differing affinities [132]. Loss of the insulin receptor under standard plasma insulin and IGF-1 levels might then lead to increased activation of the IGF-1 receptor. To test for an additional beneficial effect after loss of the IGF-1 receptor, triple podocyte-specific knockout mice lacking PHB2, the insulin receptor and IGF-1 receptor (*Phb2<sup>pko</sup>/Insr<sup>pko</sup>/Igf1r<sup>pko</sup>* mice) were generated and survival was monitored. Deletion of just one *Igf1r* allele in addition to homozygous *Phb2*- and *Insr*-deletions did not show any overt effect on survival compared to *Phb2<sup>pko</sup>/Insr<sup>pko</sup>* mice (50% mortality rate of *Phb2<sup>pko</sup>/Insr<sup>pko</sup>/Igf1r<sup>het</sup>* mice at day 37, mean lifespan of ~36 days vs. 50% mortality rate of *Phb2<sup>pko</sup>/Insr<sup>pko</sup>* mice at day 38 and a mean lifespan of ~38 days). Intriguingly, *Phb2<sup>pko</sup>/Insr<sup>pko</sup>/Igf1r<sup>pko</sup>* mice showed a 50% mortality rate at day 43 and a mean lifespan of ~86 days. However, the survival rate of *Phb2<sup>pko</sup>/Insr<sup>pko</sup>/Igf1r<sup>pko</sup>* mice was extremely diverse. While some mice did not die by the end of the study others showed a medium survival and some died in the same time frame as *Phb2<sup>pko</sup>* mice. These differences could be caused by insufficient and differing Cre activity in this triple knockout mouse model. Arguing against an ineffective Cre recombinase, all *Phb2<sup>pko</sup>/Insr<sup>pko</sup>/Igf1r<sup>pko</sup>* mice developed massive albuminuria which was present until they died. Since double knockouts of the insulin and IGF-1 receptor alone do not show any overt albuminuria until at least 8 weeks after birth (data not shown), the

## Discussion

development of albuminuria in the triple knockout mouse model is probably due to the loss of PHB2 and cannot be rescued by interfering with metabolic signaling.

### 7.2.2 Dysregulated mTOR signaling leads to glomerular diseases

The beneficial effect of the loss of insulin signaling in *Phb2<sup>pko</sup>* mice raised the question whether activation of the downstream mediator mTORC1 is involved in podocyte damage in this model.

Interestingly, staining for phosphorylated S6 ribosomal protein - a downstream target of mTORC1 signaling widely used to assess the activation status of mTORC1 - revealed enhanced phosphorylation of S6 ribosomal protein not only in *Phb2*-depleted podocytes *in vitro* but also *in vivo*. Hyperactivation of mTORC1 has been shown to cause glomerular diseases in mice and humans before [95,104,160,161]. For example, diabetic mice show increased mTORC1 activation but benefit from podocyte-specific mTORC1 suppression and are less proteinuric under mTORC1 inhibition. Furthermore, constitutive podocyte-specific activation of mTORC1 by ablation of the upstream negative regulator TSC1 results in the development of a glomerular disease similar to diabetic nephropathy including proteinuria. Treatment with rapamycin ameliorated proteinuria in that study [104]. Rats treated with puromycin aminonucleoside (PAN) to induce nephrosis show hyperactivation of mTORC1 as well and can be protected from proteinuria by treatment with rapamycin or a rapamycin derivate [160,161].

Compared to *Phb2<sup>pko</sup>* mice the progression of the disease in both, PAN-induced nephrosis rats and *Tsc1*-knockout mice, is much slower and animal models with hyperactive mTORC1 rather developed features of diabetic nephropathy with GBM thickening and mesangial expansion while *Phb2<sup>pko</sup>* mice presented with a FSGS-like pathology [104,160,161]. Additionally, *Phb2<sup>pko</sup>* mice died around 31-37 days after birth while e.g. *Tsc1*-knockout mice survived at least eight weeks when they were analyzed in the less susceptible C57BL/6 background which was also used for the *Phb2<sup>pko</sup>* study. Rapamycin treatment before onset of the disease suppressed the development of proteinuria in *Tsc1*-knockout mice completely [104] but shows no effect on albuminuria in *Phb2<sup>pko</sup>* mice. Therefore, it can be speculated that the hyperactivation of mTORC1 is not the initial cause of albuminuria and

## Discussion

glomerulosclerosis in *Phb2<sup>pk0</sup>* mice but rather the consequence of PHB2 depletion at the slit diaphragm as discussed under 7.1.2.

Intriguingly, lifespan of *Phb2<sup>pk0</sup>* mice is clearly increased under rapamycin treatment, suggesting that the fast progression of the disease and severity of podocyte damage in this model depends on mTORC1 activity. This hypothesis is in line with the studies discussed here, illustrating that dysregulation of mTOR signaling in podocytes causes glomerular diseases [95,104,160,161]. Gödel et al. [95] raised the hypothesis that under pathologic conditions like diabetic nephropathy in patients mTOR is activated to counteract the metabolic changes in the disease. But despite of short-term beneficial effects of the increased mTORC1 activation this dysregulation ultimately facilitates disease progression. Clearly, this could hold true for *Phb2<sup>pk0</sup>* mice as well, but the underlying molecular mechanism needs to be investigated further. One hypothesis could be that the development of any glomerular disease sensitizes the same pathway which ultimately leads to activation of mTOR as a common final effector pathway. Another hypothesis could be that mTOR activation is mediated via distinct pathways specific for the underlying podocyte defect. So far, hyperactivation of mTORC1 has only been shown in diabetic nephropathy [95,104,161] and glomerulonephritis [160,162] models as well as glomerulosclerosis arising from *Phb2*-deficiency. To be able to draw any conclusive result more glomerular disease models need to be analyzed for hyperactivity of mTORC1 and mechanisms of activation. Clearly, so far it cannot be ruled out that mTOR activation could also be a secondary effect caused by the development of albuminuria as a metabolic switch meant to counteract the disease. But there is no actual data available showing that albuminuria *per se* causes mTOR activation, neither in this model nor in any other published report on mTOR activation and proteinuria.

*Phb2<sup>pk0</sup>* mice treated with rapamycin showed a 50% mortality rate at day 42 and a mean lifespan of ~44 days whereas *Phb2<sup>pk0</sup>/Insr<sup>pk0</sup>/Igf1r<sup>pk0</sup>* mice showed a 50% mortality rate at day 43 and a mean lifespan of ~86 days. This high increase in mean lifespan of *Phb2<sup>pk0</sup>/Insr<sup>pk0</sup>/Igf1r<sup>pk0</sup>* mice can be explained by the fact that some *Phb2<sup>pk0</sup>/Insr<sup>pk0</sup>/Igf1r<sup>pk0</sup>* mice did not die by renal failure in the end but survived until the end of the study. In contrast, in the rapamycin-treated *Phb2<sup>pk0</sup>* study group only one mouse survived until the end of the study. This could be on the one hand due to unequal numbers of mice that were analyzed. The rapamycin-treated *Phb2<sup>pk0</sup>* study

## Discussion

group included only 8 mice while the *Phb2<sup>pk0</sup>/Insr<sup>pk0</sup>/Igf1r<sup>pk0</sup>* study group contained 19 individual subjects. On the other hand, this could also be explained by the fact that the effect of an intraperitoneally administered drug might not be as pronounced as a knockout model. For this study, it is not known which concentration of rapamycin reaches the podocyte in the end and for how long the rapamycin concentration is high enough to exert its beneficial effects. In this regard, the triple knockout mouse might serve as a better model to study metabolic effects in *Phb2*-deficient mice.

### 7.2.3 Hypothesis: Loss of PHB2 sensitizes the insulin receptor

Investigation of the molecular mechanism how loss of PHB2 leads to increased mTORC1 activity *in vitro* and *in vivo* might provide novel insights into the crosstalk of mitochondria and insulin/mTOR signaling in health and disease. This thesis work suggests that the effect of *Phb2*-deficiency on mTOR activity is mediated via activation of the insulin and IGF-1 receptor and that dysregulated signaling is detrimental to cell metabolism and survival as reflected by slowing progression of glomerular disease with rapamycin treatment or knockout of the insulin receptor and IGF-1 receptor.

A possible mechanism could be that loss of mitochondrially localized PHB2 leads to the production of reactive oxygen species (ROS) including H<sub>2</sub>O<sub>2</sub> in podocytes. These effect has already been shown for several other but not all cell types *in vitro* and *in vivo* [53,69,121,142–144]. A mild but not high increase in ROS production has been suggested to enhance insulin sensitivity by two mechanisms: first, facilitation of the insulin-stimulated tyrosine autophosphorylation of the insulin receptor; second, oxidation and inhibition of PTEN, a suppressor of the insulin/IGF-1 receptor downstream target AKT [163–165]. Furthermore, oxidative stress can also induce activation of the IGF-1 receptor [166]. Therefore, an increase in ROS production could enhance insulin/IGF-1 signaling and activate mTORC1. The study in worms showed that *Phb2*-deficiency leads to increased mitochondrial content [70]. This ROS-induced enhanced insulin sensitivity model could provide two explanations for this finding. Firstly, the activation of the mTORC1 pathway could result in the inhibition of autophagy [167], thereby preventing the breakdown of structurally disorganized and maybe dysfunctional mitochondria further promoting disease progression. Secondly, enhanced activation of insulin/IGF-1 signaling leads to

## Discussion

phosphorylation of the transcription factor FOXO1 thereby preventing FOXO1 from translocation into the nucleus [168–170]. FOXO1 is amongst others necessary for the transcription of a gene that encodes for an enzyme leading to heme depletion [171]. Heme is an important co-factor for the OXPHOS system. Loss of heme results in reduced electron transfer from e.g. NADH and FADH<sub>2</sub> and alters the ratio of NAD<sup>+</sup>/NADH which is a sensor for mitochondrial biogenesis. When FOXO1 translocates to the nucleus the NAD<sup>+</sup>/NADH ratio decreases and blocks mitochondrial biogenesis [171]. Lack of PHB2 and subsequent activation of the insulin/IGF-1 signaling pathway retain FOXO1 in the cytoplasm and allow mitochondrial biogenesis leading to more ROS production and again enhanced insulin sensitivity. This would foster a vicious circle from which escape is possible by directly interfering with signaling on the level of the insulin receptor and IGF-1 receptor. However, this does not explain the beneficial effect of mTORC1 inhibition in *Phb2<sup>dko</sup>* mice. But with regard to the function of active mTORC1 in promoting gene transcription and protein translation, inhibition of mTORC1 could deplete the cell of components necessary for mitochondrial biogenesis leading to a similar effect as loss of the insulin and IGF-1 receptor.

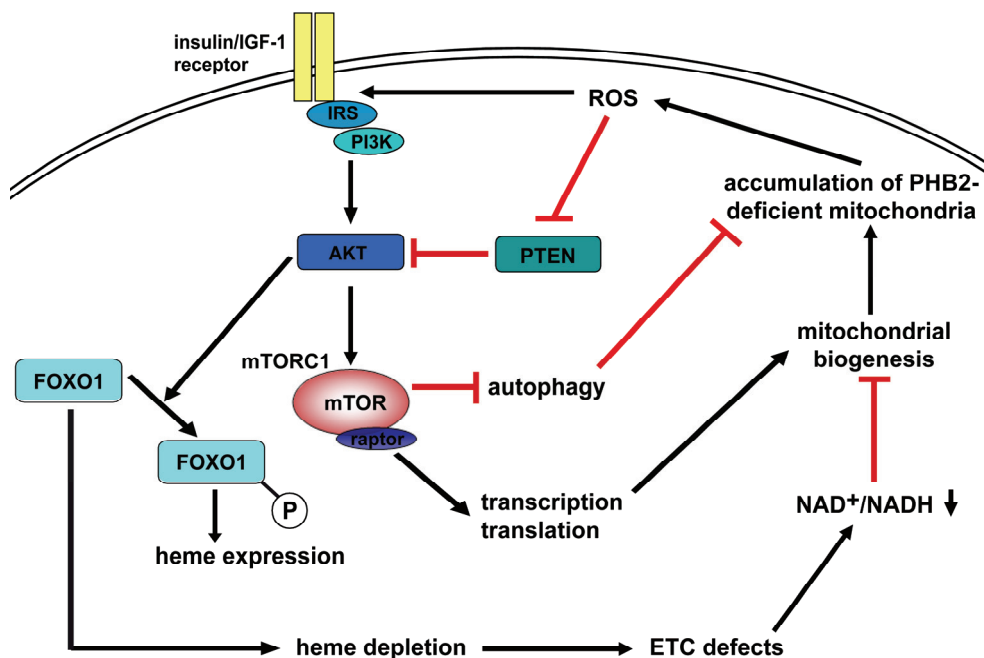


**Figure 17. Hypothesis: Loss of PHB2 sensitizes the insulin receptor**

Loss of PHB2 in mitochondria could increase ROS production which on the one hand might lead to activation of the insulin and IGF-1 receptor and thereby signaling via

## Discussion

AKT. On the other hand, increased ROS could inhibit PTEN which under normal conditions would inhibit AKT. AKT activation would lead not only to mTORC1 activation but also to the inhibition of FOXO1-phosphorylation, resulting in heme depletion and a decreasing NAD<sup>+</sup>/NADH ratio. This could promote mitochondrial biogenesis, leading to the accumulation of more *Phb2*-deficient mitochondria. Increased mitochondrial biogenesis could be further supported by elevated transcription and translation processes via mTORC1 activation and the inhibition of autophagy by mTORC1 may further promote accumulation of the dysfunctional mitochondria. (ETC = electron transport chain; ROS = reactive oxygen species)

Clearly, the hypothesis that increased ROS production from *Phb2*-deficient podocytes leads to enhanced insulin sensitivity needs further testing. Of course, it is very well conceivable that other factors than ROS activate the insulin and IGF-1 receptor in PHB2-depleted conditions to mediate hyperactivation of mTORC1 and the potentially deleterious effects of this dysregulation.

## 8 Conclusion

By using different techniques like immunofluorescence, immunogold-labeling and co-immunoprecipitation PHB2 was not only shown to localize to mitochondria but also to the podocyte slit diaphragm protein-lipid supercomplex. Podocyte-specific *Phb2*-deficient mice (*Phb2<sup>pko</sup>* mice) developed progressive albuminuria and glomerulosclerosis and died prematurely from renal failure, thereby resembling phenotypes of mice lacking other slit diaphragm protein knockout mice. Experiments in the nematode *C. elegans* further supported the localization of PHB2 to the protein-lipid supercomplex and revealed an essential impact of PHB2 on the functionality of this mechanosensitive complex in worms. Collectively, this thesis works suggests an extramitochondrial function of PHB2 at the slit diaphragm of podocytes.

Furthermore, inhibition of mTORC1 signaling by either rapamycin-treatment of podocyte-specific *Phb2*-deficient mice or loss of the insulin receptor and IGF-1 receptor prolonged lifespan of the *Phb2<sup>pko</sup>* mice by a so far unknown mechanism. Interestingly, albuminuria developed in these animals despite suppression of mTORC1 activity. In conclusion, this indicates that the development of albuminuria could be the result of the loss of function of PHB2 at the slit diaphragm but the fast progression of the glomerular disease depends on hyperactive mTORC1 after PHB2-depletion.

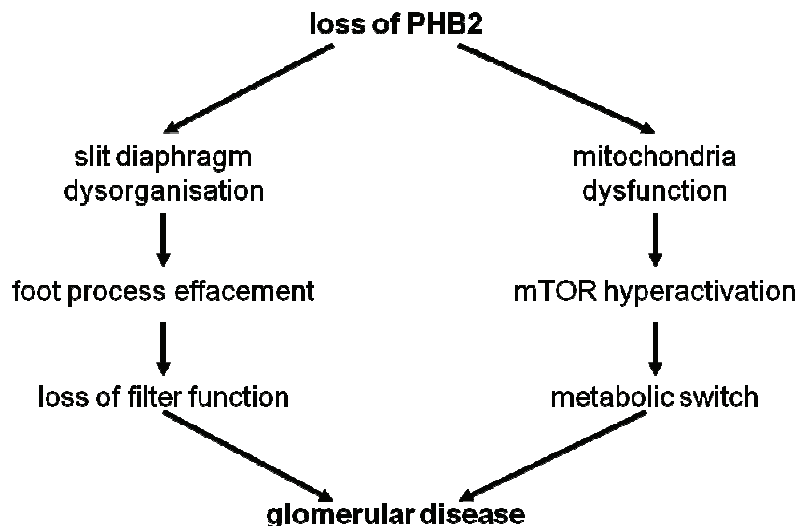


**Figure 18. Why does loss of PHB2 lead to glomerular disease?**

Loss of PHB2 ultimately leads to glomerular disease via two probably distinct pathways. On the one hand, PHB2-depletion results in foot process effacement

## Conclusion

because of its localization to the slit diaphragm, which results in loss of filter function (resulting in albuminuria). On the other hand, *Phb2*-deficiency leads to mitochondria dysfunction which enhances mTOR activation, resulting in a detrimental metabolic switch in podocytes (leading to podocyte loss). These two pathways together underlie the severe glomerular disease seen in *Phb2*<sup>pk0</sup> mice.

### 9 Publications

#### 9.1 Publications in academic journals

Brinkkoetter PT, **Ising C**, Benzing T. (2013). The role of the podocyte in albumin filtration. *Nat Rev Nephrol.* 9(6):328-36.

Höhne M, **Ising C**, Hagmann H, Völker LA, Brähler S, Schermer B, Brinkkoetter PT, Benzing T. (2013). Light microscopic visualization of podocyte ultrastructure demonstrates oscillating glomerular contractions. *Am J Pathol.* 182(2):332-8.

Brähler S, **Ising C**, Hagmann H, Rasmus M, Hoehne M, Kurschat C, Kisner T, Goebel H, Shankland S, Addicks K, Thaiss F, Schermer B, Pasparakis M, Benzing T, Brinkkoetter PT. (2012). Intrinsic proinflammatory signaling in podocytes contributes to podocyte damage and prolonged proteinuria. *Am J Physiol Renal Physiol.* 303(10):F1473-85.

#### 9.2 Publications in international academic conferences

Kidney Week 2013, American Society of Nephrology, Atlanta, Georgia, USA; Talk.

Kongress für Nephrologie, 5. Jahrestagung der Deutschen Gesellschaft für Nephrologie 2013, Berlin, Germany; Talk.

Kidney Week 2012, American Society of Nephrology, San Diego, California, USA; Poster.

9<sup>th</sup> International Podocyte Conference 2012, Miami, Florida, USA; Poster.

Kongress für Nephrologie, 3. Jahrestagung der Deutschen Gesellschaft für Nephrologie 2011, Berlin, Germany; Talk.

Kidney Week 2010, American Society of Nephrology, Denver, Colorado, USA; Poster.

### 10 References

1. Sarnak MJ, Levey AS, Schoolwerth AC, Coresh J, Culleton B, et al. (2003) Kidney disease as a risk factor for development of cardiovascular disease: a statement from the American Heart Association Councils on Kidney in Cardiovascular Disease, High Blood Pressure Research, Clinical Cardiology, and Epidemiology and Prevention. *Hypertension* 42: 1050–1065. doi:10.1161/01.HYP.0000102971.85504.7c.
2. Parfrey PS, Foley RN (1999) The clinical epidemiology of cardiac disease in chronic renal failure. *J Am Soc Nephrol* 10: 1606–1615.
3. Huber TB, Benzing T (2005) The slit diaphragm: a signaling platform to regulate podocyte function. *Curr Opin Nephrol Hypertens* 14: 211–216.
4. Jarad G, Miner JH (2009) Update on the glomerular filtration barrier. *Curr Opin Nephrol Hypertens* 18: 226–232.
5. Elger M, Kriz W (1998) Podocytes and the development of segmental glomerulosclerosis. *Nephrol Dial Transplant* 13: 1368–1373.
6. Brinkkoetter PT, Ising C, Benzing T (2013) The role of the podocyte in albumin filtration. *Nat Rev Nephrol* 9: 328–336. doi:10.1038/nrneph.2013.78.
7. D'Agati VD (2008) Podocyte injury in focal segmental glomerulosclerosis: Lessons from animal models (a play in five acts). *Kidney Int* 73: 399–406. doi:10.1038/sj.ki.5002655.
8. Zoja C, Abbate M, Remuzzi G (2006) Progression of chronic kidney disease: insights from animal models. *Curr Opin Nephrol Hypertens* 15: 250–257. doi:10.1097/01.mnh.0000222691.53970.83.
9. Lasagni L, Lazzeri E, Shankland SJ, Anders H-J, Romagnani P (2013) Podocyte mitosis - a catastrophe. *Curr Mol Med* 13: 13–23.
10. Shih NY, Li J, Karpitskii V, Nguyen A, Dustin ML, et al. (1999) Congenital nephrotic syndrome in mice lacking CD2-associated protein. *Science* 286: 312–315.
11. Kim JM, Wu H, Green G, Winkler CA, Kopp JB, et al. (2003) CD2-associated protein haploinsufficiency is linked to glomerular disease susceptibility. *Science* 300: 1298–1300. doi:10.1126/science.1081068.
12. Beltcheva O, Martin P, Lenkkeri U, Tryggvason K (2001) Mutation spectrum in the nephrin gene (NPHS1) in congenital nephrotic syndrome. *Hum Mutat* 17: 368–373. doi:10.1002/humu.1111.

## References

13. Philippe A, Nevo F, Esquivel EL, Reklaityte D, Gribouval O, et al. (2008) Nephtrin mutations can cause childhood-onset steroid-resistant nephrotic syndrome. *J Am Soc Nephrol* 19: 1871–1878. doi:10.1681/ASN.2008010059.
14. Reiser J, Polu KR, Möller CC, Kenlan P, Altintas MM, et al. (2005) TRPC6 is a glomerular slit diaphragm-associated channel required for normal renal function. *Nat Genet* 37: 739–744. doi:10.1038/ng1592.
15. Winn MP, Conlon PJ, Lynn KL, Farrington MK, Creazzo T, et al. (2005) A mutation in the TRPC6 cation channel causes familial focal segmental glomerulosclerosis. *Science* 308: 1801–1804. doi:10.1126/science.1106215.
16. Boute N, Gribouval O, Roselli S, Benessy F, Lee H, et al. (2000) NPHS2, encoding the glomerular protein podocin, is mutated in autosomal recessive steroid-resistant nephrotic syndrome. *Nat Genet* 24: 349–354. doi:10.1038/74166.
17. Frishberg Y, Rinat C, Megged O, Shapira E, Feinstein S, et al. (2002) Mutations in NPHS2 encoding podocin are a prevalent cause of steroid-resistant nephrotic syndrome among Israeli-Arab children. *J Am Soc Nephrol* 13: 400–405.
18. Roselli S, Heidet L, Sich M, Henger A, Kretzler M, et al. (2004) Early glomerular filtration defect and severe renal disease in podocin-deficient mice. *Mol Cell Biol* 24: 550–560.
19. Philippe A, Weber S, Esquivel EL, Houbron C, Hamard G, et al. (2008) A missense mutation in podocin leads to early and severe renal disease in mice. *Kidney Int* 73: 1038–1047. doi:10.1038/ki.2008.27.
20. Tavernarakis N, Driscoll M, Kyripides NC (1999) The SPFH domain: implicated in regulating targeted protein turnover in stomatins and other membrane-associated proteins. *Trends Biochem Sci* 24: 425–427.
21. Morrow IC, Parton RG (2005) Flotillins and the PHB domain protein family: rafts, worms and anaesthetics. *Traffic* 6: 725–740. doi:10.1111/j.1600-0854.2005.00318.x.
22. Rivera-Milla E, Stuermer CAO, Málaga-Trillo E (2006) Ancient origin of reggie (flotillin), reggie-like, and other lipid-raft proteins: convergent evolution of the SPFH domain. *Cell Mol Life Sci* 63: 343–357. doi:10.1007/s00018-005-5434-3.
23. Browman DT, Resek ME, Zajchowski LD, Robbins SM (2006) Erlin-1 and erlin-2 are novel members of the prohibitin family of proteins that define lipid-raft-like domains of the ER. *J Cell Sci* 119: 3149–3160. doi:10.1242/jcs.03060.

## References

24. Huber TB, Schermer B, Müller RU, Höhne M, Bartram M, et al. (2006) Podocin and MEC-2 bind cholesterol to regulate the activity of associated ion channels. *Proc Natl Acad Sci USA* 103: 17079–17086. doi:10.1073/pnas.0607465103.
25. Snyers L, Umlauf E, Prohaska R (1998) Oligomeric nature of the integral membrane protein stomatin. *J Biol Chem* 273: 17221–17226.
26. Gu G, Caldwell GA, Chalfie M (1996) Genetic interactions affecting touch sensitivity in *Caenorhabditis elegans*. *Proc Natl Acad Sci USA* 93: 6577–6582.
27. Langhorst MF, Reuter A, Stuermer CAO (2005) Scaffolding microdomains and beyond: the function of reggie/flotillin proteins. *Cell Mol Life Sci* 62: 2228–2240. doi:10.1007/s00018-005-5166-4.
28. Tatsuta T, Model K, Langer T (2005) Formation of membrane-bound ring complexes by prohibitins in mitochondria. *Mol Biol Cell* 16: 248–259. doi:10.1091/mbc.E04-09-0807.
29. Bickel PE, Scherer PE, Schnitzer JE, Oh P, Lisanti MP, et al. (1997) Flotillin and epidermal surface antigen define a new family of caveolae-associated integral membrane proteins. *J Biol Chem* 272: 13793–13802.
30. Foster LJ, De Hoog CL, Mann M (2003) Unbiased quantitative proteomics of lipid rafts reveals high specificity for signaling factors. *Proc Natl Acad Sci USA* 100: 5813–5818. doi:10.1073/pnas.0631608100.
31. Garin J, Diez R, Kieffer S, Dermine JF, Duclos S, et al. (2001) The phagosome proteome: insight into phagosome functions. *J Cell Biol* 152: 165–180.
32. Kobayakawa K, Hayashi R, Morita K, Miyamichi K, Oka Y, et al. (2002) Stomatin-related olfactory protein, SRO, specifically expressed in the murine olfactory sensory neurons. *J Neurosci* 22: 5931–5937.
33. Schwarz K, Simons M, Reiser J, Saleem MA, Faul C, et al. (2001) Podocin, a raft-associated component of the glomerular slit diaphragm, interacts with CD2AP and nephrin. *J Clin Invest* 108: 1621–1629. doi:10.1172/JCI12849.
34. Snyers L, Umlauf E, Prohaska R (1999) Association of stomatin with lipid-protein complexes in the plasma membrane and the endocytic compartment. *Eur J Cell Biol* 78: 802–812. doi:10.1016/S0171-9335(99)80031-4.
35. Brown DA, Rose JK (1992) Sorting of GPI-anchored proteins to glycolipid-enriched membrane subdomains during transport to the apical cell surface. *Cell* 68: 533–544.

## References

36. Roselli S, Gribouval O, Boute N, Sich M, Benessy F, et al. (2002) Podocin localizes in the kidney to the slit diaphragm area. *Am J Pathol* 160: 131–139. doi:10.1016/S0002-9440(10)64357-X.
37. Caridi G, Bertelli R, Di Duca M, Dagnino M, Emma F, et al. (2003) Broadening the spectrum of diseases related to podocin mutations. *J Am Soc Nephrol* 14: 1278–1286.
38. Caridi G, Bertelli R, Carrea A, Di Duca M, Catarsi P, et al. (2001) Prevalence, genetics, and clinical features of patients carrying podocin mutations in steroid-resistant nonfamilial focal segmental glomerulosclerosis. *J Am Soc Nephrol* 12: 2742–2746.
39. Karle SM, Uetz B, Ronner V, Glaeser L, Hildebrandt F, et al. (2002) Novel mutations in NPHS2 detected in both familial and sporadic steroid-resistant nephrotic syndrome. *J Am Soc Nephrol* 13: 388–393.
40. Koziell A, Grech V, Hussain S, Lee G, Lenkkeri U, et al. (2002) Genotype/phenotype correlations of NPHS1 and NPHS2 mutations in nephrotic syndrome advocate a functional inter-relationship in glomerular filtration. *Hum Mol Genet* 11: 379–388.
41. Tsukaguchi H, Sudhakar A, Le TC, Nguyen T, Yao J, et al. (2002) NPHS2 mutations in late-onset focal segmental glomerulosclerosis: R229Q is a common disease-associated allele. *J Clin Invest* 110: 1659–1666. doi:10.1172/JCI16242.
42. Huang M, Gu G, Ferguson EL, Chalfie M (1995) A stomatin-like protein necessary for mechanosensation in *C. elegans*. *Nature* 378: 292–295. doi:10.1038/378292a0.
43. Zhang S, Arnadottir J, Keller C, Caldwell GA, Yao CA, et al. (2004) MEC-2 is recruited to the putative mechanosensory complex in *C. elegans* touch receptor neurons through its stomatin-like domain. *Curr Biol* 14: 1888–1896. doi:10.1016/j.cub.2004.10.030.
44. Goodman MB, Ernstrom GG, Chelur DS, O'Hagan R, Yao CA, et al. (2002) MEC-2 regulates *C. elegans* DEG/ENaC channels needed for mechanosensation. *Nature* 415: 1039–1042. doi:10.1038/4151039a.
45. O'Hagan R, Chalfie M, Goodman MB (2005) The MEC-4 DEG/ENaC channel of *Caenorhabditis elegans* touch receptor neurons transduces mechanical signals. *Nat Neurosci* 8: 43–50. doi:10.1038/nn1362.

## References

46. Spassova MA, Hewavitharana T, Xu W, Soboloff J, Gill DL (2006) A common mechanism underlies stretch activation and receptor activation of TRPC6 channels. *Proc Natl Acad Sci USA* 103: 16586–16591. doi:10.1073/pnas.0606894103.
47. Huber TB, Schermer B, Benzing T (2007) Podocin organizes ion channel-lipid supercomplexes: implications for mechanosensation at the slit diaphragm. *Nephron Exp Nephrol* 106: e27–31. doi:10.1159/000101789.
48. Winter A, Kämäräinen O, Hofmann A (2007) Molecular modeling of prohibitin domains. *Proteins* 68: 353–362. doi:10.1002/prot.21355.
49. Back JW, Sanz MA, De Jong L, De Koning LJ, Nijtmans LGJ, et al. (2002) A structure for the yeast prohibitin complex: Structure prediction and evidence from chemical crosslinking and mass spectrometry. *Protein Sci* 11: 2471–2478. doi:10.1110/ps.0212602.
50. Berger KH, Yaffe MP (1998) Prohibitin family members interact genetically with mitochondrial inheritance components in *Saccharomyces cerevisiae*. *Mol Cell Biol* 18: 4043–4052.
51. Osman C, Merkwirth C, Langer T (2009) Prohibitins and the functional compartmentalization of mitochondrial membranes. *J Cell Sci* 122: 3823–3830. doi:10.1242/jcs.037655.
52. Nijtmans LG, de Jong L, Artal Sanz M, Coates PJ, Berden JA, et al. (2000) Prohibitins act as a membrane-bound chaperone for the stabilization of mitochondrial proteins. *EMBO J* 19: 2444–2451. doi:10.1093/emboj/19.11.2444.
53. Merkwirth C, Dargazanli S, Tatsuta T, Geimer S, Löwer B, et al. (2008) Prohibitins control cell proliferation and apoptosis by regulating OPA1-dependent cristae morphogenesis in mitochondria. *Genes Dev* 22: 476–488. doi:10.1101/gad.460708.
54. Fusaro G, Dasgupta P, Rastogi S, Joshi B, Chellappan S (2003) Prohibitin induces the transcriptional activity of p53 and is exported from the nucleus upon apoptotic signaling. *J Biol Chem* 278: 47853–47861. doi:10.1074/jbc.M305171200.
55. Supale S, Thorel F, Merkwirth C, Gjinovci A, Herrera PL, et al. (2013) Loss of prohibitin induces mitochondrial damages altering ss-cell function and survival and responsible for gradual diabetes development. *Diabetes*. doi:10.2337/db13-0152.

## References

56. Zhang L, Ji Q, Ni Z-H, Sun J (2012) Prohibitin induces apoptosis in BGC823 gastric cancer cells through the mitochondrial pathway. *Asian Pac J Cancer Prev* 13: 3803–3807.
57. Delage-Mourroux R, Martini PG, Choi I, Kraichely DM, Hoeksema J, et al. (2000) Analysis of estrogen receptor interaction with a repressor of estrogen receptor activity (REA) and the regulation of estrogen receptor transcriptional activity by REA. *J Biol Chem* 275: 35848–35856. doi:10.1074/jbc.M001327200.
58. Kurtev V, Margueron R, Kroboth K, Ogris E, Cavailles V, et al. (2004) Transcriptional regulation by the repressor of estrogen receptor activity via recruitment of histone deacetylases. *J Biol Chem* 279: 24834–24843. doi:10.1074/jbc.M312300200.
59. Park S-E, Xu J, Frolova A, Liao L, O'Malley BW, et al. (2005) Genetic deletion of the repressor of estrogen receptor activity (REA) enhances the response to estrogen in target tissues in vivo. *Mol Cell Biol* 25: 1989–1999. doi:10.1128/MCB.25.5.1989-1999.2005.
60. Wang S, Fusaro G, Padmanabhan J, Chellappan SP (2002) Prohibitin co-localizes with Rb in the nucleus and recruits N-CoR and HDAC1 for transcriptional repression. *Oncogene* 21: 8388–8396. doi:10.1038/sj.onc.1205944.
61. Jupe ER, Liu XT, Kiehlbauch JL, McClung JK, Dell'Orco RT (1996) Prohibitin in breast cancer cell lines: loss of antiproliferative activity is linked to 3' untranslated region mutations. *Cell Growth Differ* 7: 871–878.
62. Kang X, Zhang L, Sun J, Ni Z, Ma Y, et al. (2008) Prohibitin: a potential biomarker for tissue-based detection of gastric cancer. *J Gastroenterol* 43: 618–625. doi:10.1007/s00535-008-2208-3.
63. Lee JH, Nguyen KH, Mishra S, Nyomba BLG (2010) Prohibitin is expressed in pancreatic beta-cells and protects against oxidative and proapoptotic effects of ethanol. *FEBS J* 277: 488–500. doi:10.1111/j.1742-4658.2009.07505.x.
64. Guo W, Xu H, Chen J, Yang Y, Jin JW, et al. (2007) Prohibitin suppresses renal interstitial fibroblasts proliferation and phenotypic change induced by transforming growth factor-beta1. *Mol Cell Biochem* 295: 167–177. doi:10.1007/s11010-006-9286-4.
65. Duvezin-Caubet S, Jagasia R, Wagener J, Hofmann S, Trifunovic A, et al. (2006) Proteolytic processing of OPA1 links mitochondrial dysfunction to alterations

## References

- in mitochondrial morphology. *J Biol Chem* 281: 37972–37979. doi:10.1074/jbc.M606059200.
66. Frezza C, Cipolat S, Martins de Brito O, Micaroni M, Beznoussenko GV, et al. (2006) OPA1 controls apoptotic cristae remodeling independently from mitochondrial fusion. *Cell* 126: 177–189. doi:10.1016/j.cell.2006.06.025.
67. Griparic L, van der Wel NN, Orozco IJ, Peters PJ, van der Bliek AM (2004) Loss of the intermembrane space protein Mgm1/OPA1 induces swelling and localized constrictions along the lengths of mitochondria. *J Biol Chem* 279: 18792–18798. doi:10.1074/jbc.M400920200.
68. Olichon A, Baricault L, Gas N, Guillou E, Valette A, et al. (2003) Loss of OPA1 perturbs the mitochondrial inner membrane structure and integrity, leading to cytochrome c release and apoptosis. *J Biol Chem* 278: 7743–7746. doi:10.1074/jbc.C200677200.
69. Merkwirth C, Martinelli P, Korwitz A, Morbin M, Brönneke HS, et al. (2012) Loss of prohibitin membrane scaffolds impairs mitochondrial architecture and leads to tau hyperphosphorylation and neurodegeneration. *PLoS Genet* 8: e1003021. doi:10.1371/journal.pgen.1003021.
70. Artal-Sanz M, Tavernarakis N (2009) Prohibitin couples diapause signalling to mitochondrial metabolism during ageing in *C. elegans*. *Nature* 461: 793–797. doi:10.1038/nature08466.
71. Schleit J, Johnson SC, Bennett CF, Simko M, Trongtham N, et al. (2013) Molecular mechanisms underlying genotype-dependent responses to dietary restriction. *Aging Cell*. doi:10.1111/accel.12130.
72. Hara K, Maruki Y, Long X, Yoshino K, Oshiro N, et al. (2002) Raptor, a binding partner of target of rapamycin (TOR), mediates TOR action. *Cell* 110: 177–189.
73. Jacinto E, Loewith R, Schmidt A, Lin S, Rüegg MA, et al. (2004) Mammalian TOR complex 2 controls the actin cytoskeleton and is rapamycin insensitive. *Nat Cell Biol* 6: 1122–1128. doi:10.1038/ncb1183.
74. Kim D-H, Sarbassov DD, Ali SM, King JE, Latek RR, et al. (2002) mTOR interacts with raptor to form a nutrient-sensitive complex that signals to the cell growth machinery. *Cell* 110: 163–175.

## References

75. Loewith R, Jacinto E, Wullschleger S, Lorberg A, Crespo JL, et al. (2002) Two TOR complexes, only one of which is rapamycin sensitive, have distinct roles in cell growth control. *Mol Cell* 10: 457–468.
76. Sarbassov DD, Ali SM, Kim D-H, Guertin DA, Latek RR, et al. (2004) Rictor, a novel binding partner of mTOR, defines a rapamycin-insensitive and raptor-independent pathway that regulates the cytoskeleton. *Curr Biol* 14: 1296–1302. doi:10.1016/j.cub.2004.06.054.
77. Wullschleger S, Loewith R, Hall MN (2006) TOR signaling in growth and metabolism. *Cell* 124: 471–484. doi:10.1016/j.cell.2006.01.016.
78. Brugarolas J, Lei K, Hurley RL, Manning BD, Reiling JH, et al. (2004) Regulation of mTOR function in response to hypoxia by REDD1 and the TSC1/TSC2 tumor suppressor complex. *Genes Dev* 18: 2893–2904. doi:10.1101/gad.1256804.
79. Feng Z, Zhang H, Levine AJ, Jin S (2005) The coordinate regulation of the p53 and mTOR pathways in cells. *Proc Natl Acad Sci USA* 102: 8204–8209. doi:10.1073/pnas.0502857102.
80. Inoki K, Zhu T, Guan K-L (2003) TSC2 mediates cellular energy response to control cell growth and survival. *Cell* 115: 577–590.
81. Reiling JH, Hafen E (2004) The hypoxia-induced paralogs Scylla and Charybdis inhibit growth by down-regulating S6K activity upstream of TSC in *Drosophila*. *Genes Dev* 18: 2879–2892. doi:10.1101/gad.322704.
82. Gao X, Zhang Y, Arrazola P, Hino O, Kobayashi T, et al. (2002) Tsc tumour suppressor proteins antagonize amino-acid-TOR signalling. *Nat Cell Biol* 4: 699–704. doi:10.1038/ncb847.
83. Inoki K, Li Y, Zhu T, Wu J, Guan K-L (2002) TSC2 is phosphorylated and inhibited by Akt and suppresses mTOR signalling. *Nat Cell Biol* 4: 648–657. doi:10.1038/ncb839.
84. Tee AR, Manning BD, Roux PP, Cantley LC, Blenis J (2003) Tuberous sclerosis complex gene products, Tuberin and Hamartin, control mTOR signaling by acting as a GTPase-activating protein complex toward Rheb. *Curr Biol* 13: 1259–1268.
85. Kimura N, Tokunaga C, Dalal S, Richardson C, Yoshino K, et al. (2003) A possible linkage between AMP-activated protein kinase (AMPK) and mammalian target of rapamycin (mTOR) signalling pathway. *Genes Cells* 8: 65–79.

## References

86. Brunn GJ, Williams J, Sabers C, Wiederrecht G, Lawrence JC Jr, et al. (1996) Direct inhibition of the signaling functions of the mammalian target of rapamycin by the phosphoinositide 3-kinase inhibitors, wortmannin and LY294002. *EMBO J* 15: 5256–5267.
87. Li J, DeFea K, Roth RA (1999) Modulation of insulin receptor substrate-1 tyrosine phosphorylation by an Akt/phosphatidylinositol 3-kinase pathway. *J Biol Chem* 274: 9351–9356.
88. Garami A, Zwartkruis FJT, Nobukuni T, Joaquin M, Rocco M, et al. (2003) Insulin activation of Rheb, a mediator of mTOR/S6K/4E-BP signaling, is inhibited by TSC1 and 2. *Mol Cell* 11: 1457–1466.
89. Jaeschke A, Hartkamp J, Saitoh M, Roworth W, Nobukuni T, et al. (2002) Tuberous sclerosis complex tumor suppressor-mediated S6 kinase inhibition by phosphatidylinositol-3-OH kinase is mTOR independent. *J Cell Biol* 159: 217–224. doi:10.1083/jcb.jcb.200206108.
90. Sekulić A, Hudson CC, Homme JL, Yin P, Otterness DM, et al. (2000) A direct linkage between the phosphoinositide 3-kinase-AKT signaling pathway and the mammalian target of rapamycin in mitogen-stimulated and transformed cells. *Cancer Res* 60: 3504–3513.
91. Brunn GJ, Hudson CC, Sekulić A, Williams JM, Hosoi H, et al. (1997) Phosphorylation of the translational repressor PHAS-I by the mammalian target of rapamycin. *Science* 277: 99–101.
92. Burnett PE, Barrow RK, Cohen NA, Snyder SH, Sabatini DM (1998) RAFT1 phosphorylation of the translational regulators p70 S6 kinase and 4E-BP1. *Proc Natl Acad Sci USA* 95: 1432–1437.
93. Hay N, Sonenberg N (2004) Upstream and downstream of mTOR. *Genes Dev* 18: 1926–1945. doi:10.1101/gad.1212704.
94. Rangan GK, Coombes JD (2007) Renoprotective effects of sirolimus in non-immune initiated focal segmental glomerulosclerosis. *Nephrol Dial Transplant* 22: 2175–2182. doi:10.1093/ndt/gfm191.
95. Gödel M, Hartleben B, Herbach N, Liu S, Zschiedrich S, et al. (2011) Role of mTOR in podocyte function and diabetic nephropathy in humans and mice. *J Clin Invest* 121: 2197–2209. doi:10.1172/JCI44774.

## References

96. Lloberas N, Cruzado JM, Franquesa M, Herrero-Fresneda I, Torras J, et al. (2006) Mammalian target of rapamycin pathway blockade slows progression of diabetic kidney disease in rats. *J Am Soc Nephrol* 17: 1395–1404. doi:10.1681/ASN.2005050549.
97. Mori H, Inoki K, Masutani K, Wakabayashi Y, Komai K, et al. (2009) The mTOR pathway is highly activated in diabetic nephropathy and rapamycin has a strong therapeutic potential. *Biochem Biophys Res Commun* 384: 471–475. doi:10.1016/j.bbrc.2009.04.136.
98. Sakaguchi M, Isono M, Isshiki K, Sugimoto T, Koya D, et al. (2006) Inhibition of mTOR signaling with rapamycin attenuates renal hypertrophy in the early diabetic mice. *Biochem Biophys Res Commun* 340: 296–301. doi:10.1016/j.bbrc.2005.12.012.
99. Yang Y, Wang J, Qin L, Shou Z, Zhao J, et al. (2007) Rapamycin prevents early steps of the development of diabetic nephropathy in rats. *Am J Nephrol* 27: 495–502. doi:10.1159/000106782.
100. Aliabadi AZ, Pohanka E, Seebacher G, Dunkler D, Kammerstätter D, et al. (2008) Development of proteinuria after switch to sirolimus-based immunosuppression in long-term cardiac transplant patients. *Am J Transplant* 8: 854–861. doi:10.1111/j.1600-6143.2007.02142.x.
101. Letavernier E, Pe'raldi M-N, Pariente A, Morelon E, Legendre C (2005) Proteinuria following a switch from calcineurin inhibitors to sirolimus. *Transplantation* 80: 1198–1203.
102. Sennesael JJ, Bosmans JL, Bogers JP, Verbeelen D, Verpooten GA (2005) Conversion from cyclosporine to sirolimus in stable renal transplant recipients. *Transplantation* 80: 1578–1585.
103. Welsh GI, Hale LJ, Eremina V, Jeansson M, Maezawa Y, et al. (2010) Insulin signaling to the glomerular podocyte is critical for normal kidney function. *Cell Metab* 12: 329–340. doi:10.1016/j.cmet.2010.08.015.
104. Inoki K, Mori H, Wang J, Suzuki T, Hong S, et al. (2011) mTORC1 activation in podocytes is a critical step in the development of diabetic nephropathy in mice. *J Clin Invest* 121: 2181–2196. doi:10.1172/JCI44771.

## References

105. Inoki K, Huber TB (2012) Mammalian target of rapamycin signaling in the podocyte. *Curr Opin Nephrol Hypertens* 21: 251–257. doi:10.1097/MNH.0b013e3283520f38.
106. Griffin SV, Olivier JP, Pippin JW, Roberts JM, Shankland SJ (2006) Cyclin I protects podocytes from apoptosis. *J Biol Chem* 281: 28048–28057. doi:10.1074/jbc.M513336200.
107. Shankland SJ, Pippin JW, Reiser J, Mundel P (2007) Podocytes in culture: past, present, and future. *Kidney Int* 72: 26–36. doi:10.1038/sj.ki.5002291.
108. Calixto A, Chelur D, Topalidou I, Chen X, Chalfie M (2010) Enhanced neuronal RNAi in *C. elegans* using SID-1. *Nat Methods* 7: 554–559. doi:10.1038/nmeth.1463.
109. Brenner S (1974) The genetics of *Caenorhabditis elegans*. *Genetics* 77: 71–94.
110. Fire A, Xu S, Montgomery MK, Kostas SA, Driver SE, et al. (1998) Potent and specific genetic interference by double-stranded RNA in *Caenorhabditis elegans*. *Nature* 391: 806–811. doi:10.1038/35888.
111. Kamath RS, Ahringer J (2003) Genome-wide RNAi screening in *Caenorhabditis elegans*. *Methods* 30: 313–321.
112. Artal-Sanz M, Tsang WY, Willems EM, Grivell LA, Lemire BD, et al. (2003) The mitochondrial prohibitin complex is essential for embryonic viability and germline function in *Caenorhabditis elegans*. *J Biol Chem* 278: 32091–32099. doi:10.1074/jbc.M304877200.
113. Chalfie M, Sulston J (1981) Developmental genetics of the mechanosensory neurons of *Caenorhabditis elegans*. *Dev Biol* 82: 358–370.
114. Finney M, Ruvkun G (1990) The *unc-86* gene product couples cell lineage and cell identity in *C. elegans*. *Cell* 63: 895–905.
115. Bharill P, Ayyadevara S, Alla R, Shmookler Reis RJ (2013) Extreme Depletion of PIP3 Accompanies the Increased Life Span and Stress Tolerance of PI3K-null *C. elegans* Mutants. *Front Genet* 4: 34. doi:10.3389/fgene.2013.00034.
116. Moeller MJ, Sanden SK, Soofi A, Wiggins RC, Holzman LB (2003) Podocyte-specific expression of cre recombinase in transgenic mice. *Genesis* 35: 39–42. doi:10.1002/gene.10164.
117. Wang J, Wang Y, Long J, Chang BHJ, Wilson MH, et al. (2010) Tamoxifen-inducible podocyte-specific iCre recombinase transgenic mouse provides a simple

## References

- approach for modulation of podocytes in vivo. *Genesis* 48: 446–451. doi:10.1002/dvg.20635.
118. Zeng L-H, Xu L, Gutmann DH, Wong M (2008) Rapamycin prevents epilepsy in a mouse model of tuberous sclerosis complex. *Ann Neurol* 63: 444–453. doi:10.1002/ana.21331.
119. Yang J-S, Nam H-J, Seo M, Han SK, Choi Y, et al. (2011) OASIS: online application for the survival analysis of lifespan assays performed in aging research. *PLoS ONE* 6: e23525. doi:10.1371/journal.pone.0023525.
120. Bewick V, Cheek L, Ball J (2004) Statistics review 12: survival analysis. *Crit Care* 8: 389–394. doi:10.1186/cc2955.
121. Baris OR, Klose A, Kloepper JE, Weiland D, Neuhaus JFG, et al. (2011) The mitochondrial electron transport chain is dispensable for proliferation and differentiation of epidermal progenitor cells. *Stem Cells* 29: 1459–1468. doi:10.1002/stem.695.
122. Wu Q, Wu S (2012) Lipid rafts association and anti-apoptotic function of prohibitin in ultraviolet B light-irradiated HaCaT keratinocytes. *Exp Dermatol* 21: 640–642. doi:10.1111/j.1600-0625.2012.01547.x.
123. Kriz W, LeHir M (2005) Pathways to nephron loss starting from glomerular diseases-insights from animal models. *Kidney Int* 67: 404–419. doi:10.1111/j.1523-1755.2005.67097.x.
124. Wharram BL, Goyal M, Wiggins JE, Sanden SK, Hussain S, et al. (2005) Podocyte depletion causes glomerulosclerosis: diphtheria toxin-induced podocyte depletion in rats expressing human diphtheria toxin receptor transgene. *J Am Soc Nephrol* 16: 2941–2952. doi:10.1681/ASN.2005010055.
125. Kretzler M (2005) Role of podocytes in focal sclerosis: defining the point of no return. *J Am Soc Nephrol* 16: 2830–2832. doi:10.1681/ASN.2005080841.
126. Kim YH, Goyal M, Kurnit D, Wharram B, Wiggins J, et al. (2001) Podocyte depletion and glomerulosclerosis have a direct relationship in the PAN-treated rat. *Kidney Int* 60: 957–968. doi:10.1046/j.1523-1755.2001.060003957.x.
127. Ruotsalainen V, Ljungberg P, Wartiovaara J, Lenkkeri U, Kestilä M, et al. (1999) Nephrin is specifically located at the slit diaphragm of glomerular podocytes. *Proc Natl Acad Sci USA* 96: 7962–7967.

## References

128. Chalfie M, Thomson JN (1979) Organization of neuronal microtubules in the nematode *Caenorhabditis elegans*. *J Cell Biol* 82: 278–289.
129. Zhang Y, Ma C, Delohery T, Nasipak B, Foat BC, et al. (2002) Identification of genes expressed in *C. elegans* touch receptor neurons. *Nature* 418: 331–335. doi:10.1038/nature00891.
130. Schermer B, Benzing T (2009) Lipid-protein interactions along the slit diaphragm of podocytes. *J Am Soc Nephrol* 20: 473–478. doi:10.1681/ASN.2008070694.
131. Ishii N, Fujii M, Hartman PS, Tsuda M, Yasuda K, et al. (1998) A mutation in succinate dehydrogenase cytochrome b causes oxidative stress and ageing in nematodes. *Nature* 394: 694–697. doi:10.1038/29331.
132. Hale LJ, Coward RJM (2013) Insulin signalling to the kidney in health and disease. *Clin Sci* 124: 351–370. doi:10.1042/CS20120378.
133. Kasashima K, Sumitani M, Satoh M, Endo H (2008) Human prohibitin 1 maintains the organization and stability of the mitochondrial nucleoids. *Exp Cell Res* 314: 988–996. doi:10.1016/j.yexcr.2008.01.005.
134. Rajalingam K, Wunder C, Brinkmann V, Churin Y, Hekman M, et al. (2005) Prohibitin is required for Ras-induced Raf-MEK-ERK activation and epithelial cell migration. *Nat Cell Biol* 7: 837–843. doi:10.1038/ncb1283.
135. Shih NY, Li J, Cotran R, Mundel P, Miner JH, et al. (2001) CD2AP localizes to the slit diaphragm and binds to nephrin via a novel C-terminal domain. *Am J Pathol* 159: 2303–2308. doi:10.1016/S0002-9440(10)63080-5.
136. Putaala H, Soininen R, Kilpeläinen P, Wartiovaara J, Tryggvason K (2001) The murine nephrin gene is specifically expressed in kidney, brain and pancreas: inactivation of the gene leads to massive proteinuria and neonatal death. *Hum Mol Genet* 10: 1–8.
137. Ma L-J, Fogo AB (2003) Model of robust induction of glomerulosclerosis in mice: importance of genetic background. *Kidney Int* 64: 350–355. doi:10.1046/j.1523-1755.2003.00058.x.
138. Anderson M, Kim EY, Hagmann H, Benzing T, Dryer SE (2013) Opposing effects of podocin on the gating of podocyte TRPC6 channels evoked by membrane stretch or diacylglycerol. *Am J Physiol, Cell Physiol* 305: C276–289. doi:10.1152/ajpcell.00095.2013.

## References

139. Zheng YZ, Berg KB, Foster LJ (2009) Mitochondria do not contain lipid rafts, and lipid rafts do not contain mitochondrial proteins. *J Lipid Res* 50: 988–998. doi:10.1194/jlr.M800658-JLR200.
140. Huber TB, Simons M, Hartleben B, Sernetz L, Schmidts M, et al. (2003) Molecular basis of the functional podocin-nephrin complex: mutations in the NPHS2 gene disrupt nephrin targeting to lipid raft microdomains. *Hum Mol Genet* 12: 3397–3405. doi:10.1093/hmg/ddg360.
141. Kriz W, Shirato I, Nagata M, LeHir M, Lemley KV (2013) The podocyte's response to stress: the enigma of foot process effacement. *Am J Physiol Renal Physiol* 304: F333–347. doi:10.1152/ajprenal.00478.2012.
142. Schleicher M, Shepherd BR, Suarez Y, Fernandez-Hernando C, Yu J, et al. (2008) Prohibitin-1 maintains the angiogenic capacity of endothelial cells by regulating mitochondrial function and senescence. *J Cell Biol* 180: 101–112. doi:10.1083/jcb.200706072.
143. Kathiria AS, Butcher LD, Feagins LA, Souza RF, Boland CR, et al. (2012) Prohibitin 1 modulates mitochondrial stress-related autophagy in human colonic epithelial cells. *PLoS ONE* 7: e31231. doi:10.1371/journal.pone.0031231.
144. Liu D, Lin Y, Kang T, Huang B, Xu W, et al. (2012) Mitochondrial dysfunction and adipogenic reduction by prohibitin silencing in 3T3-L1 cells. *PLoS ONE* 7: e34315. doi:10.1371/journal.pone.0034315.
145. Alexander C, Votruba M, Pesch UE, Thiselton DL, Mayer S, et al. (2000) OPA1, encoding a dynamin-related GTPase, is mutated in autosomal dominant optic atrophy linked to chromosome 3q28. *Nat Genet* 26: 211–215. doi:10.1038/79944.
146. Delettre C, Lenaers G, Griffoin JM, Gigarel N, Lorenzo C, et al. (2000) Nuclear gene OPA1, encoding a mitochondrial dynamin-related protein, is mutated in dominant optic atrophy. *Nat Genet* 26: 207–210. doi:10.1038/79936.
147. Züchner S, Mersiyanova IV, Muglia M, Bissar-Tadmouri N, Rochelle J, et al. (2004) Mutations in the mitochondrial GTPase mitofusin 2 cause Charcot-Marie-Tooth neuropathy type 2A. *Nat Genet* 36: 449–451. doi:10.1038/ng1341.
148. Tatsuta T, Langer T (2008) Quality control of mitochondria: protection against neurodegeneration and ageing. *EMBO J* 27: 306–314. doi:10.1038/sj.emboj.7601972.

## References

149. Chen H, Chomyn A, Chan DC (2005) Disruption of fusion results in mitochondrial heterogeneity and dysfunction. *J Biol Chem* 280: 26185–26192. doi:10.1074/jbc.M503062200.
150. Cipolat S, Martins de Brito O, Dal Zilio B, Scorrano L (2004) OPA1 requires mitofusin 1 to promote mitochondrial fusion. *Proc Natl Acad Sci USA* 101: 15927–15932. doi:10.1073/pnas.0407043101.
151. Barisoni L, Madaio MP, Eraso M, Gasser DL, Nelson PJ (2005) The kd/kd mouse is a model of collapsing glomerulopathy. *J Am Soc Nephrol* 16: 2847–2851. doi:10.1681/ASN.2005050494.
152. Hagiwara M, Yamagata K, Capaldi RA, Koyama A (2006) Mitochondrial dysfunction in focal segmental glomerulosclerosis of puromycin aminonucleoside nephrosis. *Kidney Int* 69: 1146–1152. doi:10.1038/sj.ki.5000207.
153. Güçer S, Talim B, Aşan E, Korkusuz P, Ozen S, et al. (2005) Focal segmental glomerulosclerosis associated with mitochondrial cytopathy: report of two cases with special emphasis on podocytes. *Pediatr Dev Pathol* 8: 710–717. doi:10.1007/s10024-005-0058-z.
154. Hotta O, Inoue CN, Miyabayashi S, Furuta T, Takeuchi A, et al. (2001) Clinical and pathologic features of focal segmental glomerulosclerosis with mitochondrial tRNA<sup>Leu</sup>(UUR) gene mutation. *Kidney Int* 59: 1236–1243. doi:10.1046/j.1523-1755.2001.0590041236.x.
155. Markowitz GS, Appel GB, Fine PL, Fenves AZ, Loon NR, et al. (2001) Collapsing focal segmental glomerulosclerosis following treatment with high-dose pamidronate. *J Am Soc Nephrol* 12: 1164–1172.
156. Vienberg SG, Bouman SD, Sørensen H, Stidsen CE, Kjeldsen T, et al. (2011) Receptor-isoform-selective insulin analogues give tissue-preferential effects. *Biochem J* 440: 301–308. doi:10.1042/BJ20110880.
157. Coward RJM, Welsh GI, Yang J, Tasman C, Lennon R, et al. (2005) The human glomerular podocyte is a novel target for insulin action. *Diabetes* 54: 3095–3102.
158. Amri K, Freund N, Duong Van Huyen JP, Merlet-Bénichou C, Lelièvre-Pégorier M (2001) Altered nephrogenesis due to maternal diabetes is associated with increased expression of IGF-II/mannose-6-phosphate receptor in the fetal kidney. *Diabetes* 50: 1069–1075.

## References

159. Bridgewater DJ, Ho J, Sauro V, Matsell DG (2005) Insulin-like growth factors inhibit podocyte apoptosis through the PI3 kinase pathway. *Kidney Int* 67: 1308–1314. doi:10.1111/j.1523-1755.2005.00208.x.
160. Daniel C, Ziswiler R, Frey B, Pfister M, Marti HP (2000) Proinflammatory effects in experimental mesangial proliferative glomerulonephritis of the immunosuppressive agent SDZ RAD, a rapamycin derivative. *Exp Nephrol* 8: 52–62. doi:20648.
161. Ito N, Nishibori Y, Ito Y, Takagi H, Akimoto Y, et al. (2011) mTORC1 activation triggers the unfolded protein response in podocytes and leads to nephrotic syndrome. *Lab Invest* 91: 1584–1595. doi:10.1038/labinvest.2011.135.
162. Kurayama R, Ito N, Nishibori Y, Fukuhara D, Akimoto Y, et al. (2011) Role of amino acid transporter LAT2 in the activation of mTORC1 pathway and the pathogenesis of crescentic glomerulonephritis. *Lab Invest* 91: 992–1006. doi:10.1038/labinvest.2011.43.
163. Schmid E, El Benna J, Galter D, Klein G, Dröge W (1998) Redox priming of the insulin receptor beta-chain associated with altered tyrosine kinase activity and insulin responsiveness in the absence of tyrosine autophosphorylation. *FASEB J* 12: 863–870.
164. Schmid E, Hotz-Wagenblatt A, Hacj V, Dröge W (1999) Phosphorylation of the insulin receptor kinase by phosphocreatine in combination with hydrogen peroxide: the structural basis of redox priming. *FASEB J* 13: 1491–1500.
165. Loh K, Deng H, Fukushima A, Cai X, Boivin B, et al. (2009) Reactive Oxygen Species Enhance Insulin Sensitivity. *Cell Metabolism* 10: 260–272. doi:10.1016/j.cmet.2009.08.009.
166. Handayaningsih A-E, Takahashi M, Fukuoka H, Iguchi G, Nishizawa H, et al. (2012) IGF-I enhances cellular senescence via the reactive oxygen species-p53 pathway. *Biochem Biophys Res Commun* 425: 478–484. doi:10.1016/j.bbrc.2012.07.140.
167. Noda T, Ohsumi Y (1998) Tor, a Phosphatidylinositol Kinase Homologue, Controls Autophagy in Yeast. *J Biol Chem* 273: 3963–3966. doi:10.1074/jbc.273.7.3963.
168. Zheng WH, Kar S, Quirion R (2000) Insulin-like growth factor-1-induced phosphorylation of the forkhead family transcription factor FKHRL1 is mediated by

## References

Akt kinase in PC12 cells. *J Biol Chem* 275: 39152–39158. doi:10.1074/jbc.M002417200.

169. Ogg S, Paradis S, Gottlieb S, Patterson GI, Lee L, et al. (1997) The Fork head transcription factor DAF-16 transduces insulin-like metabolic and longevity signals in *C. elegans*. *Nature* 389: 994–999. doi:10.1038/40194.

170. Rena G, Guo S, Cichy SC, Unterman TG, Cohen P (1999) Phosphorylation of the transcription factor forkhead family member FKHR by protein kinase B. *J Biol Chem* 274: 17179–17183.

171. Cheng Z, Guo S, Copps K, Dong X, Kollipara R, et al. (2009) Foxo1 integrates insulin signaling with mitochondrial function in the liver. *Nat Med* 15: 1307–1311. doi:10.1038/nm.2049.

### 11 Danksagung

Mein Dank gilt Prof. Dr. Thomas Benzing, Prof. Dr. Thomas Langer und Prof. Dr. Bernhard Schermer für die gute Betreuung und Unterstützung sowie viele beratende Gespräche zur Durchführung meiner Doktorarbeit.

Ein besonderer Dank gilt PD Dr. Paul Brinkkötter, von dem ich viel gelernt habe, der stets all meinen Fragen zugehört, mit anregenden Ideen entscheidend zum Fortschritt meiner Doktorarbeit beigetragen und mich immer unterstützt hat.

Vielen Dank an alle MitarbeiterInnen des Nephrologischen Forschungslabors für die gute und kommunikative Zusammenarbeit und die angenehme Arbeitsatmosphäre. Hier geht ein besonderer Dank an PD Dr. Christine Kurschat sowie das gesamte Podozyten-Team, für ihr unablässiges Interesse an meinem Projekt und hilfreichen Diskussionen.

Des Weiteren möchte ich Dr. Sibylle Brinkkötter und Dr. Puneet Bharill danken, die mir bei der Durchführung einiger Experimente eine große Hilfe waren und immer als Ansprechpartner zur Verfügung standen. Mein Dank gilt natürlich auch allen weiteren Kooperationspartnern: Prof. Dr. Wilhelm Bloch, Prof. Dr. Donscho Kerjaschki, Dr. Andreas Linkermann, Dr. Carsten Merkwirth.

.Außerdem möchte ich Sybille Köhler, Fabian Braun, Dr. Lori Borgal und Dr. Claudia Dafinger danken, denn sie standen mir in jeder Lebens- und Laborlage zur Seite. Sie haben mich nicht nur bei Experimenten unterstützt, wenn ich mal wieder in Zeitnot war, sondern auch dazu beigetragen, dass ich nicht vergessen habe, dass es auch noch ein Leben außerhalb des Labores gibt.

Auch spreche ich meiner Familie einen besonderen Dank aus für ihre Unterstützung und Verständnis dafür, dass manchmal die Arbeit Vorrang haben musste. Ganz besonders möchte ich meinem Freund Dr. Sebastian Brähler dafür danken, dass er immer großes Vertrauen in mich und meine Arbeit hatte und mich bei allem unterstützt hat. Ohne sein Verständnis für meine ständigen Wochenend-Einsätze im Labor und ohne seine Hilfe wäre diese Arbeit nicht möglich gewesen.

## 12 Erklärung

Ich versichere, dass ich die von mir vorgelegte Dissertation selbständig angefertigt, die benutzten Quellen und Hilfsmittel vollständig angegeben und die Stellen der Arbeit – einschließlich Tabellen, Karten und Abbildungen –, die anderen Werken im Wortlaut oder dem Sinn nach entnommen sind, in jedem Einzelfall als Entlehnung kenntlich gemacht habe; dass diese Dissertation noch keiner anderen Fakultät oder Universität zur Prüfung vorgelegen hat; dass sie – abgesehen von unten angegebenen Teilpublikationen – noch nicht veröffentlicht worden ist, sowie, dass ich eine solche Veröffentlichung vor Abschluss des Promotionsverfahrens nicht vornehmen werde.

Die Bestimmungen der Promotionsordnung sind mir bekannt. Die von mir vorgelegte Dissertation ist von Prof. Dr. Thomas Langer und Prof. Dr. Thomas Benzing betreut worden.

Teilpublikationen liegen nicht vor.

Christina Ising, Köln den 18.11.2013

### **13 Curriculum vitae**

#### *Persönliche Angaben*

Name: Ising  
Vorname: Christina  
Geburtsdatum: 23.12.1985  
Geburtsort: Steinfurt, Deutschland  
Nationalität: Deutsch

#### *Akademische Ausbildung*

04/2010 – 01/2014 Promotion an der Universität zu Köln  
Im Rahmen der „International Graduate School for Development Health and Disease“ (IGS DHD),  
Universität zu Köln  
Betreuer: Prof. Dr. Thomas Langer,  
Prof. Dr. Thomas Benzing

01/2009 - 09/2009 Diplomarbeit an der Rheinischen Friedrich-  
Wilhelms-Universität Bonn  
Titel der Diplomarbeit: Analyse des  
Myelinproteomes von Fettsäure-2-Hydroxylase-  
defizienten Mäusen  
Betreuer: Prof. Dr. Volkmar Gieselmann,  
Prof. Dr. Jochen Walter

10/2005 - 09/2009 Exzellenz-Studiengang Molekulare Biomedizin an  
der Rheinischen Friedrich-Wilhelms-Universität  
Bonn

#### *Schulische Ausbildung*

08/1996 - 06/2005 Städtisches Gymnasium Borghorst, Steinfurt,  
Deutschland

08/1992 – 06/1996 Marienschule, Steinfurt, Deutschland